LEGIBILITY NOTICE

A major purpose of the Technical Information Center is to provide the broadest dissemination possible of information contained in DOE's Research and Development Reports to business, industry, the academic community, and federal, state and local governments.

Although portions of this report are not reproducible, it is being made available in microfiche to facilitate the availability of those parts of the document which are legible.

3

ORNL/FEDC--87/7

DE88 010756

Dist. Category UC- 423,424

Fusion Energy Division

ETR/ITER SYSTEMS CODE

R. L. Reid, Editor[a]

W. L. Barr[b]
C. G. Bathke[c]
J. N. Brooks[d]
R. H. Bulmer[b]
A. Busigin[e]
P. F. DuBois[b]
M. E. Fenstermacher[b,f]
J. Fink[b]
P. A. Finn[d]
J. D. Galambos[a]
Y. Gohar[d]
G. E. Gorker[a,g]
J. R. Haines[a,h]
A. M. Hassanein[d]
D. R. Hicks[a]
S. K. Ho[b]
S. S. Kalsi[a,g]
K. M. Kalyanam[e]
J. A. Kerns[b]
J. D. Lee[b]
J. R. Miller[b]
R. L. Miller[c]
J. O. Myall[b]
Y-K. M. Peng[a]
L. J. Perkins[b]
P. T. Spampinato[a,g]
D. J. Strickler[a]
S. L. Thomson[a,i]
C. E. Wagner[b,f]
R. S. Willms[c]

[a]Fusion Engineering Design Center, Oak Ridge National Laboratory.

[b]Lawrence Livermore National Laboratory.

[c]Los Alamos National Laboratory.

[d]Argonne National Laboratory.

[e]Canadian Fusion Fuels Technology Project.

[f]TRW, Inc.

[g]Grumman Aerospace Corporation.

[h]McDonnell Douglas Astronautics Company.

[i]Bechtel Group, Inc.

Date Published - April 1988

Prepared by the
OAK RIDGE NATIONAL LABORATORY
Oak Ridge, Tennessee 37831
operated by
MARTIN MARIETTA ENERGY SYSTEMS, INC.
for the
U.S. DEPARTMENT OF ENERGY
under contract DE-AC05-84OR21400

CONTENTS

LIST OF FIGURES

LIST OF FIGURES (Continued)

Figure

LIST OF TABLES

ABSTRACT

A tokamak systems code capable of modeling experimental test reactors has been developed and is described in this document. The code, named TETRA (for Tokamak Engineering Test Reactor Analysis), consists of a series of modules, each describing a tokamak system or component, controlled by an optimizer/driver. This code development was a national effort in that the modules were contributed by members of the fusion community and integrated into a code by the Fusion Engineering Design Center. The code has been checked out on the Cray computers at the National Magnetic Fusion Energy Computing Center and has satisfactorily simulated the Tokamak Ignition/Burn Experimental Reactor II (TIBER II) design. A feature of this code is the ability to perform optimization studies through the use of a numerical software package, which iterates prescribed variables to satisfy a set of prescribed equations or constraints. This code will be used to perform sensitivity studies for the proposed International Thermonuclear Experimental Reactor (ITER).

1. INTRODUCTION

1.1 BACKGROUND OF THE DEVELOPMENT OF THE ETR/ITER SYSTEMS CODE

A national effort to develop an Experimental Test Reactor/International Thermonuclear Experimental Reactor (ETR/ITER) systems code was initiated this past year and led to the first version of the TETRA code, which is described in this document. This effort was motivated by the following reasons:

1. There has been a strong need to improve the projected cost effectiveness of near-term ETRs; assessments for the Engineering Test Facility,[1] the Fusion Engineering Device,[2] and the Tokamak Fusion Core Experiment[3] indicated cost levels beyond the projected resources available in the U.S. magnetic fusion program in the near future.

2. The systems analysis efforts that guided the evolution of the Compact Ignition Tokamak (CIT) design[4] highlighted the challenge and the potential benefits of comprehensive systems tradeoffs among the physics and engineering design assumptions. The emphasis on high performance and minimum cost in CIT accentuated the role of an efficient and comprehensive systems analysis[5] during the early phases of the CIT design effort.

3. The Tokamak Ignition/Burn Experimental Reactor (TIBER) design concepts,[6] which emphasized aggressive physics and engineering assumptions, represent design regimes significantly different from the design concepts of the International Tokamak Reactor (INTOR),[7] the Next European Torus (NET),[8] Fusion Engineering Reactor (FER),[9] and OTR[10] and project significant savings in cost. A strong need presented itself to compare these designs on an equitable basis of performance, cost, uncertainties, and risks.[11]

4. The possibility of an international design effort for ITER, beginning during FY 1988 and lasting no more than three years, points to the need of a comprehensive systems code to assist in an early development of the ITER concept.[12]

The systems code development effort obtained valuable and major contributions from Lawrence Livermore National Laboratory (LLNL), Argonne National Laboratory (ANL), Los Alamos National Laboratory (LANL), Idaho National Engineering Laboratory (INEL), TRW, the Canadian Fusion Fuels Test Program (CFFTP), and the Fusion Engineering Design Center (FEDC); the effort was managed at the FEDC.

1.2 ROLE AND NATURE OF SYSTEMS ANALYSIS OF ETR/ITER

The basic step of systems analysis is the calculation of changes to a design (the parameters characterizing the design) when a single change is introduced. This single change can be in a parameter (e.g., the gap between the shield and the toroidal field coil case), a feature (e.g., single-null vs double-null divertor), or a constraint (e.g., the average neutron wall load). Relative to this single change, other features, constraints, objectives, and some parameters are held invariant as long as they are consistent with the principles of design. The impact of a single change on the design is therefore well defined when the invariants are clarified. A properly devised systems code should adequately model the design principles of the plasma and the components and allow efficient execution of this basic step of systems analysis.

By the method of constrained optimization, the ETR/ITER systems code TETRA (Tokamak Engineering Test Reactor Analysis) allows one to choose the collection of parameters, features, constraints, and objectives that are held invariant when a single change is introduced into the design. The code automatically "homes-in," by repeated calculations of nearby designs, on a design that minimizes or maximizes a chosen figure of merit. The TETRA code identifies this design efficiently by its numerical approach. Once such a design is identified, any systems code can verify it by the "benchmark" process.

It is worth noting that the use of a single figure of merit in systems analysis is not necessarily the sole consideration in arriving at a design. Systems analysis deals with a systems view of designs in the parameter space. That is, many parameters are viewed simultaneously in the evaluation of designs as useful yardsticks of comparison.

Examples of figures of merit include plasma major radius, direct cost, neutron wall load, fusion power, ignition margin, fluence, and their ratios (such as the fusion power divided by nuclear island mass). A good design should nearly optimize a number of figures of merit while satisfying a set of performance objectives, assuming a set of design features, and while being constrained by a set of design limits. This design should be able to operate over a sizable region in the parameter space above the minimum performance objectives and below the allowable limits (Fig. 1.1). Once we have chosen the desired figures of merit, performance objectives, performance margins, design constraints, and safety margins, design efforts can begin to identify acceptable designs. Systems analysis that uses a powerful tool such as TETRA can rapidly provide much of the information needed in identifying these designs.

In addition, much uncertainty remains in the performance, constraints, and margins we choose and in the basis with which they are calculated. We are also often uncertain about the impact of the uncertainties and about the identification of design issues with critical needs of analysis and data base.

To assist in conducting this process of design assessments, systems analysis can be applied to calculate the dependence of designs on changes in any of the design assumptions with significant uncertainties. Critical issues are identified when the dependences are strong over the accepted range of uncertainty. The tradeoffs among performance, cost, features, and limits (risks) can be rapidly assessed by using the systems code to provide valuable and timely input to choices of design concepts, issues, and innovations.

It is therefore clear that systems analysis aims to help elucidate the dependence of ITER/ETR designs in the multidimensional design parameter space and to quantify the sensitivity of this dependence to changes in any of the design objectives, features, and constraints. A broad understanding of the properties of this dependence is needed in making conceptual design decisions. The TETRA code is produced with up-to-date models and methods for this purpose.

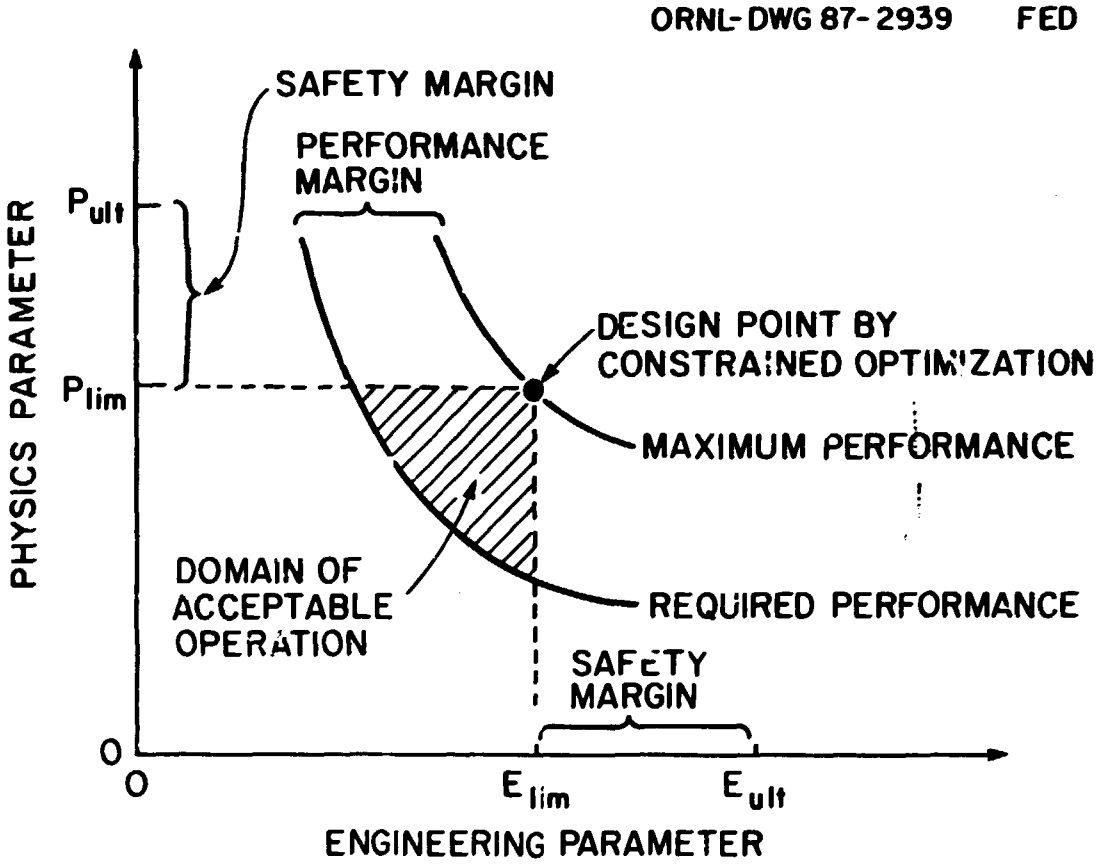

Fig. 1.1. Constrained optimization of a figure of merit leads to acceptable and unique design points.

1.3 ORGANIZATION OF THE REPORT

This volume is organized in the following manner. The architecture of the code is first discussed in summary form in Sect. 2. Then, an in-depth discussion of the "optimizer driver" is presented in Sect. 3 along with instructions for code retrieval and execution. Summary discussions of each module in the systems code, written by the respective authors of the modules, appear in Sect. 4. The modules are grouped into functional areas, namely plasma performance and requirements, mechanical systems, electrical systems, magnet systems, nuclear systems, and miscellaneous systems. The names of the authors of the modules appear in the introductory sections preceding the write-ups for each functional group of modules. Finally, Sect. 5 presents output from an execution of the systems code, which in this case is the simulation or benchmark of the TIBER II design.

The systems analysis work presented in this document was part of the effort on the ETR/TIBER study for FY 1987. The reader is referred to the companion document, TIBER II/ETR Final Design Report, UCID-21150 (to be published), which presents the design work on the TIBER II project.

1.4 REFERENCES FOR SECTION 1

1. ETF Design Team, ETR Mission Statement, ORNL/TM-6733, Oak Ridge National Laboratory, April 1980.

2. The Fusion Engineering Device, DOE/TIC-11600, Vols. 1-6, U.S. Department of Energy, October 1981.

3. C. A. Flanagan, Ed., Tokamak Fusion Core Experiment: Design Studies Based on Superconducting and Hybrid Toroidal Field Coils--Design Overview, ORNL/FEDC-84/3, Oak Ridge National Laboratory, October 1984.

4. C. A. Flanagan, Ed., Interim Report on the Assessment of Engineering Issues for Compact High-Field Ignition Devices, ORNL/FEDC-86/1, Oak Ridge National Laboratory, April 1986.

5. J. D. Galambos et al., System Studies of Compact Ignition Tokamaks, ORNL/FEDC-86/5, Oak Ridge National Laboratory, August 1987.

6. C. D. Henning and B. G. Logan, TIBER II, Tokamak Ignition/Burn Experimental Reactor 1986 Status Report, UCID-20863, October 1986.

7. INTOR, International Tokamak Reactor: Phase Two A, Part II, STI/PUB/714, International Atomic Energy Agency, Vienna, Austria, 1986.

8. R. Toschi, "The Next European Torus (NET)," Nucl. Eng. Des./Fusion 3(4), 325 (1986).

9. Japanese Atomic Energy Research Institute, "The Fusion Experimental Reactor (FER)," in Proceedings of the INTOR-Related Specialists Meeting on Information on Engineering Test Reactor Design Concepts, International Atomic Energy Agency Report, Vienna, Austria, to be published.

10. I. V. Kurchatov Institute of Atomic Energy, "OTR," in Proceedings of the INTOR-Related Specialists Meeting on Information on Engineering Test Reactor Design Concepts, International Atomic Energy Agency Report, Vienna, Austria, to be published.

11. C. A. Flanagan, J. D. Galambos, and Y-K. M. Peng, "Comparative Analysis of Next-Generation INTOR-Like Device," to be published in proceedings of the IEEE 12th Symposium on Fusion Engineering, October 1987.

12. Y-K. M. Peng et al., "Initial Results of Systems Analysis of the ETR/ITER Design Space," to be published in proceedings of the IEEE 12th Symposium on Fusion Engineering, October 1987.

2. CODE ARCHITECTURE

The Experimental Test Reactor (ETR) tokamak systems code consists of a series of modules, each describing a system or component of a tokamak reactor, controlled by a driver or optimizer routine. The modules are shown in Fig. 2.1. In the hierarchy of module execution, the modules downstream depend on the upstream modules to supply input (i.e., the energy storage module requires input from the magnet modules and the plasma heating modules).

The overall ETR systems code schematic is shown in Fig. 2.2. The code is controlled by an optimizer or nonlinear equation solver. All of the modules from Fig. 2.1, which describes the tokamak reactor, serve as a function generator and are represented as a single block (Tokamak

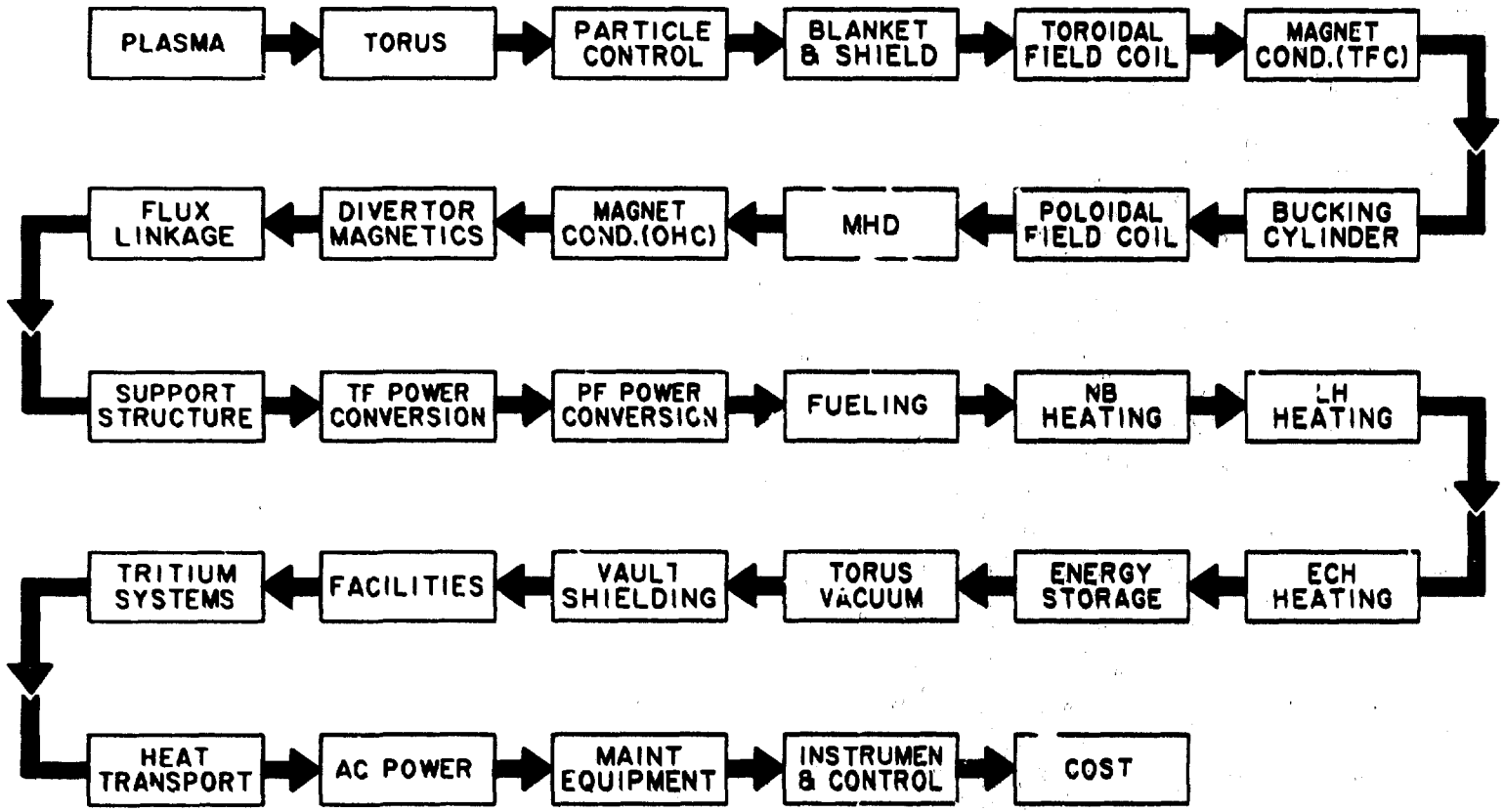

Fig. 2.1. Tokamak reactor systems flow diagram.

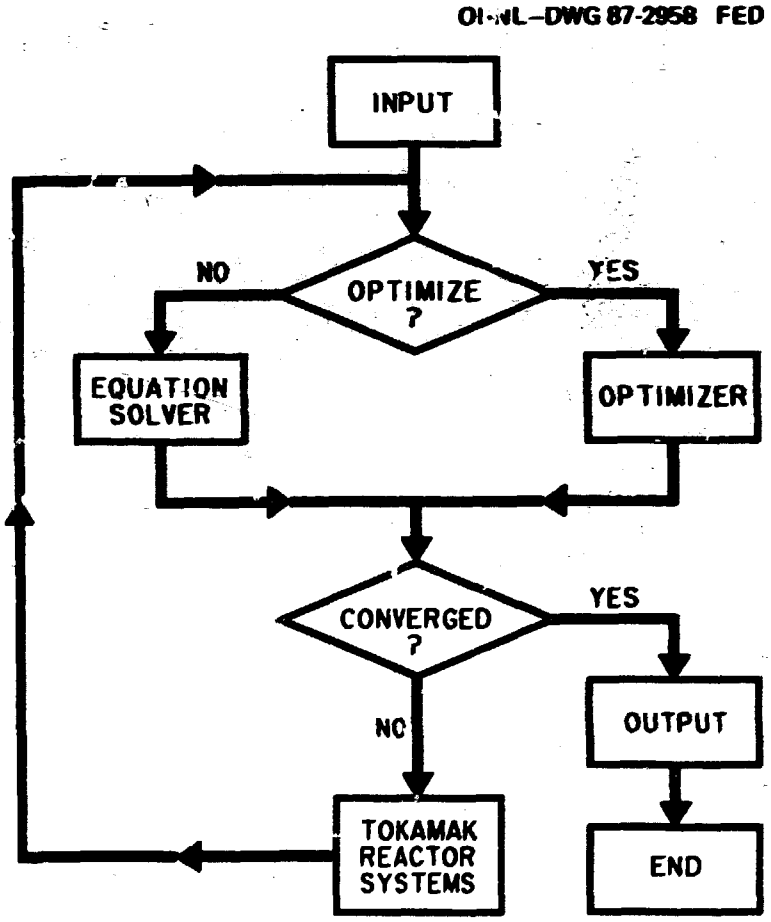

Fig. 2.2. Experimental test reactor tokamak systems code schematic.

Reactor Systems) in Fig. 2.2. This block returns to the driver computed values of physics and engineering quantities, which are used in evaluating specified constraints. If constraints are not satisfied within tolerance, the driver changes specified variables for iteration and recalls the Tokamak Reactor Systems modules until convergence criteria are satisfied. When using the optimizer option, the variables are iterated within prescribed bounds until the constraints are satisfied and a maximum or minimum of a selected figure of merit (such as cost or major radius) is achieved. (Section 3 contains an in-depth discussion of code formulation and usage.)

The constraints that link the tokamak reactor modules include the following:

1. beta limits,
2. plasma density limits,
3. ignition margin,
4. neutron wall loading,
5. magnetic flux capability of the poloidal field coil set,
6. coil stresses,
7. superconducting coil current limits,
8. shield requirements for superconducting coils,
9. shielding requirements for biological considerations,
10. plasma power balance, and
11. Q (the ratio of fusion power to current drive power).

3. OPTIMIZATION DRIVER AND USER INSTRUCTIONS

3.1 INTRODUCTION

The TETRA code is organized in a standard "equation solver" format and consists of a numerical software package that iterates prescribed variables to satisfy a set of prescribed equations (or constraints). In this case, the engineering and physics modules serve as the "function evaluator" of the equation solver, which provides information used in the solution of the equations. This section describes how the variables and equations are set up and explains how to use the code to examine problems.

The two equation-solving packages included in TETRA are VMCON and HYBRID. VMCON is an "optimizer" package, or more specifically, a generalized nonlinear programming subroutine. This option requires (1) iterating more variables than constraints being considered, (2) incorporating upper and lower bounds on all variables being iterated, and (3) specifying a prescribed figure of merit to be minimized or maximized. As an example, this option is useful for finding the minimum-cost machine that satisfies some physics and engineering constraints, and it has the freedom of not specifying plasma and coil sizes, field strengths, etc. HYBRID is a nonlinear equation solver with no "optimization." HYBRID iterates the same number of variables as constraints being satisfied and does not include any bounds on the variables. This option is useful for performing benchmark comparisons when the sizes, fields, plasma parameters, etc. are required to remain fixed (at the values of the comparison case) and one wishes to see how the calculated stress compares to the allowable stress, the beta compares to the beta limit, etc. Details of how to execute these types of runs are given in later sections. First, a description of the mechanics of using VMCON or HYBRID is given and the constraints that may be incorporated are summarized.

3.2 OPTIMIZER

To use the optimizer (VMCON), set the input switch IOPTIMZ to a value > 0. Initial decisions to be made in setting up the input involve what constraints should be incorporated for the task being considered and what quantities should be varied to satisfy these constraints (the constraints are described in Sect. 3.4). The number of constraints to be considered is specified by the variable NEQNS, and the numbers of the constraints being used (see Table 3.1) should be entered in the first NEQNS elements of the input array ICC. For example, if 20 constraints are being used and one of them is the beta limit constraint, NEQNS should be 20 and one of the first 20 elements of the array ICC should be "8" (the order of the constraint numbers in array ICC doesn't matter). The number of quantities to be iterated is NVAR, which should be greater

Table 3.1. Description of candidate ICC array elements[a]

Constraint	Description of the constraint	Corresponding ICC variables
1	Poloidal beta equation	2
2	Hot ion beam density equation	10
3	Beta calculation	14
4	Global power balance equation (ti/te - fixed)	4, 12, 15
5	Ion power balance	4, 11, 15
6	Electron power balance	4, 12, 15
7	*Density limit equation	15, 17
8	*Beta limit equation	12, 15, 16
9	Radial build	9, 18, 19, 30, 8, 31
10	*Volt-second equation	25, 20, 29, 18, 19
11	*Bucking cylinder buckling stress	32, 31
12	*Bucking cylinder bearing stress	23, 31
13	*Neutron wall load equation	24, 12, 15
14	*Inner shield equation (old first wall model)	28, 22
15	*Outer shield equation (old first wall model)	35, 13
16	*Ohmic heating (OH) coil stress	27, 20, 45
17	*Toroidal field (TF) coil stress	36, 21, 30, 6, 3
18	Field at TF coil (= required field at TF coil)	1, 9, 21, 30
19	*Insulator dose	42, 22
20	*Shut-down dose rate	43, 13
21	*TF coil port size equation	5, 40
22	*OH coil superconductor current	33, 20, 47, 46, 45
23	*TF coil superconductor current	26, 21, 41, 7, 3
24	*Sheffield figure of merit	39, 8, 9, 1
25	*Peak TF coil nuclear heating	44, 22
26	*Maximum TF coil field	37, 1, 9, 21
27	*Big Q value (injected power/fusion power)	34, 12, 15, 1, 9
28	*TF conductor stability margin	48, 41, 7, 3
29	*OH coil conductor stability margin	49, 47, 46, 45

[a]The constraints are numbered, and the number should be included in array ICC for the constraint to be considered. Some (non-exhaustive) variable numbers (see Table 3.2 for the quantities corresponding to these numbers) that directly affect the associated constraint and can be used to satisfy them are also given. Constraints marked by an asterisk (*) are set up as inequality constraints as described in the text.

than NEQNS when using the optimizer. The variable numbers (see Table 3.2) of the quantities to be iterated should be included in the first NVAR elements of array IXC. For example, if 25 quantities are to be iterated and one of them is electron temperature, then one of the first 25 elements of IXC should be "12."

An additional feature of the optimizer is to use bounds on the quantities being varied. These bounds are input through arrays BOUNDU and BOUNDL for the upper and lower bounds, respectively. The upper [lower] bound for variable i should be entered in BOUNDU(i) [BOUNDL(i)]. For example, if the upper bound on electron temperature is 100.0, set BOUNDU(12) = 100.0.

Some of the constraints are formulated as "inequality" constraints and are indicated by an asterisk (*) in Table 3.1. These constraints are arranged as

calculated quantity = "f-value" × allowable value.

Examples of "calculated quantities" are plasma beta and coil stress, and the corresponding "allowable values" are beta limit and stress limit, respectively. (Note: Sometimes the allowable value is computed, as with the case of the beta limit, and sometimes it is input, as with the case of stress limits.) The "f-values" can be used as variables, and by appropriately bounding them, the constraints become inequalities. Generally, it is desirable for the calculated quantity to be less than the allowable value, in which case the "f-value" should have an upper bound of 1. For example, if constraint 8 (beta limit) is being used, and variable 16 (fbeta) is used with an upper bound of 1.0, then a solution that satisfies the beta limit must be found. The two possible exceptions are the wall-load and Sheffield figure-of-merit constraints (as discussed below), where it may be desirable for the calculated quantity (wall-load) to be greater than the allowable or reference value (wall-load limit), in which case the f-value should have a lower bound of 1.0. The f-values corresponding to the constraints are listed in Table 3.2 along with their variable numbers. It is possible to use these constraints as equality constraints by keeping the f-value fixed (not including it in the array IXC).

Table 3.2. Quantities that can be used as variables for iteration[a]

Variable No.		Symbol	Description
1		bt	Toroidal field (TF) on axis (T)
2		betap	Poloidal beta
3		thwcndut	TF coil conduit case thickness
4		dign	Plasma ignition margin
5	*	ftfport	f-value for Eq. (21)
6		thkcas	TF coil external case average thickness (m)
7		vftf	He fraction on inside of TF coil winding pack
8		aspect	Plasma aspect ratio
9		rmajor	Plasma major radius
10		rnbeam	Hot beam ion density/electron density
11		tratio	Ion temperature/electron temperature
12		te	Average electron temperature (vol. averaged) (keV)
13		dsho	Outer shield thickness (m)
14		beta	Plasma beta
15		dene	Average electron density (m^{-3})
16	*	fbeta	f-value for beta limit, Eq. (8)
17	*	fdene	f-value for density limit, Eq. (7)
18		soltx	Thickness of ohmic heating (OH) coil (including case) (m)
19		boresol	Radius of OH coil inner bore (m)
20		coheof	Overall current density in OH coil at end of flattop (A)
21		rjcontf	Conductor current density in TF coil (A)
22		dshi	Inner shield thickness (m)
23	*	fbcbr	f-value for bucking cylinder stress, Eq. (12)
24	*	fwalld	f-value for neutron wall load, Eq. (13)
25	*	fvs	f-value for volt-second, Eq. (10)
26	*	fcpttf	f-value for TF coil current, Eq. (23)
27	*	fohsts	f-value for OH coil stress, Eq. (16)
28	*	fdshi	f-value for inner shield thickness, Eq. (14)
29		cohbop	Overall current density in OH coil at beginning of pulse (A)
30		tfthki	TF coil thickness (including case) (m)
31		bcylth	Bucking cylinder thickness (m)
32	*	fbckl	f-value for bucking cylinder, Eq. (11)
33	*	fcptoh	f-value for OH coil current, Eq. (22)
34	*	fqval	f-value for Q, Eq. (27)
35	*	fdsho	f-value for outer shield thickness, Eq. (15)
36	*	ftfsts	f-value for TF coil stress, Eq. (17)
37	*	fbmax	f-value for maximum TF coil field, Eq. (26)
38		fefac	H-factor in Kaye-Goldston confinement scaling
39	*	ffigmr	f-factor in figure of merit, Eq. (24)
40		dago	Gap between outboard TF coil leg and shield (m)
41		fcutf	Copper fraction of TF coil winding pack conductor
42	*	ffwlrad	f-value for radiation dose limit, Eq. (19)
43	*	ffwlsdd	f-value for shut-down dose limit, Eq. (20)
44	*	ffwlht	f-value for TF coil nuclear heating, Eq. (25)
45		twcdtoh	OH coil conduit case thickness (m)
46		vfohc	He fraction on inside of OH coil winding pack
47		fcuoh	Copper fraction of OH coil winding pack conductor
48	*	feptf	f-value for TF coil conductor stability, Eq. (28)
49	*	fepoh	f-value for OH coil conductor stability, Eq. (29)

[a]Including the associated variable No. in the array IXC allows these quantities to be iterated to satisfy the constraints being considered in Table 3.1. Variables marked with an asterisk (*) are used as "f-values" in inequality constraints, as described in the text.

An important consideration when using VMCON is the choice of a figure of merit (or objective function) to be minimized or maximized. In TETRA, this is determined by the input switch MINMAX (see Table 3.3). When the absolute value of MINMAX is positive, the figure of merit is minimized; when it is zero or negative, the figure of merit is maximized. That is, if MINMAX = 1, the minimum major radius solution is found. For the case when MINMAX = 0 (ignition margin), the maximum ignition margin is always found. It is possible to incorporate different figures of merit in subroutine FUNCT1.

3.3 NON-OPTIMIZER EQUATION SOLVER

To use the equation solver HYBRID (non-optimizer), set IOPTIM < 0 and specify the number of constraints to be considered with NEQNS. With this mode of operation, the number of variables used is automatically set equal to NEQNS. Also, when not optimizing, the bounds on the variables are not included, which precludes the use of inequality constraints as described above. As previously noted, the non-optimizing equation solver is useful for benchmarking. The constraints that are formulated as inequalities for VMCON can still be used by letting the appropriate f-value be a variable, even though it is not bounded. This provides information about how calculated values compare with limiting values, without having to change characteristics of the device being benchmarked to find a solution.

3.4 CONSTRAINT DESCRIPTION

This section contains a brief description of the constraints presently included in TETRA. These are also listed in Table 3.1, along with some variables that directly affect each constraint (and that can be used to find a solution when using that constraint). In general, other variables may also affect the constraints through the complicated interactions of the different systems. More complete descriptions of the methods used in calculating the terms used in the constraints are given in the summaries of the appropriate sections.

Table 3.3. Figure-of-merit choices determined by the input parameter MINMAX

MINMAX	Figure of merit	Description
0	dign	Plasma ignition margin
1	rmajor	Plasma major radius
2	totdcst	Total direct cost
3	wallmw	Neutron wall load
4	te	Plasma electron temperature

3.4.1 General Constraints

Several constraints that should always be used when analyzing tokamaks are the poloidal beta equation [Eq. (1) in Table 3.1], the plasma beta equation [Eq. (3)], the radial build equation [Eq. (9)], the relationship between the field at the toroidal field (TF) coil and the field-on-axis [Eq. (18)], and a plasma power balance relation--either the global balance [Eq. (4)] or the separate ion and electron balance equations [Eqs. (5) and (6)].

3.4.2 Plasma Constraints

The plasma beta and density can be limited to FBETA and FDENE times their respective limits with Eqs. (7) and (8) of Table 3.1. These inequality constraints are set up as described above. The neutron wall load is set equal to FWALLD times the input allowable wall load (WALALW) in constraint 13. The Sheffield figure of merit [i.e., plasma current (MA) $\times$ ASPECT^{SBAR}] is set equal to FFIGMR times the input allowable figure of merit (FGMRIN) in constraint 24. (Note: Setting SBAR = 0, where SBAR is a user input exponent, permits using this constraint as a minimum plasma current condition.) The injected current drive power is set equal to FQVAL times the fusion power in constraint 27; thus, bounding FQVAL $<$ 0.2 results in a solution with the big "Q" $>$ 5. Also, the volt-second requirement is set equal to FVS times the volt-second

capability of the poloidal field system in constraint 10. When using neutral beam current drive, the hot ion beam density constraint (2) should be used along with variable RNBEAM (variable 10). Otherwise, the hot beam density RNBEAM should be set equal to 0. Also, when using neutral beam injection, outer leg TF coil port size constraint 21 should be used; this sets the minimum allowable port size equal to FTFPORT times the actual port size.

3.4.3 Stress Constraints

The in-plane stress in the TF coil conduit is set equal to FTFSTS times the allowable stress in constraint 17, and the peak ohmic heating (OH) coil conduit in-plane stress is set equal to FOHSTS times the allowable in constraint 16. If a bucking cylinder is used, constraint 11 is used to set the buckling stress equal to FBCBKL times the critical buckling pressure, and constraint 12 is used to set the bearing stress equal to FBCBR times the input yield strength of the bucking cylinder material (YBUCK).

3.4.4 Superconductor Constraints

The current per turn in the TF coil is set equal to FCPTTF times the allowable current per turn in constraint 23. The allowable current is based on four considerations: (1) magnetic field, temperature, and strain effects; (2) heat transfer effects; (3) protection effects; and (4) quench pressure effects. Similarly, the OH coil current per turn is set equal to FCPTOH times its allowable in constraint 22. The minimum allowable TF (OH) coil conduit stability parameter is set equal to FEPTF (FEPOH) times the actual TF (OH) coil stability parameter in constraint 28 (29). It is possible to limit the maximum field at the TF coil explicitly with constraint 26, which sets the peak field at the coil equal to FBMAX times the input allowable (BMAXO).

3.4.5 Shielding Constraints

When using the new first-wall, blanket, and shield module (controlled by input switch ITIBER = 1), the following constraints

should be used. The TF coil nuclear heating rate is set equal to FFWLHT times the input allowable (HTFMAX) in constraint 25, the insulator radiation dose rate is set equal to FFLWRAD times the input allowable (DOSEMAX) in constraint 19, and the shutdown dose rate is set equal to FFWLSDD times the input allowable (SDDRMAX) in constraint 20. If the old first-wall, shield modules are used (ITIBER = 0--use with caution), then constraint 14 (15) should be used to set the minimum inner (outer) shield thickness equal to FDSHI (FDSHO) times the inner (outer) shield thickness, where the minimum thicknesses are based on the TF coil heating, insulator dose rate, and shut-down dose rate requirements. If the shield thicknesses are held fixed, it is not necessary to use any of these constraints.

3.4.6 Code Execution

First, obtain a copy of the systems code and required input data files from filem. The code and data files are stored in a global read directory call .TETRA. The Fortran listing of the code is designated tetra1, and a copy of the executable is called xtetra1. The reference input data files are called itetra1 and etrd. The file itetra1 contains user input consistent with the Tokamak Ignition/Burn Experimental Reactor (TIBER II) configuration. Definitions of the user input parameters are given in the Fortran listing of the code immediately following the subroutine "Input." The file etrd is an "expert" input data file necessary for code execution and should not be changed by the user. This data file contains detailed neutronic data used by the first-wall, blanket, and shield modules to determine the nuclear components' size and will only be changed by the module author. To extract the necessary codes and data from filem, enter the following filem command:

```
read 1057 .tetra xtetra1 itetra1 etrd
```

To execute the code, enter

```
xtetra1 in = itetra1  out = otetra1 / t v
```

An output file called otetra1 will be generated, and it is the TIBER II benchmark. To run other points, make the desired changes to the input

data file itetra1 and execute the code. The input and output file names may be changed from the reference names at the discretion of the user.

Succeeding versions of the code will be stored in filem under the TETRA directory and will be called tetra2, tetra3, etc., with reference input files itetr2, itetra3, etc.

The TIBER II benchmark case is included in Sect. 5 of the report.

3.5 REFERENCES FOR SECTION 3

1. R. L. Crane, K. E. Hillstrom, and M. Minkoff, Solution of the Generalized Nonlinear Programming Problem with Subroutine VMCON, ANL-80-64, Argonne National Laboratory, 1980.

2. J. J. More, B. S. Garbow, and K. E. Hillstrom, User Guides for MINPACK-1, ANL-80-74, Argonne National Laboratory, 1980.

4. MODULES

A brief description of each module of the experimental test reactor (ETR) tokamak systems code is presented. The summaries, in general, describe what is accomplished within the module, list major assumptions, and inform the reader where more detailed information on the subject can be obtained. The summaries are grouped into the following functional areas:

1. plasma performance and requirements,
2. mechanical systems
3. electrical systems,
4. magnet systems,
5. nuclear systems,
6. miscellaneous systems, and
7. cost.

4.1 PLASMA PERFORMANCE AND REQUIREMENTS

This section contains summaries for the following modules. Lead authors and their affiliations are indicated.

Module	Lead Author	Organization
Physics	J. D. Galambos	Fusion Engineering Design Center (FEDC)/ Oak Ridge National Laboratory (ORNL)
Current drive	M. E. Fenstermacher	TRW, Inc./Lawrence Livermore National Laboratory (LLNL)
Poloidal magnetics	D. J. Strickler	FEDC/ORNL
Flux linkage/inductance	J. D. Galambos	FEDC/ORNL
Divertor magnetics interface	R. L. Miller	Los Alamos National Laboratory (LANL)

(Note: The divertor magnetics interface module is not incorporated in this first version of the systems code, TETRA1. The module will be included in an upgraded version of TETRA. The summary description of the module will remain in this document.)

4.1.1 Physics Module

The physics module uses global, profile-averaged, steady-state plasma physics similar to that used in the MUMAK code[1] and described in ref. 2. Input to this module is lengthy and is described more completely in the code listing. Primary input includes the plasma size and shape, toroidal field (TF) on axis, edge safety factor, plasma density and temperature (and profiles), and Z-effective. We note that the electron and ion temperatures in this code (TE and TI) are volume-averaged temperatures as opposed to the density-weighted volume-averaged temperatures used in refs. 1 and 2. Key output includes the plasma current, plasma composition, power balance terms, volt-second requirements, limits on density and beta, and some other quantities used in other modules. The calculations are summarized here, and more detailed descriptions of the methods can usually be found in the references.

4.1.1.1 Plasma current

The plasma current scaling can be chosen from several options. In all cases, the edge safety factor, plasma major and minor radius, and

plasma shape are input. For limiter plasmas, one can choose from ICURR = 1 (scaling derived for a spherical torus[3]), ICURR = 3 [Compact Ignition Tokamak (CIT) physics panel recommendation], ICURR = 4 [fit to magnetohydrodynamic (MHD) equilibria[4]], or ICURR = 5 (the GAT scaling[5]). All these scalings use the safety factor (q) as the "q-psi" at the outermost closed flux surface. For divertors, ICURR = 2, the scaling described in ref. 6 can be used; it uses q as the mean safety factor at the separatrix (see ref. 6). The cylindrical safety factor (QSTAR) is also calculated using the method described in ref. 1.

4.1.1.2 Plasma composition

The plasma ion composition consists of fuel, alpha ash, impurity species, and hot neutral beam ions. The fractional makeup is determined by inputting the thermal alpha ash density fraction [relative to the electron density (RALPNE)], the neutral beam fast ion density fraction (RNBEAM), the charge of the impurity species (ZIMP), and the effective charge of the plasma (ZEFF). Then, the fuel ion density (DENI), impurity ion density (DNZ), and other mass and charge-averaged quantities are calculated. The plasma density limit can be chosen from either the Murakami (IDENL = 1) or Greenwald (IDENL = 2) limit. The beta limit is the Troyon limit if IBETAIN = 2 [see ref. 2, Eq. (27)], with the coefficient (DNBETA) being an input parameter. If IBETAIN = 1, a simplified scaling suggested by the CIT physics panel is used.

4.1.1.3 Fusion power

The fusion power is found by integrating over the plasma volume as described in ref. 1. Profile effects can be explicitly accounted for in the fusion power because the integration is performed for each iteration. The fusion cross sections are taken from ref. 7 for TI < 20 keV and from ref. 8 for TI > 20 keV. The fraction of the alpha power going to the electrons is taken from Eq. (3.12) in ref. 1. A simplified fit to the fast alpha beta fraction, which does not account for profile effects, is presently used.[9] The average neutron wall load

(WALLMW) is found by dividing the neutron power by the first-wall surface area (FWSUR).

4.1.1.4 Other power balance terms

The Bremsstrahlung radiation power calculation is an analytic integration over the plasma volume (including profile effects) and is equivalent to that described in ref. 1. No synchrotron radiation power is presently accounted for. The ohmic power term uses the average plasma temperature to calculate plasma resistivity and includes a neoclassical correction to the resistivity.[10] The ohmic heating (OH) term is negligible for all steady-state cases for which the code is presently constructed. The equilibration power between the bulk ions and electrons uses the same formulation as ref. 1, except that the volume-averaged temperatures are used in the expression, and the equation is analytically volume averaged to account for profile effects.

Transport power losses for ions and electrons are modeled as $1.5\ (N \times T)/\tau$, where N is the density, T is the density-weighted average temperature, and τ is an energy confinement time. For ions, the confinement is neoclassical, as formulated in ref. 2. The losses can be enhanced by increasing the input factor FIFAC. Also the ion confinement time can be forced to be equal to the electron confinement by setting TAUPRE = 2 Electron confinement can be chosen from a variety of scalings. For ISC = 1, Neo-Alcator scaling[11] is used; for ISC = 2, Mirnov scaling is used [Eq. (A.3) in ref. 1]; for ISC = 3, Kaye-Goldston L-mode scaling is used [Eq. (A.1) in ref. 1, with Hfac = 1]; for ISC = 4, ASDEX H-mode is used [Eq. (A.11) in ref. 1); and for ISC = 5, IAEA-ASDEX H-mode is used (ref. 11). The Kaye-Goldston confinement time is multiplied by the input factor FEFAC. Also, for the Kaye-Goldston confinement time, if IINVQD is set not equal to 0, the confinement time is combined with neoclassical scaling via inverse quadrature.

4.1.1.5 Volt-second requirements

Plasma volt-second requirements are calculated in subroutine VSBT. The requirements are broken into three parts: inductive, startup

losses, and flattop-burn losses. The inductive requirement has internal and external components as described in ref. 12, except that the normalized plasma internal inductance (RLI) is now an input. The external inductance comes from ref. 13. The startup resistive volt-second requirement is taken to be a fraction (GAMMA) of the internal inductive volt-second requirement. The default value for GAMMA is 0.5, which was determined through comparisons with WHIST calculations. For the volt-second requirements during burn (VSB = CSAWTH × loop voltage × burn time), the loop voltage is calculated using the plasma resistance, which is based on average plasma parameters and a neoclassical correction factor. The coefficient CSAWTH is input and can be used to enhance the burn requirement to mimic the effects of sawteeth activity. Comparison with 1.5-D WHIST calculations showed that CSAWTH should be 3 for CIT regime studies (refs. 12 and 14).

4.1.1.6 Auxiliary calculations

Some auxiliary calculations done by the physics module are for particle loss rates from the plasma. The convective particle loss rate is found using a particle confinement time (TAUP) = 5 times the effective energy confinement time (where the effective energy confinement time is the average for the ions and electrons). Also, an input recycling ratio (RECYCLE) is included in the particle loss rate where the particle loss rate = (1.0 - RECYCLE) × ion density × volume/TAUP. The fractional burnup is defined as the fusion burn rate over the convective particle loss rate. A maximum fractional burnup of 0.5 is set, and when this is exceeded, TAUP is lowered so that the specified maximum fractional burnup is met. The plasma volume (VOL) is found with the crescent-shaped model used in ref. 1. The average poloidal field (BP) is found using Ampere's law and using the poloidal path length around the plasma perimeter as described in ref. 1.

4.1.1.7 Constraint formulation

No iterations exist for solving equations internal to the physics module. However, several physics constraints should be included in the

set of equations satisfied by the equation solver or optimizer. An important one is the power balance relationship. The power balance can be solved as a global power balance equation [Eq. (4)] in which case the ion-to-electron temperature ratio (TRATIO) is specified on input. This equation requires the sum of the power source terms (fusion, current drive, and ohmic) to be DIGN times the loss terms (radiation and transport), where DIGN is the ignition margin. Separate power balance equations for the ions [Eq. (5)] and electrons [Eq. (6)] can be used, in which case TRATIO should be made a variable (see Sect. 3 for the method of including quantities to be iterated on). Other physics variables that can be iterated to satisfy the power balance equation(s) are electron temperature, electron density, ignition margin, the H-factor in Kaye-Goldston scaling, major radius, aspect ratio, and TF on axis.

The plasma beta (BETA) is held equal to the plasma pressure over the magnetic pressure in Eq. (3). The plasma pressure includes the thermal component (from electrons, fuel ions, alpha ash, and impurity ions) and energetic components from the fast alphas (BETAFT) and from the fast neutral beams ions (BETANB).

Another physics constraint is that the poloidal beta (BETAP) equals the toroidal beta (BETA) times (BT/BP) squared, where BT is the TF on axis and BP is the average poloidal field. This equation is necessary because several of the plasma current scalings depend on BETAP. When using this constraint, BETAP should be included as a variable for iteration.

Several inequality-type physics equations can be employed. The plasma beta (BETA) is held to FBETA times the beta limit (BETALIM) in Eq. (8), and the density (DENE) is held to FDENE times the density limit (DNELIMT) in Eq. (7). FBETA and FDENE can be bounded however desired. Also, the neutron wall load (WALLMW) is held to FWALLD times the input value WALALW. Restricting FWALLD to < 1 results in a maximum wall load condition, and restricting FWALLD to > 1 results in a minimum wall load condition.

4.1.2 Non-Inductive Current Drive Models

The models used in the TETRA code to calculate amps-per-watt conversion efficiencies for various non-inductive current drive schemes

are described in Sects. 4.1.2.1 through 4.1.2.7. These models are found in subroutine CURDRIV of the TETRA code. This subroutine is modular so that any of these models can be modified without affecting the others. Models of current drive schemes that are not presently included can be added easily.

As in all modules of the TETRA code, a balance has been struck here between the need for accuracy in the computations and the requirement that the models be simple enough for use in a systems code environment. References will be made in the following sections to areas where more work is required to develop systems-code-compatible adaptations of more detailed calculations, which can be installed in the TETRA code next year.

4.1.2.1 Neutral beam injection current drive

The conversion efficiency for current drive by neutral beam injection (NBI), η_{nb}, is calculated in a subroutine ETANB, which is called by CURDRIV. The modeling equations in ETANB are described in detail in refs. 1 and 15 through 19. The equation for the efficiency is

$$\eta_{nb} = \frac{f_d \; T_e \; J(x,y) \; F_{nb} \; [1 - \exp(-\tau_{nb})]}{R_o \; n_{e2o} \; \ln \Lambda} \; (A/W) \quad , \tag{4.1}$$

where f_d is a coefficient that calibrates this scaling formula to Fokker-Planck results (f_d = 2.65 is used at present), T_e is the electron temperature (keV), $J(x,y)$ is a function[15] of the beam energy ($x^2 = E_{beam}/E_{critical}$) and the plasma effective charge [$y = f(Z_{eff})$], F_{nb} is a degradation factor[17,18] to account for electron spin-up effects (F_{nb} = 0.76 is used at present), τ_{nb} is the effective optical depth for the beam ions[15] [i.e., the shine through fraction is $f_s = \exp(-\tau_{nb})$], R_o is the plasma major radius (m), n_{e20} is the electron density (10^{20} m^{-3}), and $\ln \Lambda$ is the Coulomb logarithm. For typical Tokamak Ignition/Burn Experimental Reactor II (TIBER II) parameters (T_e = 18-20 keV, n_{e20} = 1.0, R_o = 3.0 m), the efficiency is η_{nb} = 0.08 - 0.10 (A/W).

The required neutral beam power for current drive, P_{nb}, is calculated as $P_{nb} = I_{nb}/\eta_{nb}$ where I_{nb} is the current to be driven by the beams. At this writing, the models in the code assume that all of the neutral beam power is eventually transferred to the background plasma ions as the beam ions slow down. Models for calculating the partitioning of the beam power between background electrons and ions, which are described in refs. 1 and 19, will be adapted for use in the TETRA code next year. This partitioning is important for the power balance calculation (see Sect. 4.1.1) when solutions are computed for the electron and ion power balances separately.

4.1.2.2 Lower hybrid current drive

The scaling formula used in the TETRA code for calculating lower hybrid (LH) current drive efficiencies is a fit by Logan[20] to efficiencies calculated by Karney and Fisch[21]. For parallel indices of refraction, $N_{\parallel}$, of the LH waves in the range $1.5 \leq N_{\parallel} \leq 2.0$, the efficiency is approximated well by

$$\eta_{lh} = 0.36 \left[\frac{1 + \left(\frac{T_e}{25} \right)^{1.16}}{(R_o n_{e20})} \right] \quad (A/W) \quad , \tag{4.2}$$

where T_e, n_{e20}, and R_o have been defined previously. An option also exists in the code for using a scaling recommended for the INTOR studies,[22]

$$\eta_{lh}^{INTOR} = 0.3/(n_{e20} R_o) \quad (A/W) \quad . \tag{4.3}$$

Equation (4.2) tends to overestimate the efficiency at high T_e (>25 keV) because it does not include the effect of relativistic mass increase of the current-carrying electrons in the tail of the distribution as T_e increases. Equation (4.3) represents present experimental results but tends to give lower efficiencies than detailed theoretical calculations

for TIBER-like parameters. Neither formula takes into account trapped electron effects, which reduce the efficiency, nor do they take into account any LH wave power which may be launched in a direction opposite to the current. Detailed models for some of these effects (given in ref. 1) will soon be adapted for use in the TETRA code. Finally, the required LH power is calculated from $P_{lh} = I_{lh}/\eta_{lh}$, where I_{lh} is the lower hybrid driven current. The code models assume that all of this power eventually couples from the fast current-carrying electrons to the bulk plasma electrons.

4.1.2.3 Electron cyclotron resonance current drive

The efficiency of current drive by electron cyclotron resonance (ECR) waves is calculated in the TETRA code from the formula

$$\eta_{ecr} = 0.21\ T_e/(R_o n_{e20} \ell n\Lambda)\ (A/W) \quad . \tag{4.4}$$

This scaling reproduces the result by Karney and Fisch[21] for a narrow spectrum of cyclotron waves, fundamental frequency, in the non-relativistic limit, for a background plasma with $Z_{eff} = 1$ when the resonance parallel velocity of the current-carrying electrons is approximately 2.5 times the thermal velocity of the bulk electrons. Linear theory (see refs. 1, 23, 24) indicates that, for TIBER-like parameters ($T_e = 20$ keV, $R_o = 3.0$ m, $\omega_{pe}^2/\omega_{ce}^2 = 0.5$), the optical depth for ECR waves at the fundamental is in the range $100 \leq \tau \leq 500$ so that the resonance parallel velocity is in the range $2 \leq v_{\parallel} \leq 3$. For the systems code, we have chosen an intermediate value. Equation (4.4) does not include degradation of the efficiency due to electron trapping effects, relativistic detuning of the resonance, or the phenomenon of higher harmonic overlap[25] when ECR waves with high $N_{\parallel}$ (for efficient current drive) are injected into a plasma with high T_e (>10 keV). Models for some of these effects (see ref. 1) will be adapted for use in the TETRA code in the next year. Simple models for the harmonic overlap effect have yet to be developed. It should be stressed at this point that Eq. (4.4) should be used with caution in systems studies of configurations for which the electron temperature exceeds 10 keV (harmonic overlap effect) and/or the aspect ratio of the tokamak is less

than 4.0 (electron trapping effect). Finally, the ECR power is calculated from $P_{ecr} = I_{ecr}/\eta_{ecr}$ where I_{ecr} is the current to be driven by ECR waves. The model assumes that all of this power eventually couples to the bulk electrons.

4.1.2.4 Lower hybrid fast-wave current drive

The models for LH fast-wave current drive in the TETRA code have been formulated by Ehst.[26] The conversion efficiency formula is

$$\eta_{fw} = Z_c(0.034 + 0.196\beta_t)\, T_e^{0.77}/\,(R_o\, n_{e20})\ (A/W) \quad , \tag{4.5}$$

where

$$Z_c = 0.08\,[32/(5 + Z_{eff}) + 2 + Z_f] \tag{4.6}$$

and

$$Z_f = \frac{12(6 + Z_{eff})}{(5 + Z_{eff})\,(3 + Z_{eff})} + \frac{3.76}{Z_{eff}} \quad , \tag{4.7}$$

where Z_{eff} is the bulk plasma effective charge and β_t is the total beta. This parameterization was derived from a series of radio frequency (rf) current drive and MHD equilibria calculations. Linear Landau damping was assumed, and the effects of transit time magnetic pumping were not included. In addition, the parasitic damping of the fast waves by high-energy fusion alphas was not considered in obtaining Eq. (4.5).

4.1.2.5 Bootstrap current

Neoclassical bootstrap current effects are modeled in the TETRA code with a scaling formula that includes the dependence on poloidal beta, aspect ratio, and plasma effective charge. The bootstrap current is calculated as

$$I_{bs} = I_p\,(0.4)\,\beta_{p,th}\,\sqrt{\epsilon}\,(1 + 0.94/Z_{eff} + 0.43/Z_{eff}^2) \quad , \tag{4.8}$$

where I_p is the total toroidal current, $\beta_{p,th}$ is the thermal component of the poloidal beta, $\epsilon = a/R_o$ is the inverse aspect ratio, and Z_{eff} is the plasma effective charge. The total current that must be driven by

the current drive system(s) is $I_{cd} = I_p - I_{bs}$. Equation (4.8) was developed from a series of Fokker-Planck and power balance calculations[27] for TIBER-like conditions.

4.1.2.6 Combinations of current drive systems

For some configurations, it may be advantageous to use two or more current drive systems to drive the total current. For systems analysis, this requires that the partitioning of the required current for each system be calculated. At present, the only option implemented in the TETRA code is a combination of NBI and LH current drive with $I_{nb} = f\, I_{lh}$. The value $f = 1.13$ corresponds roughly to the results of more detailed calculations for TIBER-like conditions (see ref. 1). Simplified calculations of this partitioning have been adapted from the detailed calculations in ref. 1 and are in the process of being added to the TETRA code.

4.1.2.7 Summary

At present, simplified models of current drive by NBI, LH slow and fast waves, and ECR are available in the TETRA code. LH slow waves and NBI current drive may be combined in a rudimentary way. Simplified models of more detailed calculations for each current drive method are under development and will be included in the systems code as soon as they are available.

Limitations on the parameter ranges over which the models are valid vary from one current drive method to another. The NBI model is valid except in cases with very high plasma density ($n_e \geq 4 \times 10^{20}$ m^{-3}) or low beam energy ($E_{beam} \leq 200$ keV) for which a more detailed penetration calculation is required to ensure that the beams reach the core of the plasma. The LH model is valid if the bulk electron temperature in the region of LH wave propagation satisfies $T_e \leq 15$ keV. At higher temperatures, the model overestimates the current drive efficiency. The ECR model is valid only for low-temperature ($T_e < 10$ keV) plasmas in devices with large aspect ratio ($R_o/a > 4$). Electron trapping effects and the phenomenon of higher harmonic overlap must be included in the

model to remove these limitations. Finally, the LH fast-wave model is valid only for the outer radial regions of the plasma, where alpha particle damping of the waves will not be important. Work continues to develop algorithms that extend the ranges of validity for each of these models.

4.1.3 Poloidal Magnetics

The poloidal magnetics subroutine computes coil currents at the beginning of pulse (BOP) and end of flattop (EOF) for the coil configuration determined in the poloidal field (PF) coil subroutine PFCOIL. Input includes data defining a reference PF system and the PF system of a design point. The output array contains the PF coil currents, where those currents designated as variables are scaled from the reference point to the design point. The data defining the reference point consist of the geometry (major and minor radius), plasma pressure and profile parameters (poloidal beta, internal inductance), and PF system (number of coils, coil coordinates, and coil currents) associated with a free-boundary MHD equilibrium solution at EOF. The input data describing the design point are similar, with the addition of arrays giving the coordinates and currents of coils designated as fixed current and arrays describing the coordinates and group numbers of coils designated as variable current, where coils in the same group carry the same current.

The scaling procedure is based on the Shafranov formula (ref. 28) for the external vertical field of a large-aspect-ratio plasma, and it scales the reference equilibrium vertical field along the plasma midplane to that of the design point. Coil currents at the design point are obtained by approximating this scaled vertical field with the field of the PF coil currents associated with the design point. More specifically, the scaling procedure may be summarized as follows:

1. compute the reference external field along the midplane of the reference point;

2. scale this external field to the adjusted design point by the ratio of the Shafranov vertical field at the design point to that of the reference point; and

3. determine the coil currents approximating the scaled external field by solving a least-squares problem.

As an example, for 5-25% changes in plasma parameters between a systems code final design point and the reference point, an equilibrium based on the scaled coil currents varied by <1% in major and minor radius with the major and minor radius of the final design point given by the systems code.

4.1.4 Inductance/Flux Linkage Module

The inductance/flux linkage routines calculate the mutual and self-inductances of the PF coils, OH coil, and plasma. These inductances are used in the stored energy, pulsed power requirement, and volt-second calculations. Inputs to the routines are the coil locations and sizes, number of turns per coil, and the coil currents.

The primary calculation is for the mutual inductance matrix SXLG(i,j), which is the mutual inductance (H) between coils i and j times the number of turns in coil i and in coil j. When i = j, this is a self-inductance. This is performed by subroutine INDUCT and uses the same method as in the original tokamak systems code (ref. 29), which is borrowed from ref. 30. This procedure approximates the coils as a system of rectangular cross-sectioned, coaxial solenoids. The inner and outer radii of each coil [RA(i) and RB(i) in m] and the upper and lower height [ZH(i) and ZL(i) in m] are input, as is the number of turns per coil [TURNS(i)]. All inputs are evaluated in the PF coil subroutine.

The volt-second capability of the PF coil system (i.e., the flux linkage between the coils and the plasma) is evaluated in subroutine VSEC. The volt-seconds linked to the plasma from each PF coil are equal to cpt(i,EOR) - cpt(i,BOP) * sxlg(plasma,i), where cpt(i,EOR) is the current (A) per turn of coil i at the end of flattop and cpt(i,BOP) is the corresponding quantity at the BOP. The CPT arrays are calculated in the PF coil subroutine. The sum of contributions from all coils to the PF system volt-second capability is stored as VSSTT. Setting VSEF = 0 in the input file results in inclusion of only the OH coil volt-second contribution in VSSTT.

4.1.5 Divertor Magnetics Module

The divertor magnetics module, DIVMAG, interfaces between the PF coil module and the (magnetic divertor) particle control system module. A double-null (top and bottom) PF divertor configuration is assumed for the TIBER II reference design and modeled with the ORNL magnetics code NEQ (refs. 31 and 32) using as input the reference configuration designated K69B (ref. 33). In addition to modifications to NEQ made by R. Bulmer, a number of LANL modifications, derived from the ATR/ST study (ref. 34), have been incorporated into NEQ. These latter modifications model the divertor magnetics, including calculations of flux surfaces outside the plasma boundary, connection lengths along flux surfaces between the watershed (i.e., plasma equatorial plane, $z = 0.0$ m) and the nominal divertor "plate" (at various locations), flux-tube expension factors, angle of incidence of the flux tube at the plate, and strike-point coordinates (R_s, z_s) at the plate. This divertor-magnetics information is used by the particle control system module.

The reference TIBER II configuration assumes a plasma with major radius $R = 3.0$ m, minor radius $a = 0.83$ m, elongation $\kappa = 2.4$, and triangularity $\delta = 0.406$; the magnetic null coordinates for this configuration are $R_x = 2.352$ m and $z_x = \pm 2.365$ m. The reference scrapeoff thicknesses are $\Delta_{sci} = 0.06$ m for the inboard and $\Delta_{sco} = 0.12$ m for the outboard. The nominal plasma surface areas are $A_{pi} = 61.5$ m^2 and $A_{po} = 108.8$ m^2 for the inboard and outboard, respectively, for a total plasma surface area $A_p = 170.3$ m^2. The reference TIBER II divertor-magnetics configuration as calculated by NEQ is illustrated in Fig. 4.1. The open flux surfaces (dashed lines, inboard and outboard) are shown extending to the "plate" located at $R = 2.0$ m and $z = \pm 2.75$ m, and representative internal closed flux surfaces (solid lines) are also shown. PF coil positions are indicated by the squares with areas proportional to the coil currents.

Figure 4.2 illustrates the upper divertor flux plumes of the same configuration; a magnified scale is used to enhance the details. The

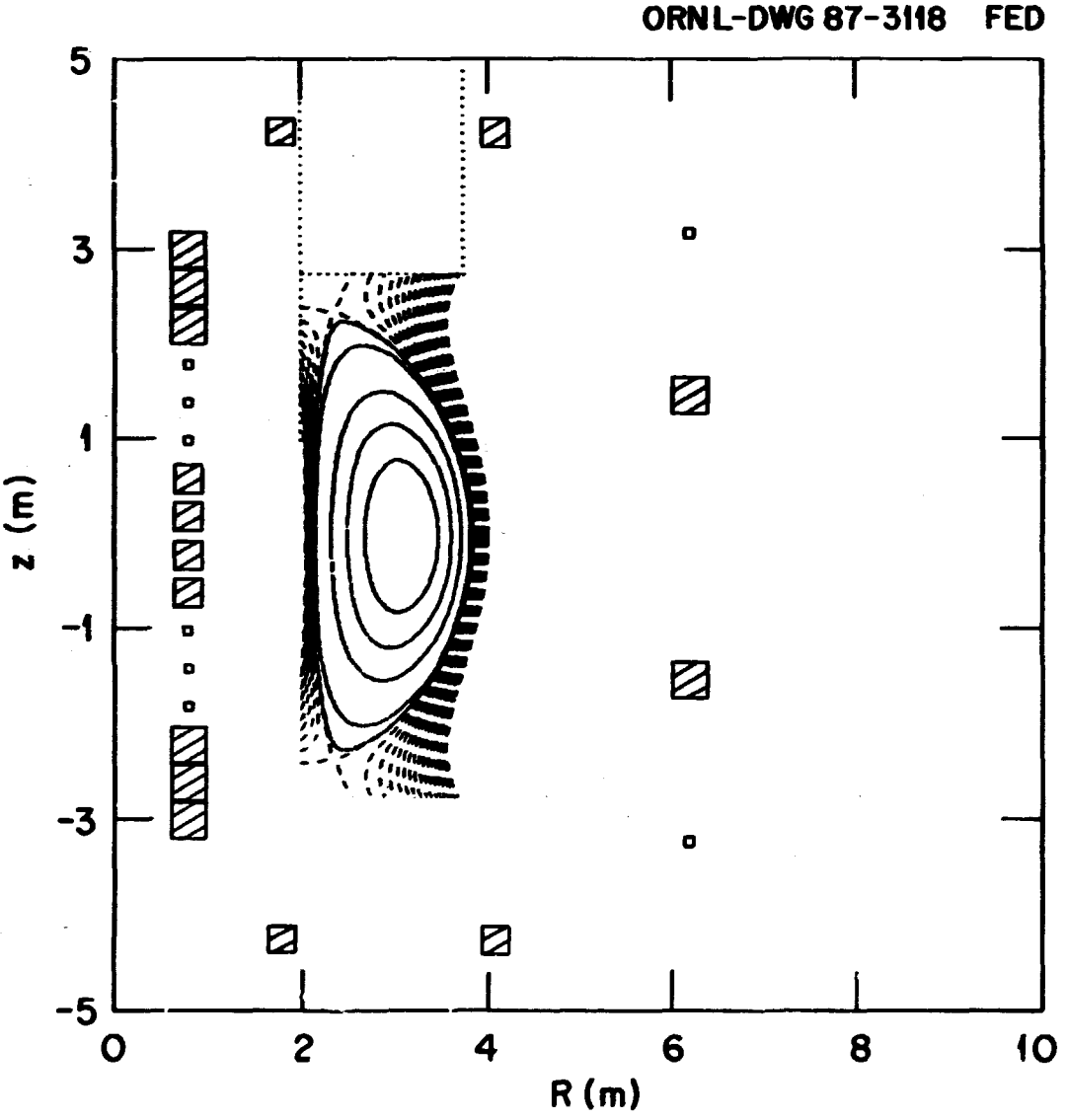

Fig. 4.1. Reference TIBER II poloidal field divertor magnetics configuration (K69B) illustrating closed internal flux surfaces (solid lines) and open external flux surfaces (dashed lines) leading to an idealized divertor "plate" at $R = 2.0$ m and $z = \pm 2.75$ m (dotted lines). Poloidal field coils are shown as squares. Plasma major radius $R_0 = 3.0$ m, minor radius $a = 0.83$ m, vertical elongation $\kappa = 2.4$, and triangularity $\delta = 0.406$.

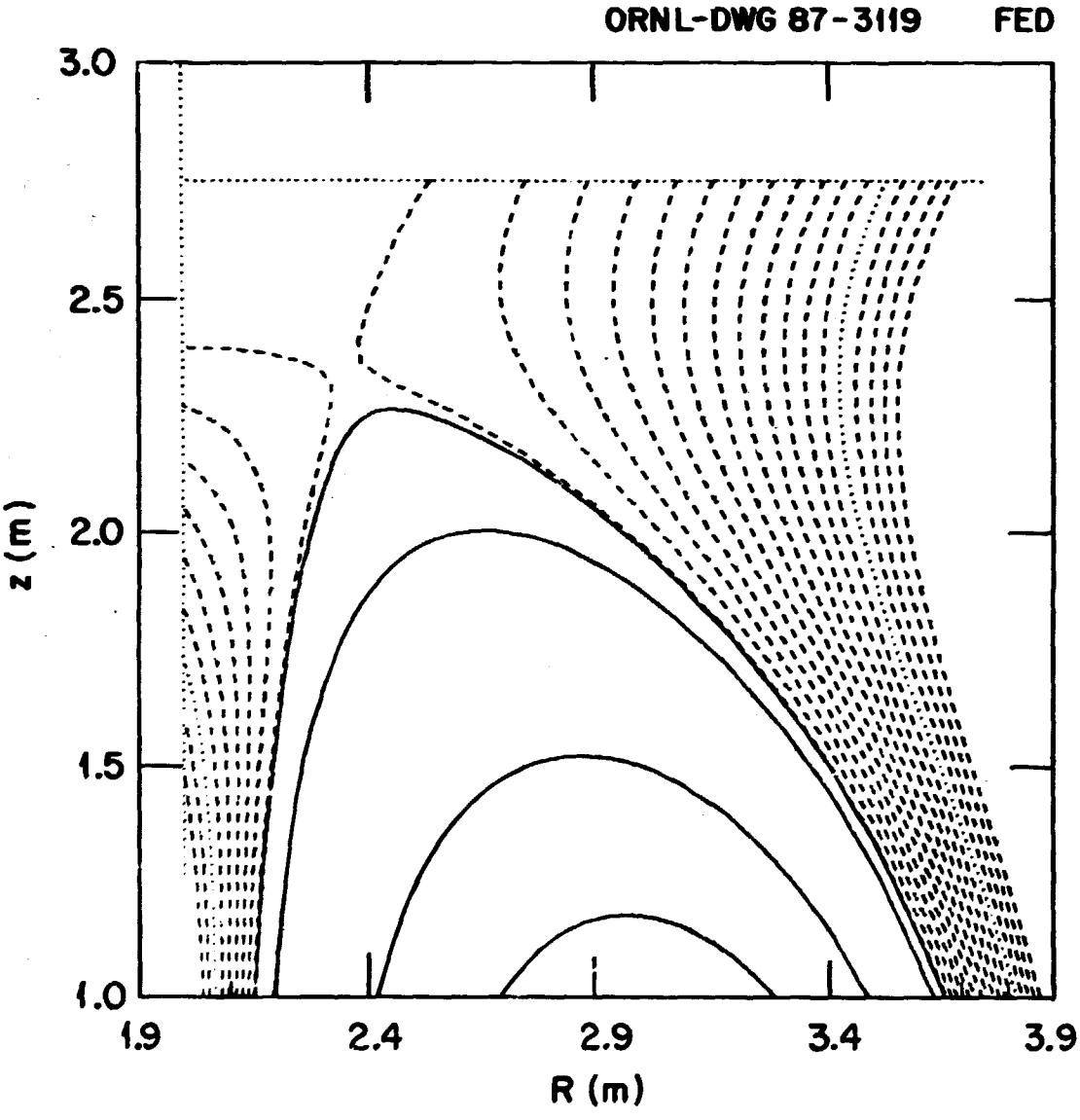

Fig. 4.2. Expanded view of TIBER II poloidal field divertor magnetics configuration (K69B). Flux surfaces (dashed lines) are spaced at R = 0.01 m intervals at the equatorial plane (z = 0.0 m). The nominal boundaries of the inboard scrapeoff at Δ_{sci} = 0.06 m and outboard scrapeoff Δ_{sco} = 0.12 m are denoted by the dotted lines. An idealized divertor "plate" (dotted lines) at R = 2.0 m and z = ±2.75 m is shown.

calculated flux surfaces are launched from the watershed (z = 0.0 m), spaced at intervals of ΔR = 0.01 m from the inboard and outboard plasma surfaces ($R = R_o \pm a$), and they cover a maximum Δ_i = 0.08 m and Δ_o = 0.16 m on the inboard and outboard sides, respectively. The reference TIBER II scrapeoff thicknesses (Δ_{sci} = 0.06 m and Δ_{sco} = 0.12 m) are denoted by dotted lines in Fig. 4.2. By redefining the idealized "plate" locations, a computational grid is obtained onto which the reference divertor plate geometry (R,z) can be mapped. Interpolation and scaling relationships for the several divertor magnetics parameters are under development. Typically, the divertor plate is positioned so as to ameliorate the local heat-flux peaking or sputtering as well as for thermohydraulic and maintenance considerations. This plate may be located by using DIVMAG results, but a reference TIBER II divertor plate design is being produced as part of the TIBER II design effort; however, a plate geometry consistent with the K69B magnetics configuration is not yet available (ref. 35). The grid for DIVMAG results is summarized in Table 4.1.

4.1.6 References for Section 4.1

1. M. E. Fenstermacher, MUMAK--A Computer Code for Modeling Plasma Power Balance and Current Drive in Tokamaks, UCID-21038, Lawrence Livermore National Laboratory, April 1987.

2. N. Uckan and J. Sheffield, A Simple Procedure for Establishing Ignition Conditions in Tokamaks, ORNL/TM-9722, Oak Ridge National Laboratory, 1985.

3. M. Peng and D. Strickler, Nucl. Fusion **26**, 769 (1986).

4. J. Miller and D. Strickler, System Code Scaling of Plasma Current, FEDC-M-85-PE-002, Oak Ridge National Laboratory, 1985.

5. T. N. Todd, in 2nd European Tokamak Programme Workshop (Proc. Workshop Saulx-les-Chartreux), 1983.

6. D. Strickler, Mean Field Safety Factor, FEDC-M-87-PE-027, Oak Ridge National Laboratory, 1987.

7. N. Jarmie, R. E. Brown, and R. A. Hardekopf, Phys. Rev. C **29(6)**, 2031 (1984); and Phys. Rev. C **33(1)**, 385 (1986) erratum.

8. L. Hively, Nucl. Fusion **17**, 873 (1977).

Table 4.1. DIVMAG scaling database from NEQ results[a]

Plasma edge (m)	Connection length, L (m)	Expansion factor	Incidence angle (rad)	Coordinates (R_s, z_s) (m)
Outboard, $+\Delta_o$				
~0.0	95.75	14.99	0.610	2.544, 2.750
0.02	24.76	8.15	0.430	2.890, 2.750
0.04	19.08	5.96	0.433	3.087, 2.750
0.06	16.46	4.84	0.445	3.232, 2.750
0.08	14.87	4.14	0.466	3.351, 2.750
0.10	13.77	3.66	0.47	3.452, 2.750
0.12[b]	12.95	3.30	0.490	3.541, 2.750
0.14	12.31	3.03	0.496	3.620, 2.750
0.16	11.79	2.81	0.505	3.693, 2.750
Inboard, $-\Delta_i$				
~0.0	86.19	12.80	0.046	2.000, 2.391
0.02	20.77	8.42	0.585	2.000, 2.151
0.04	13.48	5.22	1.034	2.000, 1.938
0.06[b]	10.06	3.37	1.238	2.000, 1.719
0.08	7.01	2.27	1.408	2.000, 1.468

[a]Refer to Fig. 4.2 for the geometry of the K69B magnetics configuration.

[b]Reference TIBER II scrapeoff thickness, Δ_{sc}.

9. N. Uckan, private communication (July 1987).

10. S. Hirshman, R. J. Hawryluk, and B. Birge, Nucl. Fusion **17**, 611 (1977).

11. International Tokamak Reactor, Phase Two A, Part II Report, STI/PUB/714, ISBN 92-0-131086-2, International Atomic Energy Agency, Vienna, 1986.

12. J. Galambos et al., System Studies of Compact Ignition Tokamaks, ORNL/FEDC-86/5, Oak Ridge National Laboratory, 1987.

13. S. Hirshman and G. H. Nielson, Phys. Fluids **29**, 790 (1986).

14. W. Houlberg, "Volt-Second Consumption in Tokamaks with Saw-Tooth Activity," accepted for publication in Nuclear Fusion (1987).

15. D. R. Mikkelsen and C. D. Singer, Nucl. Tech./Fusion 4, 237 (1983).

16. R. S. Devoto, Neutral-Beam Current Drive in Tokamaks, UCRL-95799, Lawrence Livermore National Laboratory, October 1986.

17. D. F. H. Start, J. G. Cordey, and E. M. Jones, Plasma Phys. 22, 303 (1980).

18. D. F. H. Start and J. G. Cordey, Phys. Fluids 23, 1477 (1980).

19. J. D. Gaffey, J. Plasma Phys. 16, 149 (1979).

20. C. D. Henning, B. G. Logan, et al., TIBER--Tokamak Ignition/Burn Experimental Research, Final Design Report, UCID-20589, Lawrence Livermore National Laboratory, November 1985.

21. C. F. F. Karney and N. J. Fisch, Phys. Fluids 28, 116 (1985).

22. International Tokamak Reactor--Phase Two A, Part 1, ISBN 92-0-131283-0, International Atomic Energy Agency, 1983.

23. K. I. Thomassen, Ed., Free-Electron Laser Experiments in Alcator C, LLL-PROP-00202, Lawrence Livermore National Laboratory, July 1986.

24. M. Bornatici et al., Nucl. Fusion 23, 1153 (1983).

25. G. R. Smith, R. H. Cohen, and T. K. Mau, Harmonic Overlap in Electron-Cyclotron Current Drive at High T_e, UCRL-96364 preprint, Lawrence Livermore National Laboratory, March 1987 (to be published in Physics of Fluids).

26. D. Ehst, TIBER-II, Tokamak Ignition/Burn Experimental Reactor, 1986 Status Report--Appendix C, UCID-20863, C. D. Henning and B. G. Logan, Eds., Lawrence Livermore National Laboratory, October 1986.

27. R. S. Devoto, M. E. Fenstermacher, and A. A. Mirin, "Studies of Neutral-Beam Current Drive," presented at the Sherwood Theory Meeting, San Diego, 1987 (to be submitted to Nuclear Fusion).

28. V. S. Mukovatov and V. D. Shafranov, "Plasma Equilibrium in a Tokamak," Nucl. Fusion 11, 605 (1971).

29. L. Reid, The Tokamak Systems Code, FEDC/ORNL-84-9, Oak Ridge National Laboratory, 1984.

30. M. W. Garret, An Elliptic Integral Computer Package for Magnetic Fields, Forces and Mutual Inductances of Axisymmetric Systems, ORNL-3575, Oak Ridge National Laboratory, 1965.

31. J. D. Callen and R. A. Dory, "Magnetohydrodynamic Equilibria in Sharply Curved Axisymmetric Devices," Phys. Fluids 15, 1523 (August 1972).

32. D. J. Strickler, J. B. Miller, K. E. Rothe, and Y-K. M. Peng, Equilibrium Modeling of the TFCX Poloidal Field Coil System, ORNL/FEDC-83/10, Oak Ridge National Laboratory, April 1984.

33. R. H. Bulmer, Lawrence Livermore National Laboratory, personal communication (June 1987).

34. R. L. Miller, R. A. Krakowski, C. G. Bathke, C. Copenhaver, A. Englehardt, T. J. Seed, R. M. Zubrin, and N. M. Schnurr, Advanced Tokamak Reactors Based on the Spherical Torus (ATR/ST): Preliminary Design Considerations, LA-10740-MS, Los Alamos National Laboratory, June 1986.

35. W. Barr, Lawrence Livermore National Laboratory, and J. Haines, Oak Ridge National Laboratory/Fusion Engineering Design Center, personal communications (July 1987).

4.2 MECHANICAL SYSTEMS

This section contains summaries for the following modules. Lead authors and affiliations are indicated.

Module	Lead Author	Organization
Torus configuration	J. D. Galambos	FEDC/ORNL
Torus vacuum system	J. R. Haines	FEDC/McDonnell Douglas
Fueling systems	S. K. Ho	LLNL
Torus support structure	L. J. Perkins	LLNL
Bucking cylinder	J. D. Galambos	FEDC/ORNL

4.2.1 Torus Configuration Module

The torus subroutine calculates the shield, blanket, and first-wall volumes and areas. The shields are modeled using rectangular cross sections and are situated between the TF coil and the plasma. The models are taken from ref. 1 (i.e., ITORUS = option 2 in the old tokamak systems code), except that the option to include a lead shield external

to the TF coil is no longer included. Reference 1 contains a more detailed description of the modeling algorithms.

Input includes radial build dimensions on midplane and plasma elongacion. The vertical legs of the shield and blanket are of constant thicknesses and are set equal to the midplane values. The top and bottom thicknesses are set equal to the outboard leg thickness. The volumes of the shield and blanket are calculated by rotating the rectangular cross-sectioned shape through 2π degrees in the toroidal direction (toroidal symmetry is assumed). The weight of the shield is calculated using steel, unless ioptsh = 1, in which case the inner leg is composed of tungsten. The first-wall surface area calculation uses an elliptical poloidal cross section of minor radius = (plasma minor radius + scrapeoff length) and major radius = (plasma height + scrapeoff length), where an average scrapeoff length is used. This poloidal path length is multiplied by 2(π) × the plasma major radius. This surface area is used in calculating the average neutron wall loading.

Several additional areas and volumes are calculated for use in the old shielding routines, which are also included. It is possible to use the old shielding routines by setting ITIBER not equal to 1. These routines (POWFLX and FWALL) are described in detail in ref. 1, but they do not provide all the information that the new first-wall, blanket, and shield module provides.

4.2.2 Torus Vacuum Module

The torus vacuum module of the systems code attempts to define vacuum pumping requirements, determine component sizes, and estimate the subsystem cost. The major components that are modeled are shown schematically in Fig. 4.3. These components include large vacuum pumping ducts leading from the torus to the high-vacuum pumps, nuclear shielding for the ducts, large torus isolation valves, high-vacuum pumps, and roughing/backing pumps.

Vacuum pumping requirements are determined for (1) initial pumpdown, (2) pumpdown between burns, (3) helium ash removal, and (4) removal of deuterium-tritium (D-T) that is exhausted through the divertor chamber. The initial pumpdown assessment assumes that the outgassing from internal surfaces limits the base pressure. Values for

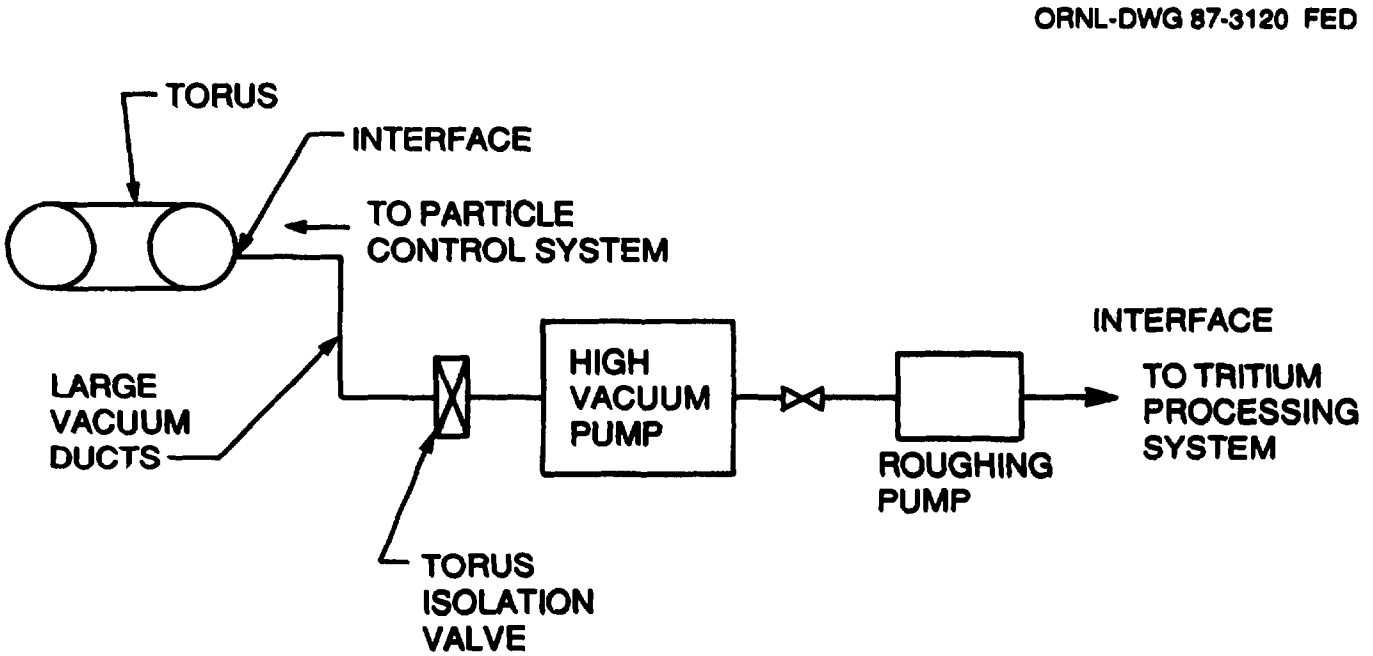

Fig. 4.3. Schematic of torus vacuum pumping system.

plasma chamber outgassing rate per unit area and major and minor radii of the plasma chamber are needed for this evaluation. The area for outgassing is estimated to be a factor of 5 greater than the first-wall area to account for other exposed surfaces.

Plasma density, pressure required in the torus before initiating a burn, and dwell time between consecutive burns are used to determine the pumping requirements for pumpdown between burns. The pressure in the chamber immediately following a burn is estimated to be equal to the pressure of neutral D-T molecules at a temperature of 300 K and a density equal to the plasma density.

Helium ash must be removed at a rate equal to its formation by fusion of deuterium and tritium. The neutral gas pressure at the divertor chamber exit is used as input to determine the required net helium pumping speed. The net pumping speed required for removal of D-T at the fueling rate by pellets, gas puffing, NBI, etc., minus the burn-up rate is also determined based on the pressure at the divertor chamber exit.

By considering each of these four requirements, the maximum pumping speed (Snet) that must be provided by the vacuum system is determined. Vacuum pumping ducts are assumed to be placed between each pair of TF coils. Results of a study performed with this code show that a minimum system cost occurs when the duct conductance (C) is given by

$$C = 1.5\ (Snet) \quad . \tag{4.9}$$

Because the net pumping speed is

$$Snet = 1/(1/C + 1/Sp) \quad , \tag{4.10}$$

where Sp is the speed of the high-vacuum pumps, the value of Sp must be

$$Sp = 3\ (Snet) \quad . \tag{4.11}$$

The ducts are assumed to consist of three segments with two 90° bends. The duct area required to obtain the value of C specified above is determined. If this area is less than the area between adjacent TF coils, the code proceeds. However, if the space between TF coils is inadequate, the requirement for the conductance (C) specified by Eq. (4.9) is relaxed. The conductance is reduced incrementally until either the duct area is able to fit between TF coils or the conductance

becomes close to Snet, which implies that infinite pumping speed is provided. If this latter condition occurs, the code provides two options. The first is to print a warning statement in the output and proceed through the remainder of the systems code. The second option causes the entire code to iterate with a larger device until the duct is able to fit.

4.2.3 Fueling Systems

The purpose of the fueling module is to calculate the fueling requirements and the design parameters of the fueling system. After implementing results from the physics module and the user's choice of the fueling scheme and desired deposition point, the module provides a set of fueling parameters that satisfies the requirement for sustaining a constant fuel in the plasma for a steady-state operation.

Two different approaches to plasma fueling are employed in this module, namely, the pellet injection and compact toroid (CT) plasma injection schemes. For the pellet fueling scheme, there are several alternatives, including the operational and conceptual methods described below. A neutral shielding ablation model[2,3] is used to describe the pellet ablation in the plasma. The effect of fusion alphas is neglected because, as suggested by a recent work,[4] the alphas contribute to a very small extent (<5%) in the ablation process. The CT injection scheme is based on a recent study by Perkins, Ho, and Hammer.[5] Their promising results have caused this novel technique to be considered as the baseline fueling scheme for the TIBER ETR.[6,7]

Input and output variables for the fueling module are as follows:

Input	Source	Description
r0	Physics	Plasma major radius (m)
ra	Physics	Plasma minor radius (m)
rkappa	Physics	Plasma elongation
alpn	Physics	Density profile exponent
alpt	Physics	Temperature profile exponent
dene0	Physics	Peak electron density (m^3)
te0	Physics	Peak electron temperature (keV)
fconv	Physics	Convective loss current (A)
fburn	Physics	Fusion burn current (A)
fbeam	Physics	Neutral beam injection current (A)
ftritbm	User Input	Fraction of the neutral beam that is tritium

fractn	User Input	Ratio of number of particles in pellet to total number of particles in plasma [typical range: 0.1 to 0.5]
dpreq	User Input	Required fuel penetration depth (m) [typical range: ra/3 to ra/2]
itype	User Input	Type of injector chosen: 1. Compact toroid plasma gun 2. Pneumatic gun 3. Centrifugal injector 4. Railgun 5. Electron beam rocket 6. Theta-pinch accelerator 7. Laser-vapor-jet injector 0. Injector selected by the module
nout2	User Input	Unit specifier for output
iprnt	User Input	Switch for output (0 = no, 1 = yes)
Output		Description
rp0		Pellet/CT radius (m)
pmass		Pellet/CT mass (kg)
fmixd2		Fraction of D_2 in the pellet/CT mixture
fmixt2		Fraction of T_2 in the pellet/CT mixture
reprate		Required repetition rate (1/s)
vpinj		Required pellet/CT injection speed to achieve the desired penetration depth (m/s)
dlaunch		Required launch length (m)
gasld		Gas load inside the torus (kg/s)
nport		No. of injector ports
power		Estimated required power for the system (W)
cost		Estimated cost of the fueling system ($)

The required fueling current is calculated from the convective loss, fusion burn, and NBI currents obtained from the physics module. Then, the mass content and the fuel mix composition of the pellet or injected CT can be determined, as can the required repetition rate to maintain the fuel particle balance. The fueling content of a single injection is controlled by the user input parameter "fractn" such that the total number of particles in a pellet is fractn times that in the

plasma. This value must be small to avoid a large density perturbation and pulsing of the fusion power generated; fractn is usually taken to be 0.1. Note that the pellet and CT injected in the two alternative approaches will have the same particle contents but very different size. Typical sizes for the pellet and CT are several millimeters and tenths of centimeters, respectively.

The most restrictive requirement for fueling in reactor-grade plasmas is the necessity to achieve very high injection velocity to accomplish the desired penetration. For pellet fueling, we use the ablation scaling law from the neutral shielding model[2,3] and integrate over the radial profiles to calculate the required injection velocity. For the CT injection fueling, the required injection velocity is projected from the results of ref. 5.

The user may select a fuel injection scheme or let the module select an appropriate one. The scheme chosen must be able to meet the injection velocity requirement. Also, a scheme with lower cost, less power consumption, and fewer technological restrictions is preferred. In the input description, we have ranked the various schemes in order of decreasing preference. The CT injection scheme is ranked first because of its likelihood for achieving the injection velocity needed to penetrate well into the plasma.

In addition to the fuel injection physics, the module also provides supplementary information on other technological aspects of the fueling system. We assume that the injector has only one port. The calculation of the gas load inside the torus resulting from the fueling injection is based on an estimation by G. Gorker.[8] The launch length for pellet injection is computed from the criterion that the maximum allowable pressure exerted on the pellet must be less than 3 MPa to avoid fracture.[9] Because no sufficient data exist for the power efficiency for the various schemes, a 15% efficiency is assumed for all schemes; 30% additional power is added for the auxiliary systems. A very rough estimate of the cost of the fueling systems is also included for reference.

4.2.4 Torus Structure and Support

This module calculates the mass and cost of the torus support structure, consisting of the outer PF coil support fence, the center post, the intercoil support between the TF coils to react the overturning moments, the cold island support, and the warm mass (shield and divertor) support structure.

It was originally intended that this module would be comprised of scaling laws obtained from parameterizing the formalism employed for the TIBER II structural analysis. Unfortunately, as of the date of this publication, the latter analysis was still not completed and, because of the complexity of this subject, general scaling laws cannot be ascertained at this time. Accordingly, this module is composed of rather simple scaling equations that scale support masses in terms of zeroth-order quantities such as component masses, major dimensions, PF currents (via plasma currents), etc.; these equations are normalized to the baseline TIBER II design (ref. 7). Costs are now obtained by applying multiplicative $/kg coefficients to the computed structural masses.

The inputs to this module are shown in Table 4.2. The corresponding computed variables for output use are shown in Table 4.3. Table 4.4 shows a typical output listing from the module based on the torus parameters for the 3-m major radius, 10-MA, TIBER II ETR (ref. 7).

The following major calculations are performed by this module. All quantities are in base SI units. The definitions of variables used below are given in Tables 4.2 and 4.3:

1. Mass of outer PF coil fence
   FNCMASS = $(5.94 \times 10^{-11}) \times AI \times AI \times RO \times AKAPPA \times A$

2. Mass of center post (this is NOT a bucking post but rather a center mandrel for location of the OH coil stack--the centering load is assumed to be taken by the OH stack alone as in the TIBER design)
   POSTMASS = $4.56 \times TRANHT \times (0.1 \times TRANBORE - 0.0025) \times RHOSTEEL$,
   where RHOSTEEL = steel density (set at 8.03×10^3 kg/m^3)

Table 4.2. Input variables for the torus structure and support module

Variable	Source	Description
ai	Physics	Plasma current (maximum design value) (A)
r0	Physics	Major radius (m)
a	Physics	Minor radius (m)
akappa	Physics	Elongation
b0	Physics	Axial B-field (T)
shldmass	Shield	Total mass of shield (kg)
dvtrmass	Impurity control	Total mass of divertor and associated structure (kg)
pfmass	PF magnets	Total mass of PF coils plus cases (kg)
tfmass	TF magnets	Total mass of TF coils plus cases (kg)
tranht	Magnets	Height of central PF stack (m)
tranbore	Magnets	Inner bore radius of central PF stack (m)
strucost	User input	Structure unit cost--materials and fabrication ($/kg) (if strucost = 0, default = 28 $/kg is used)
nout	Main	Logical unit number for output print file
iprint	Main	Instruction to print results: 0/1 = no/yes

Table 4.3. Output variables for the torus structure and support module

Component	Variable	
	Mass (kg)	Cost ($)
PF coil support fence	fncmass	fnccost
Center post	postmass	postcost
Intercoil support	aintmass	aintcost
Cold island support plus struts	cislmass	cislcost
Total cold support structure	coldmass	coldcost
Warm support structure	warmmass	warmcost
Total torus support structure	sprtmass	sprtcost

Table 4.4. Sample output file for the structural support for the 10-MA, 3-m TIBER ETR

Component	Variable	
	Mass (kg)	Cost[a] ($)
Outer PF coil fence	fncmass = 7.499×10^4	fnccost = 2.100×10^6
Center post	postmass = 1.347×10^4	postcost = 3.773×10^5
Intercoil support	aintmass = 2.498×10^5	aintcost = 6.995×10^6
Cold island support plus struts	cislmass = 9.040×10^4	cislcost = 2.531×10^6
Total cold support structure	coldmass = 4.287×10^5	coldcost = 1.200×10^6
Warm support structure	warmmass = 1.651×10^5	warmcost = 4.623×10^6
Total torus support structure (warm and cold)	sprtmass = 5.938×10^5	sprtcost = 1.663×10^7

[a]Structure unit cost = $28/kg.

3. Mass of intercoil support between TF coils to react overturning moments

   AINTMASS = $(5.17 \times 10^{-4}) \times$ AI $\times$ BO $\times$ RO $\times$ A $\times$ AKAPPA

4. Mass of cold island support [i.e., support structure for cold torus components (TF, PF coils, center post, PF fence, intercoil support)]

   CISLMASS = $(5.15 \times 10^{-2}) \times$ (PFMASS + TFMASS + FNCMASS + AINTMASS)

5. Mass of shield support structure

   SHSPMASS = 0.1 $\times$ SHLDMASS

6. Mass of warm support struts

   STRTMASS = 0.00145 $\times$ (SHLDMASS + SHSPMASS + DVTRMASS)

7. Total mass of cold support structure

   COLDMASS = FNCMASS + POSTMASS + AINTMASS + CISLMASS

8. Total mass of warm support structure

   WARMMASS = SHSPMASS + STRTMASS

9. Total mass of torus support structure

   SPRTMASS = COLDMASS + WARMMASS

10. Costs of individual support structures are given by mass $\times$ unit cost. Current default unit costs are shown in Table 4.2.

4.2.5 Bucking Cylinder

The bucking cylinder subroutine provides an option for including a bucking cylinder between the OH coil and TF coil to take the TF coil centering load. If the bucking cylinder thickness (BCYLTH) is 0, the subroutine returns without performing any calculations. Input to this module includes the bucking cylinder thickness, the OH solenoid outer radius where the outer radius = BORESOL + SOLTX where BORESOL is the radius of the solenoid and SOLTX is the thickness of the solenoid, the gap between the OH solenoid and the TF coil (GAPBOH), the height of the straight section of the inboard TF coil leg (HR1), centering force per TF coil (CFORCE), number of TF coils (TFNO), and the Young's modulus of the bucking cylinder (EBUCK, in Pa). Output includes the bearing pressure, buckling pressure, critical buckling pressure, and bucking cylinder weight.

The equations used for the bearing and buckling stresses are taken from ref. 1. The buckling pressure is the total centering force averaged over the outer surface area of the bucking cylinder. The critical buckling stress is calculated using formulas for an open (no end caps) cylinder. The routine provides an option for modeling solid bucking cylinders, but the option is presently commented out. The bearing pressure is the maximum hoop stress at the inner surface.

The two stresses calculated here are used in two global constraint equations (see Sect. 3). The bearing stress is used in Eq. (12) of Table 3.1 and is compared to an input for the allowable bearing stress (YSBUCK) (in Pa). Bounding FBCBR (variable 23) to be <1 ensures that the bearing stress is less than the allowable stress. The buckling pressure is compared to the critical buckling pressure in Eq. (11) of Table 3.1. Bounding FBCBKL (variable 32) to be ≤1 ensures that the buckling pressure is less than the critical buckling pressure.

4.2.6 References for Section 4.2

1. L. Reid et al., The Tokamak Systems Code, ORNL-FEDC-84/9, Oak Ridge National Laboratory, 1984.

2. P. B. Parks and R. J. Turnbull, Phys. Fluids 21, 1735 (1978).

3. S. L. Milora and C. A. Foster, IEEE Trans. Plasma Sci. 6, 578 (1978).

4. S. K. Ho and L. J. Perkins, Pellet Ablation Modeling in Reactor-Grade Plasmas, Lawrence Livermore National Laboratory (to be published).

5. L. J. Perkins, S. K. Ho, and J. H. Hammer, Deep Penetration Fueling of Reactor Grade Plasmas with Accelerated Compact Toroids, UCRL-96894, Lawrence Livermore National Laboratory (submitted to Nuclear Fusion).

6. S. K. Ho and L. J. Perkins, An Assessment of Fueling for the Engineering Test Reactor, Lawrence Livermore National Laboratory (to be published).

7. C. D. Henning et al., TIBER Engineering Test Reactor--Final Design Report, Lawrence Livermore National Laboratory (to be published).

8. G. E. Gorker, Grumman Aerospace/Oak Ridge National Laboratory, private communication (1987).

9. R. S. Hawke, J. Vac. Sci. Technol. 1A, 969 (1983).

4.3 ELECTRICAL SYSTEMS

This section contains summaries for the following modules. Lead authors and affiliations are indicated.

Module	Lead Author	Organization
ECH system	C. E. Wagner	TRW, Inc./LLNL
LH system	--	--
NBI system	L. J. Perkins	LLNL
Alternating current (ac) power system	D. R. Hicks	FEDC/ORNL
Instrumentation and controls (I&C)	D. R. Hicks	FEDC/ORNL

4.3.1 Electron Cyclotron Heating System

Summary is yet to be provided. The reader is referred to the Fortran listing of this module (see Sect. 3), which is fairly well commented.

4.3.2 Lower Hybrid System

The LH heating system is simply accounted for in TETRA1 based on an input value for efficiency (injected power/wall plug power) and an input value for unit cost ($/W).

4.3.3 Neutral Beam Module

For a given neutral beam energy and current (supplied by the physics/current-drive modules), this module computes all salient characteristics and features of the NBI system. The module is configured for negative-ion beams only and is based on a volume-type negative ion source coupled to a conventional neutral gas neutralizer. The allowable beam energy is in the range of 205-1000 keV. Negative ion accelerators based on rf quadrupole for energies up to 2.5 MeV, and

neutralizers based on laser photo-detachment may be included as options in future upgrades of this module should these concepts mature in the FY 1988 ITER studies.

Calculations performed by this module include number of beamlines, source configuration, beamline geometry and dimensions, losses in accelerator/neutralizer/drift sections, gas flows to reactor torus, beam losses due to skimming by collimation at beam focus, shielding requirements at entrance duct, resulting minimum separation of TF coils because of duct penetrations, power supply requirements, and cost.

Full details of the philosophy underlying NBI systems design, on which this module is based, are given in ref. 1.

The inputs to and outputs from this module are shown in Tables 4.5 and 4.6. The number in square brackets following certain input variables in Table 4.5, denotes the default value supplied by the module if that particular variable is set to zero in the input. In Table 4.7, we show a typical output listing produced by the module for an input request of 87.5 A of injected neutral beam current at an energy of 500 keV.

The following major calculations are performed by the module. Full details of the equations and formalism employed can be found in refs. 2 and 3. The results of all calculations are in base SI units.

1. Check input for consistency and range validity.
2. Apply default input values where applicable.
3. Compute beam divergence as 1/SQRT of beam energy (ref. 2).
4. Compute fractional beam loss (FA) caused by stripping loss in the accelerator (ref. 2).
5. Compute optimum neutralizer length and fractional neutralizer losses (FN) (ref. 2).
6. Compute fractional beam loss (FL) in the final drift section of the beamline after the neutralizer (ref. 2).
7. Compute number of beamlines required.
8. Compute fractional collimator skimming losses (FS) caused by the entrance duct collimator based on a 2/e collimation in the vertical direction and EFOLDA (1/p variable) in the horizontal direction. [See ref. 3 for details of two-dimensional (2-D) skimming of Gaussian beams.]

Table 4.5. Input variables for the neutral beam module[a]

Variable	Source	Description
ebeam	Physics/current drive	Injected neutral beam energy (keV)
aibeam	Physics/current drive	Injected neutral beam current (A)
ajsource	User input	Average source current-density (A/m^2) [60]
ppsource	User input	Source neutral gas pressure (Pa) [1.33]
ppneut	User input	Neutralizer inlet pressure (Pa) [1.9345×10^{-2}]
pptorus	Vacuum	Torus vacuum pressure (Pa)
ab	User input	Aspect ratio of source [80]
pmax	User input	Maximum injected power per beamline (W) [25.0×10^6]
nsource	User input	Number of source arrays per beamline [2]
tshield	Shield/user	Minimum shield thickness between neutral beam duct and TF coil case (on one side) (m) [0.25]
r0	Physics	Plasma major radius (m)
rtfouter	Magnetics	Mean radius of outer TF coil leg (m)
ttfouter	Magnetics	Radial thickness of outer TF coil leg + case (m)
efolda	User input	Collimator width in narrow direction at minimum point between TF coils (beam e-folds) [1]
iduct	User input	0 = compute minimum dimensions of torus entrance duct between TF coils and radial distance from plasma axis 1 = dimensions wduct × hduct and zduct supplied

Table 4.5. (Continued)

Variable	Source	Description
wduct	Geometry/ computed	Minimum width of entrance duct to torus (m) [*]
hduct	Geometry/ computed	Minimum height of entrance duct to torus (m) [*]
zduct and	Geometry/ computed	Tangential distance of duct from plasma axis (m) [*] (*--if iduct = 0, this module calculates the duct dimensions wduct × hduct and distance zduct to plasma axis; in this case, wduct, hduct, and zduct will initially come in as zero. If iduct = 1, the module computes beam dimensions losses consistent with the supplied values of wduct × hduct and zduct)
ucost	User input	Unit cost for NBI system in terms of $/W wall-plug power, normalized to a 500-keV system ($/W) [1.698--equivalent to approximately $4/W (injected) for TIBER parameters]
nout	Main	Logical unit number for output print file
iprint	Main	Instruction to print results: 0/1 = no/yes

[a] [ ] = default value if input is set to zero.

Table 4.6. Output variables for the neutral beam module

Variable	Description
nlines	Total number of beamlines
effcy	Total beamline efficiency-- injected power/wall-plug power
pwpop	Total wall-plug power required (W)
cost	Total cost of beamlines and power supplies ($)
qtorus	Room-temperature gas flow from beamlines into torus vacuum (D_2/s)
zsrcplsm	Source--plasma distance (m)
zfocus	Distance: source to minimum focus between outer TF coils legs (m)
zext	Length of beamline external to vacuum vessel (m)
wduct	Width of duct at minimum focus between outer TF coils (m) {*}
hduct	Height of duct (vertical direction) at minimum focus (m) {*}
	(*--if iduct = 0 in the input, this module calculates wduct, hduct, and zduct; if iduct = 1, these three variables are supplied externally and the module computes beam parameters consistent with these fixed dimensions)
wtf	Minimum permissible separation of outer TF coil legs--case to case (m)
zduct	Distance from minimum focus point between outer TF legs to tangential intercept at plasma axis (m) {*}

Table 4.7. Sample output file for an input request of 87.8 A of neutral beams at 500 keV

Variable		Description
pinj	= 43.90 MW	Total injected power requirement
ebeam	= 500.0 keV	Beam energy requirement
aibeam	= 87.80 A	Total injected current requirement
nlines	= 2	No. of beamlines
effcy	= 0.3372	Overall efficiency--injected power/wall-plug power
pwp	= 130.2 MW	Total wall-plug power
ucost	= 1.698 $/W	Neutral beam unit cost--$/W of wall-plug power
cost	= 2.210×10^{8} $	Total cost of beamlines and power supplies
nsource	= 2	No. of source arrays/beamline
ajsource	= 60.00 A/m^2	Average source current density
a	= 0.1184 m	Source array width
b	= 9.472 m	Source array height
asource	= 4.486 m^2	Total area of all sources
psource	= 0.0100 torr	Source pressure
paccl	= 1.0×10^{-4} torr	Accelerator pressure
pneut	= 1.455×10^{-4} torr	Neutralizer inlet pressure
pnout	= 1.455×10^{-5} torr	Neutralizer outlet pressure
plast	= 1.455×10^{-5} torr	Final line pressure
ptorus	= 1.0×10^{-6} torr	Torus vacuum pressure
qtorus	= 9.874×10^{19} mol/s	Room temperature gas load to torus from all beamlines
ep	= 0.9500	Power supply efficiency
ea	= 0.8499	Accelerator (current) efficiency (power efficiency = accelerator efficiency/2 + 0.5)
en	= 0.5800	Neutralizer efficiency
el	= 0.9845	Final line efficiency
es	= 0.6721	Collimator skimmer efficiency
effcyi	= 0.3262	Beamline current efficiency
plossp	= 6.509 MW	Total loss in power supplies

Table 4.7. (Continued)

Variable		Description
plossa	= 4.641 MW	Accelerator loss per beamline
plossn	= 24.02 MW	Neutralizer loss per beamline
plossl	= 0.5147 MW	Final line loss per beamline
plosss	= 10.71 MW	Collimation skimmer loss per beamline
zsrcaccl	= 3.200 m	Source/accelerator length
zneut	= 30.00 m	Neutralizer length
zlast	= 5.000 m	Final line length
zsrcplsm	= 45.71 m	Total line length from source to plasma
zfocus	= 41.10 m	Distance from source to minimum focus
zext	= 38.20 m	Length of beamline external to vacuum vessel
efolda	= 0.690	Collimator width in narrow direction (beam e-folds)
wduct	= 0.412 m	Width of duct at minimum focus between outer TF coil legs
hduct	= 0.842 m	Height of duct at minimum focus
wtf	= 1.264 m	Minimum permissible separation of outer TF coil legs
zduct	= 4.610 m	Distance from minimum focus to tangential intercept at plasma axis

9. Compute total beamline current efficiency as EFFCYI = (1 - FL) *(1 - FA)*(1 - FS)*(1 - FN).
10. Compute resulting source(s) current and dimensions.
11. Compute beamline length from source to focus at entrance duct between coils.
12. Compute duct dimensions from beamline geometry and collimation requirements.
13. Compute beam geometry from duct focus to plasma axis.
14. Compute minimum width between outer TF coil legs (case to case) from duct dimensions, beam/plasma geometry, and shielding requirements.
15. Compute gas load to torus from pressure difference between last section of beamline and torus, and impedance of entrance duct.

16. Compute power supply requirements based on unregulated supplies (for high efficiency and lower costs--series tube requirements in a regulated supply would result in appreciable voltage drop, lower efficiency, and higher cost.
17. Compute incremental power losses in each section of the beamline.
18. Compute total cost in terms of $/W of WALLPLUG (not injected) power--bulk of costs are in the power supplies.
19. Print results.

4.3.4 AC Power System Module

4.3.4.1 Module description

The ac power module (ACPOW) is a TETRA code subroutine that will calculate design and cost data for the plant electrical power system. This system includes the following major system configurations:

1. essential facility power system shown on Fig. 4.4,
2. non-essential facility power system shown on Fig. 4.4, and
3. coil power supply system options shown on Fig. 4.5 (default option) and Fig. 4.6.

Figures 4.4 through 4.6 illustrate the overall electrical power system included in this code module. The code will read pertinent input data from other code modules and calculate design and installed material cost data for the electrical power system. This system includes the following major items: switchyard equipment and protection, high-voltage transmission line interfacing equipment and components, cables, buses, structures, circuit breakers, switches, transformers, diesel generators, uninterruptible power supplies (including batteries, chargers, inverters, and associated equipment and components), protective relaying, power factor correction equipment, lighting and grounding, and all necessary low-voltage power distribution equipment and components. Lightning arresters and auxiliary cooling will be included in the cost of the transformers. Isolation switches and the local instrumentation and controls will be included in the cost of the

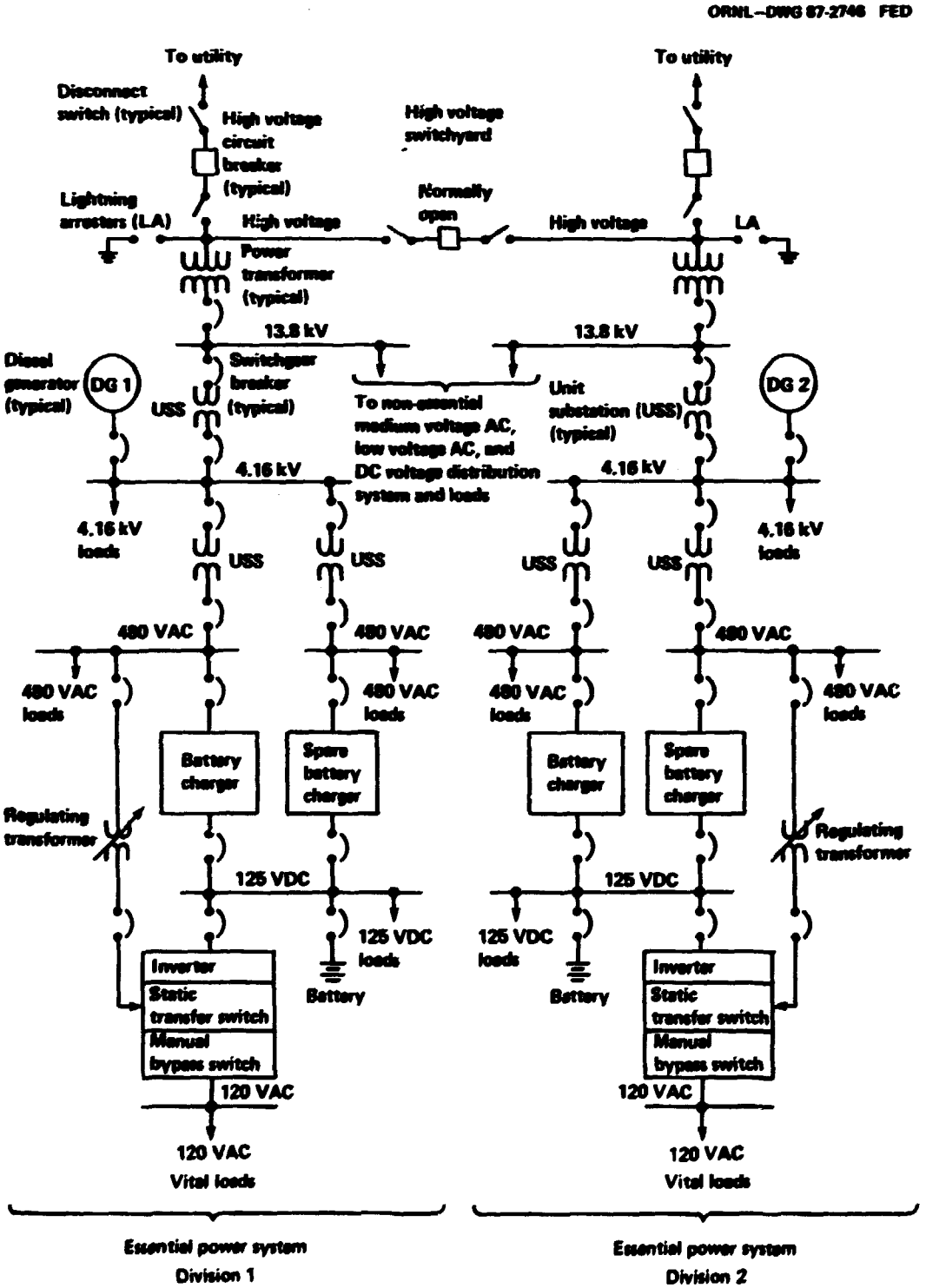

Fig. 4.4. Essential and nonessential facility power system one-line diagram.

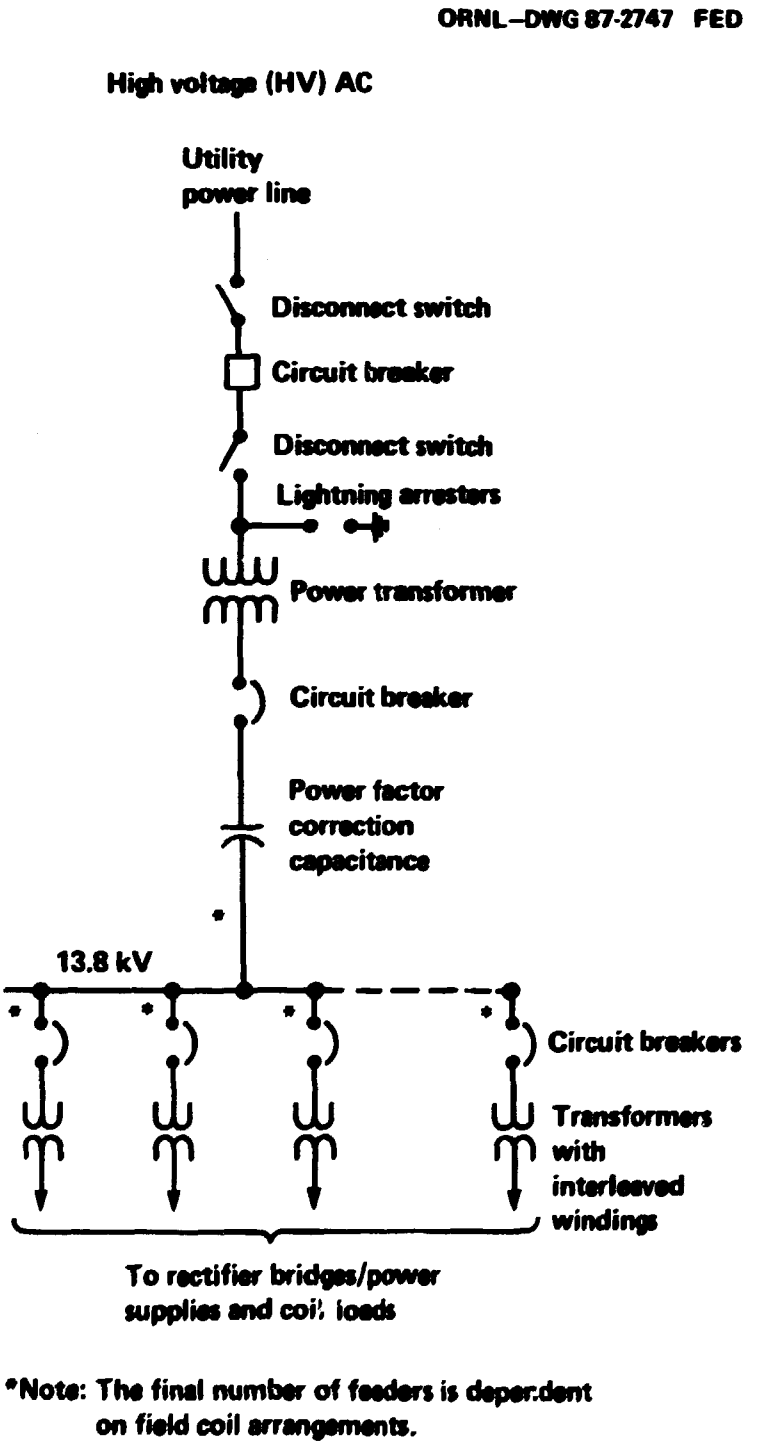

Fig. 4.5. Coil power supply system one-line diagram (direct utility line connection option).

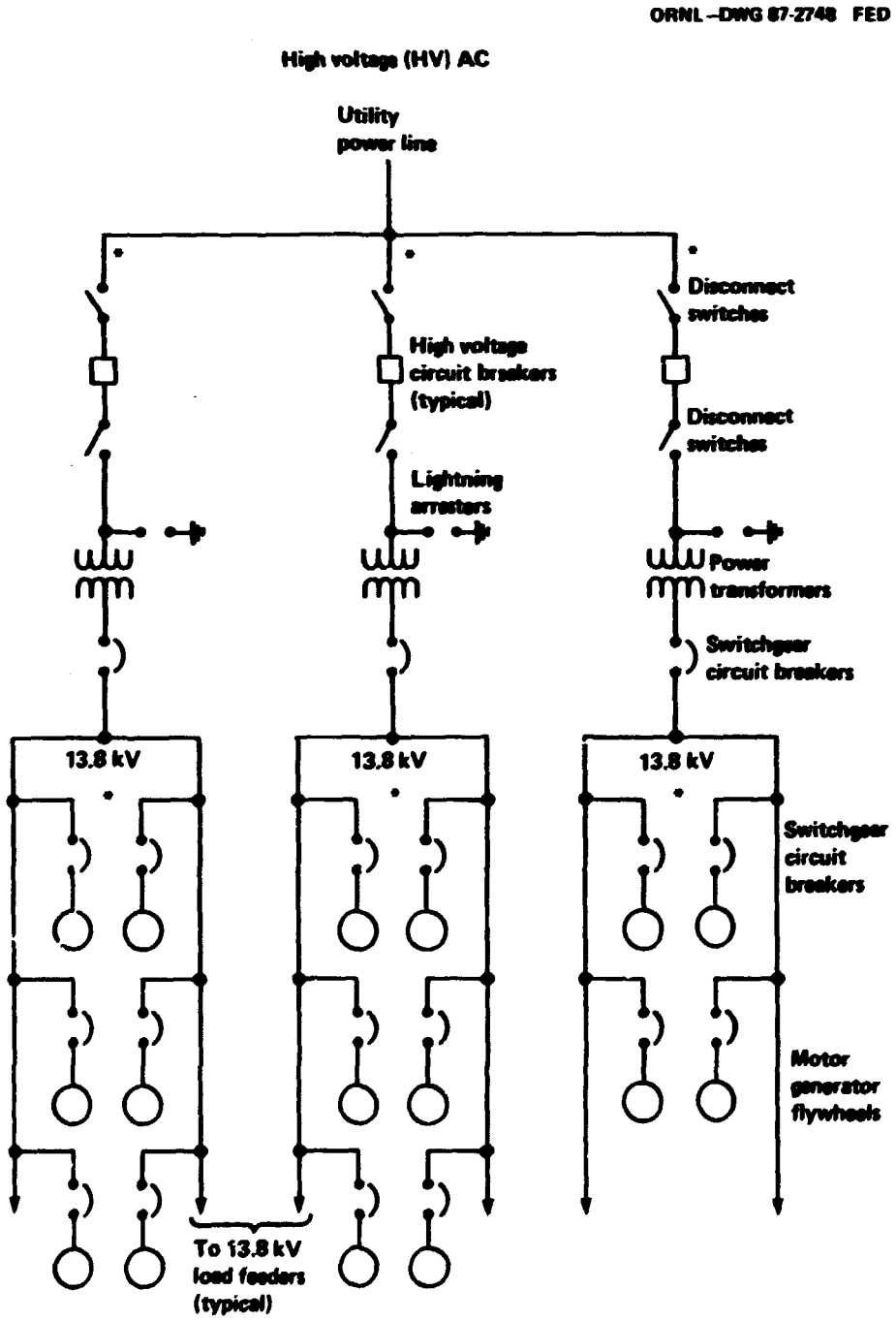

Fig. 4.6. Coil power supply system one-line diagram (motor-generator/flywheel option).

circuit breakers. Where items are not specifically identified, they are included in overall cost multipliers.

4.3.4.2 Options

The user may select the desired utility line voltages and characteristic power feeder cable length. The user may also select the type of energy supply system. The two energy supply options are (1) power supplied directly from the utility line as in Fig. 4.5 and (2) power supplied directly from a motor-generator/flywheel (MGF) system as in Fig. 4.6. Option 1, with direct utility line power and power factor correction capacitors, is the default option.

4.3.4.3 Input/output data

All variables except the following are defined in the output data and are listed in Table 4.8, a sample output from this module:

1. pcika, continuous current rating of the pulsed power system, 13.8-kV circuit breakers, kA;
2. fcika, continuous current rating of the facility power system, 13.8-kV circuit breakers, kA;
3. chvcam, cost of high-voltage cables and bussing for the pulsed power system, $ \times 10^6$;
4. cfvcam, cost of high-voltage cables and bussing for the facility power system, $ \times 10^6$;
5. chvcbm, cost of high-voltage circuit breakers of the pulsed power system, $ \times 10^6$;
6. cfvcbm, cost of high-voltage circuit breakers of the facility power system $ \times 10^6$;
7. cmvcbm, cost of 13.8-kV circuit breakers of the pulsed power system, $ \times 10^6$;
8. cfmvcb, cost of 13.8-kV circuit breakers of the facility power system, $ \times 10^6$;
9. cmvcam, cost of 13.8-kV cables of the pulsed power system, $ \times 10^6$;
10. cfmvca, cost of 13.8-kV cables of the facility power system, $ \times 10^6$;
11. clthm, characteristic length of the 13.8-kV cables, m;
12. tlvpmw, estimate of the total low-voltage (480-V) power, MW;
13. iprint, output dataprint designator:
    0 = no print,
    1 = complete output data table;
14. hvlkv, pulsed power utility line voltage, kV;
15. fvlkv, facility power line voltage, kV; and
16. basemw, facility base load (loads that are not dependent on floor area), MW.

Table 4.8. ACPOW subroutine output[a]

Variable	Description	Value
basemw	Facility base power load, MW	5.00
# efloor	Effective total floor space, m^2	90000.00
pkwpm2	Power needed per floor area, kW/m^2	0.15
fcsht	Total power to facility loads, MW	39.17
# fmgdmw	Power to motor-generator/flywheel units, MW	166.10
# acpfmva	PF pulsed power at # pwrfac = 0.60, MW	0
# bpsmw	Power to burn power supplies, MW	2.58
# bdvmw	Power to divertor coil supplies, MW	0
# wtfmw	Power to TF coil power supplies, MW	2.90
# pheatmw	Power to plasma heating supplies, MW	182.90
# crymw	Power to cryogenic compressor motors, MW	17.78
# vacmw	Power to vacuum pump motors, MW	0.50
# htpmw	Power to heat transport system pump motors, MW	10.00
# t2pmw	Power to tritium processing, MW	12.21
* pacpmw	Total pulsed power system load, MW	413.47
& hvlkv	Pulsed power utility line voltage, kV	230.00
n3pht	Number of three-phase transformers	3.00
tmva	Maximum MVA of each transformer	150.00
pnbkrs	No. of 13.8-kV circuit breakers	24.00
bkrmva	Short-circuit MVA of circuit breakers	1500.00
& fvlkv	Facility power line voltage, kV	115.00
ftmva	Maximum MVA of facility transformer	40.00
fnbkrs	No. of 13.8-kV circuit breakers	6.00
fbkmva	Short-circuit MVA of circuit breakers	500.00
	AC Power Summary	
*pacpmw	Total pulsed power system load, MW	413.47
# hvlkv	Pulsed power utility line voltage, kV	230.00
fcsht	Total facility power load, MW	39.17
#fvlkv	Facility power line voltage, kV	115.00
	AC Power Cost Summary	
cpacpm	Cost of the pulsed power system, $\$ \times 10^6$	20.72
cfacpm	Cost of facility ac power system, $\$ \times 10^6$	2.51
c2dgm	Cost of two diesel generators (480 V, 2500 kW each), $\$ \times 10^6$	2.00
c4nbpm	Cost of four no-break power supplies, $\$ \times 10^6$	0.40
clvdsm	Cost of low-voltage power distribution, $\$ \times 10^6$	4.67
*ctacpm	Installed material cost of power system, $\$ \times 10^6$	36.35

[a] # = inputs from other system code modules; & = user-selected inputs; and * = outputs to other system code modules.

4.3.5 Instrumentation and Control Module

4.3.5.1 Module description

The instrumentation and control module (IANDC) is a TETRA code subroutine that provides costs for process I&C, archival computing, and diagnostic instrumentation.

Earlier code versions included calculations for process I&C costs. However, for simplicity, the present version allows the user to select this quantity (tcopsc) because tcopsc is small compared with diagnostic instrumentation costs. The default value for tcopsc is included. Likewise, the archival computer cost (tcarch) is selectable with a default value included.

4.3.5.2 Options

Predictions of the extent of diagnostic instrumentation required for any large project are very subjective. Therefore, the diagnostics in IANDC have selectable options that permit the determination of diagnostic costs over a wide range of possibilities. The three user selections for diagnostic range are high, medium, and low, and the user selects idiag = 1, 2, or 3, respectively. The default selection is idiag = 2. The three user selections for the operation phase are hydrogen, deuterium, and tritium, and the user selects iph = 1, 2, or 3, respectively. The default is iph = 3. Table 4.9 is a listing of the output for this subroutine.

4.3.5.3 Input/output data

All inputs are user selected with default settings available. There are no inputs from other system code modules. Outputs from the IANDC module to other modules are identified in the output listing in Table 4.9.

4.3.6 References for Section 4.3

1. C. D. Henning et al., TIBER Final Design Report, Lawrence Livermore National Laboratory (to be published).

Table 4.9. IANDC subroutine sample cost estimate output using defaults of tritium phase and medium diagnostics

k	Diagnostics group	nohp[a]	nodp[b]	notp[c]	Cost ($ × 10^6) tmcpdm[d]	hpdgcm[e]	dpdgcm[f]	tpdgcm[g]	Total
					Plasma diagnostics				
1	edensity	2	2	2	1.80	3.60	3.60	3.80	11.00
2	e.temp	2	2	2	1.60	3.20	3.20	3.40	9.80
3	ion temp	3	2	2	1.80	5.40	3.60	4.00	13.00
4	impurity	3	2	2	0.85	2.55	1.70	2.00	6.25
5	pwr loss	2	2	2	0.50	1.00	1.00	1.10	3.10
6	magnetic	3	2	2	0.35	1.05	0.70	0.80	2.55
7	p.instab	3	2	1	0.85	2.55	1.70	1.05	5.30
8	fprodpar[h]	1	3	2	0.95	0.95	2.85	2.10	5.90
9	environ	3	3	2	0.85	2.55	2.55	1.80	6.90
10	miscel	6	8	10	0.50	3.00	4.00	5.10	12.10
	Subtotal[i,j]					25.85	24.90	25.15	75.90
					Archiving computer hardware				
	Subtotal[j,k]								10.00
					Process I&C				
	Subtotal[j,l]								21.45
	Total[j,m]								107.35

[a]nohp = No. of diagnostic types in group k for H_2 phase.

[b]nodp = No. of diagnostic types in group k added for deuterium phase.

[c]notp = No. of diagnostic types in group k added for tritium phase.

[d]tmcpdm = average cost of diagnostic type in group k.

[e]hpdgcm = cost of diagnostics in group k added for H_2 phase.

[f]dpdgcm = cost of diagnostics in group k added for deuterium phase.

[g]tpdgcm = cost of diagnostics in group k added for tritium phase.

[h]fprodpar = fusion product particle diagnostics group.

[i]tcopdg = total cost of plasma diagnostics. Medium-range diagnostics were used to compute total cost of diagnostics. The various defaults for the tritium phase are low diagnostics, tcsdg = $67 million; medium diagnostics, tcsdg = $107 million; and high diagnostics, tcsdg = $170 million.

[j]Outputs to other systems code modules.

[k]tcarch = total cost of archiving and processing.

[l]tcopsc = total cost of process I&C.

[m]tscdg = total cost of diagnostics and I&C.

2. J. E. Fink, A Formulary for Negative Ion Neutral Beam Design, Lawrence Livermore National Laboratory (to be published).

3. L. C. Pittenger, "Power Density Calculations for Beams from Diffuse Astigmatic, Rectangular Sources," Lawrence Livermore National Laboratory, Engineering Note ENC 77-1, 1977.

4.4 MAGNET SYSTEMS

This section contains summaries for the following modules. Lead authors and affiliations are indicated.

Module	Lead Author	Organization
TF magnet system	J. D. Galambos	FEDC/ORNL
PF magnet system	J. D. Galambos	FEDC/ORNL
Magnet conductor	J. A. Kerns	LLNL
TF power conversion system	G. E. Gorker	FEDC/Grumman
PF power conversion system	G. E. Gorker	FEDC/Grumman
Energy storage system	G. E. Gorker	FEDC/Grumman

4.4.1 TF Coil Magnet Module

The TF coil subroutine (TFCOIL) provides some basic information about the TF coil size, shape, and stress. The subroutine is a modified version of its counterpart from the original tokamak systems code.[1] Input to the routine includes guesses on geometry (major radius, coil location, coil thickness, coil component sizes) and current density. Calculated quantities include TF coil cross-sectional area required to produce the field on axis, various current density definitions, outer leg position, coil shape, coil stored energy, coil stress, and coil weights.

The first calculation is for the area available for the TF coil between the shield and the OH coil (ARTFI). Another quantity calculated is the area required to produce the field on axis with the present guess on current density (TATFI) and is based on Ampere's law. These quantities are required to be equal through an external constraint. Also, the current densities over the winding pack (including steel case), over the entire TF coil (including the external case), and over the conducting material are calculated.

Next, the outer coil leg radial location is determined based on a minimum of that required for a specified port size between the coils (case-to-case), PORTSZ, and that required for a specified ripple on axis (peak-to-average), RIPPLE.[2] This value, the outer leg radial location, is used in calculating the TF coil shape. The TF coil top-half inner surface shape is approximately represented by four arcs going through five points, and the bottom half is assumed to be symmetric. The first point is found from the radial buildup on the inboard midplane. The next point found is at the highest vertical location, which is equal to the sum of the plasma height, the inboard build thickness between the TF coil and scrapeoff, and the input gap (VGAPTF). The previously determined outer leg radius is used to place the outer leg midplane point, and additional points are put between the first and second points above and between the second and third points to smooth out the TF coil shape. These points are used to find the TF coil length and weights and are used in the TF coil stored energy calculation, which integrates B*dA throughout the coil interior to find the inductance (where B is the magnetic field in the coil and dA is the differential area).

Finally, the inplane stresses in the coil winding packs are calculated. The centering force is first calculated[3] and is used to find the compressive stress component on the inner winding.[3] All of the centering force on the winding is assumed to be taken in the steel case surrounding the winding pack. Then, the tensile component is found by spreading the vertical separating force over the cross-sectional area of the winding pack cases and the external case of the whole TF coil. This total stress is taken to be the Tresca sum of these two components. The strain induced in the winding by the electromagnetic force (EMF) is calculated using the tensile stress component.

4.4.2 PF Coil Module

The PF coil subroutine (PFCOIL) calculates information for the OH coil and the other PF coils. Input includes the number of PF coils, current in the OH coil, plasma parameters, size and location of the OH coil, and the OH coil superconductor winding pack parameters. Calculated quantities include the PF coil locations and currents, number

of turns/coil, sizes and weights of the coils, and stress in the OH coil conductor.

First, the subroutine prepares for the call to the PF coil scaling module (i.e., poloidal magnetics module), which calculates the PF coil locations and currents (at the BOP and at the EOF). This task requires modeling the OH coil as a set of discrete coils and gathering information on a reference MHD run. Once the MHD scaling is done, the sizes and weights of the PF coils are found using the calculated currents and input overall current densities. The coil current waveforms over the pulse are calculated using the BOP and EOF values provided by the MHD scaling. The coils are assumed to be ramped from zero to BOP values during the TRAMP. They swing 90% of the way from the BOP to EOF values during the ohmic swing period (TOHS) and swing the last 10% during the heating (THEAT) and burn (TBURN) times. The coils are then ramped to zero current during TQNCH. All current waveforms are assumed to be linear in the code. The waveform assumptions may be changed in subroutine WAVEFORM. Additional time periods at the beginning (TTFRAMP) and at the end (TTFQNCH) are available but are not currently being used. The sizes and weights of the PF coils are found by using assumed (input) current densities. Also, the number of turns is found by using an assumed (input) current per turn.

The OH coil size is input to the module (and may be externally iterated), as are the superconductor winding pack parameters. Various current density definitions in the OH coil are calculated along with the weight of the OH coil. The current density in the OH coil is controlled by an external constraint. The number of turns is found by using the input for the winding pack size and the OH coil size. The peak field in the OH coil is calculated by using information from ref. 4; no field effects from other coils or the plasma are included in this calculation.

Finally, the in-plane stress in the OH coil winding pack is calculated. The peak hoop stress (which usually occurs at the inner OH coil radius) is used. The stress is calculated by using the product of field, current, and radius (B*I*R) as the separating force and by using the area of the steel winding pack casing to carry the load. No effects of load sharing between the windings, external case, TF coil, etc., are considered. Also, a radial stress component is included in the total

Tresca stress (Tresca stress = sum of the hoop and radial components). The radial component modeling is taken from CIT work[5] and is much smaller than the hoop component.

4.4.3 Magnet Conductor Module

The superconducting (SC) magnet package determines the allowable current density in the coils and stability margin for a given configuration. Input for the conductor configuration includes the conduit cross-sectional area, conductor fraction (f-cond), copper fraction (f-cu), steel case thickness of the conduit, peak field in the coil (B), helium temperature (T-b), EMF-induced strain in the conductor, and inductance/turn of the coil. Using this information, the package calculates the stability margin (e-p) and allowable current density in the winding pack, or equivalently the allowable operating current (I-op). The requirements that the operating coil current be less than the allowable current and that the actual stability margin be greater than the allowable stability margin are included in the global constraints of the systems code. Some quantities that are included in the global variables are the copper fraction, conductor fraction, and steel case thickness. These constraints and variables can presently be applied to the TF coils and to the OH solenoid.

High-field and high-current-density operation of the superconducting magnet systems of an ETR provides clear benefits for reduced size and lower costs. Cable-in-conduit conductors (CICCs) capable of providing the required performance are under development. This type of conductor lends itself naturally to the use of Nb_3Sn, to the incorporation of distributed structure, and to simplification of the cryogenic system. In addition, CICC designs are generally similar, exhibiting relatively minor variations in dimensions or composition of constituents among adaptations for a variety of applications.

In an SC magnet system, the field that can be provided and the operating current density possible at that field are inextricably tied to details of the system design. Obviously, the coil size or level of field produced has an impact on stress levels in structural components, as well as on the stored energy that must be safely extracted in the event of a quench. The choice of a generic conductor design like the

CICC ameliorates the problem of evaluating the effects of such details of coil design for a broad range of systems.

Whether the performance required of a particular SC magnet system fabricated with CICCs is achievable can be determined by examining the constraints placed on the winding pack current density J_{pack} by the maximum field B_{max} and other design details. Because of the nature of CICCs, these constraints are quite general and quantifiable in terms of key CICC parameters. Although none of these parameters is completely independent of the others, a natural division occurs between those that describe what is inside the sheath (the SC composite cable and the void space for helium flow) and the rest (sheath, additional reinforcement, and insulation). Thus, it is often more natural to examine the constraints in terms of limits on the cable space current density J and then to recast these as limits on J_{pack} after a somewhat independent determination is made of the required quantities of steel and insulation.

4.4.3.1 Constraints on J

Constraints on the cable-space current density J presently included in the systems code are described in the following subsections.

Minimum acceptable stability margin

The stability margin provided by a CICC depends on the effective heat capacity of the coolant at any point along its length and the temperature margin between the normal operating temperature and the current-sharing temperature of the superconductor. After evaluating credible events that might cause a sudden deposition of energy into the SC cable strands of the CICC, we have chosen to require a stability margin of 300 $kJ \cdot m^{-3}$ of the conductor.

Such an evaluation is straightforward in principle, but it is complicated in the detail. We simplified the process by requiring that heat transfer from the conductor strands be sufficient to permit all of the interstitial helium in the vicinity of a disturbance to be used in absorbing the energy of the disturbance plus the Joule heat production during the recovery process. Empirical evidence indicates that this

requirement will be met if J is constrained as indicated in the next subsection.[6] When that constraint is satisfied, the same empirical evidence indicates that the stability margin provided will be given approximately by

$$e_p = \frac{\eta S_{He} T_c}{1 + (J^2 \rho_{Cu} Cd_w)/(f_{Cu} f^2_{cond})} \quad , \tag{4.12}$$

where the stability parameter η is given by

$$\eta = \frac{1 - f_{cond}}{f_{cond}} \left[\frac{T_c(B,\varepsilon) - T_b}{T_c(B,\varepsilon)} - \frac{J}{f_{cond}(1 - f_{Cu}) J_{c0}(B,\varepsilon)} \right] \quad . \tag{4.13}$$

We approximate the effective heat capacity S_{He} of the coolant over the temperature range T_b to T_{cs} by

$$S_{He} = \frac{\int_{T_b}^{T_{cs}} \rho_{He} C_p \, dt}{T_{cs} - T_b} \quad . \tag{4.14}$$

Fortunately, this expression exhibits surprisingly simple and slow variation with p and T over the usual range of interest.

Inspection of the relation for η shows that it is simply a dimensionless parameter constructed from the product of $(T_{cs} - T_b)/T_c$ and the ratio of helium to conductor volumes inside the sheath by assuming that critical current is a linear function of temperature in the range of interest. Note that T_c and J_{c0} in η are dependent on the intrinsic strain ε of the SC filaments. In the systems code, estimates are made of the initial strain caused by cooldown as well as of the change in this strain because of mechanical loads imposed on the CICC during operation as described in ref. 6. The effects of strain on critical current are accounted for according to the prescription of Ekin.[7] Note that critical performance capabilities of the superconductor are completely represented in this prescription by $T_{cm}(B)$, $J_{c0m}(B)$, and ε. For state-of-the-art Nb_3Sn superconductors, we use the following equations, which adequately represent a large database in the ranges of B and T important to this operation:

$$T_{cm}(B) = 18(1 - 0.036B) \quad (K) \text{ and} \tag{4.15}$$

$$J_{cOm}(B) = \frac{111(1 - 0.036B)^2}{B^{1/2}} \quad (A \times mm^{-2}) \ . \tag{4.16}$$

Adequate heat transfer to the coolant

As mentioned earlier, the validity of the estimates of stability margin depends on heat transfer being sufficient to ensure that all helium in the vicinity of the perturbation absorbs heat uniformly. Empirical evidence indicates that, even with initially stagnant helium, the heat transfer to the helium in a CICC is adequate if J is constrained according to

$$J \leq \left(\frac{f_{Cu} f_{cond}^3}{1 - f_{cond}} \right)^{1/2} \frac{[T_c(B,\varepsilon) - T_b]^{1/2} \ell_H^{2/15}}{\rho_{Cu}^{1/2} \tau_H^{1/15} d_w} \ . \tag{4.17}$$

In principle, evaluation of this expression requires some knowledge of the length and duration of the perturbation, but one can see that its value is relatively insensitive to ℓ_H and τ_H. We routinely take 10 m and 1 ms, respectively, as appropriate values unless specific situations suggest different ones.

Maximum temperature in the event of a quench

We restrict the maximum hot spot temperature in the event of a quench to 150 K. This limitation guarantees that strains caused by differential thermal expansion cannot be greater in absolute magnitude than about 0.1%, which is considered safe for both the Nb_3Sn superconductor and the steel sheath. The limitation on J because of T_{max} is related to CICC and other magnet system parameters according to

$$J \leq \left[\frac{V_D I_{op}}{E_s} (1 - f_{cond}) f_{cond} f_{Cu} I_1 + f_{Cu}^2 f_{cond}^2 I_2 \right. \tag{4.18}$$

$$\left. + (1 - f_{cu}) f_{cu} f_{cond}^2 I_3 \right]^{1/2} \ ,$$

where

$$I_1 = \int_{T_b}^{T_{max}} \frac{\mu_{He,init} C_{v,He}}{\rho_{Cu}} dT \quad , \tag{4.19}$$

$$I_2 = \int_{T_b}^{T_{max}} \frac{\mu_{Cu} C_{Cu}}{\rho_{Cu}} dT \quad , \tag{4.20}$$

$$I_3 = \int_{T_b}^{T_{max}} \frac{\mu_{core} C_{core}}{\rho_{Cu}} dT \quad . \tag{4.21}$$

Maximum pressure in the event of a quench

The maximum allowable pressure p_{max} internal to a CICC in the event of a quench depends on the sheath geometry and allowable stresses for the constituent material. In the systems code, we presently assume a square conduit with wall thickness chosen to satisfy stress allowables under the imposition of the operating electromagnetic loads. Membrane stress in the sheath resulting from an internal pressure is estimated according to a prescription in ref. 3. The limitation of J because of p_{max} and various CICC parameters is then[6]

$$J \leq \frac{6.59 p_{max}^{0.694} f_{Cu}^{1/2} f_{cond}^{1/4} (1 - f_{cond})^{3/4} d_w^{1/4}}{L^{3/4} \rho_{Cu}^{1/2}} \quad . \tag{4.22}$$

4.4.3.2 Choices of key parameters

Certain key parameters are not free but are determined by features of the machine design or manufacturability of key components. As mentioned earlier, thicknesses of the sheath and any other steel reinforcement of the CICC are chosen with regard to the mechanical load that must be borne. To determine insulation thickness, one assesses turn-to-turn voltage during ramping or dumping as well as other factors affecting minimum reasonable separation. The diameter of wires in the CICC should be near the 0.5-1.0 mm range. The copper fraction in the wires should be less than about 0.4. Resistivity of the copper matrix

in the CICC strands is affected by the radiation dose and, therefore, by the shield thickness. In the constraints on J that deal with the ability to protect the magnet system, the resistivity used must be the value expected at the end of a scheduled cycle of operation, after which the system must be warmed to anneal the copper. In the constraints on J that impact stability, it is sufficient to require a value corresponding to what can be achieved (by annealing) at the beginning of any planned cycle of operation. We predict the residual resistivity at the end of a cycle of operation by

$$\rho_0 = \rho_{0,init} + \rho_s \left\{1 - \exp\left[\frac{-i(D + D_{rtnd})}{\rho_s}\right]\right\} . \qquad (4.23)$$

Magnetic field effects are accounted for by

$$\rho_{Cu}(B) = \rho_0[1 + 0.0339(B/\rho_0)^{1.07}] \quad (n\Omega\cdot m) \quad . \qquad (4.24)$$

At the beginning of operation after N regular anneal cycles, we estimate the damage retained by

$$D_{rtnd} = \sum_j f_{rtnd}(D_j)D_j \quad , \qquad (4.25)$$

where

$$f_{rtnd}(D) = 0.1 + 0.1e^{-1000D} \quad . \qquad (4.26)$$

In these formulae, we use $\rho_s = 3.0\ n\Omega\cdot m\cdot dpa^{-1}$.

4.4.3.3 Nomenclature

B = Magnetic field at the conductor (T).

C = Empirically determined constant relating recovery time in a CICC to a perturbation energy density and the wire diameter ($m^2 \times W^{-1}$).

C_{core} = Specific heat of noncopper fraction of the composite superconductor. For MF-Nb_3Sn, this amounts to an average of the specific heats of CuSn-bronze and Nb_3Sn ($J \times kg^{-1} \times K^{-1}$).

C_{Cu} = Specific heat of copper ($J \times kg^{-1} \times K^{-1}$).

$C_{v,He}$ = Mean specific heat at constant volume for He, taken as 3100 $J \times kg^{-1} \times K^{-1}$.

C_p = Specific heat at constant pressure for He ($J \times kg^{-1} \times K^{-1}$).

D = Damage to the copper stabilizer of a conductor during operation (dpa).

D_{rtnd} = Damage retained after a room-temperature anneal (dpa).

d_w = Diameter of a composite SC strand in the CICC (m).

e_p = Energy density per unit volume of conductor that can be absorbed by a CICC without quench ($J \times m^{-3}$).

E_s = Stored energy at full field (J).

f_{cond} = Fraction of conductor inside the conduit of the CICC.

f_{Cu} = Fraction of stabilizing copper in the composite SC strands.

f_{rtnd} = Fraction of damage retained by copper after a room-temperature anneal.

I_{op} = Operating current at full field (A).

I_1, I_2, I_3 = Integral terms defined in text ($A^2 \times s^{-1} \times m^{-4}$).

J = Operating current density inside the conduit of a CICC ($A \times m^{-2}$).

$J_{c0}(B,\varepsilon)$ = Zero-temperature critical current density over the noncopper fraction of a composite SC strand at field and strain ($A \times m^{-2}$).

J_{c0m} = Maximum J_{c0} vs strain ($A \times m^{-2}$).

J_{pack} = Average current density over the winding pack ($A \times m^{-2}$).

ℓ_H = Length of CICC receiving a sudden heat impulse (m).

T_b = Bulk fluid temperature of the internal helium of a CICC at operating conditions (K).

$T_c(B,\varepsilon)$ = Critical temperature of the SC composite at a particular field and current (K).

T_{cm} = Maximum T_c vs strain (K).

T_{cs} = Current-sharing temperature of the superconductor at a particular field and current (K).

V_D = Terminal voltage resulting from a dump at full field (V).

η = Stability parameter.

$\mu_{He,init}$ = Density of the internal He in a CICC at the initial operating temperature and pressure (i.e., before a quench) (kg × m^{-3}).

μ_{core} = Density of the noncopper fraction of the composite superconductor (taken as 8920 kg × m^{-3} for MF-Nb_3Sn composites).

μ_{Cu} = Density of copper (taken as 8940 kg × m^{-3}).

$\rho_{Cu}(B)$ = Resistivity of the stabilizing copper at operating field (Ω × m).

ρ_s = Saturation value of stabilizer residual resistivity because of radiation damage (Ω × m).

ρ_0 = Residual resistivity (Ω × m). A subscript "init" indicates initial, undamaged value.

τ_H = Duration of a sudden heat impulse to the CICC (s).

4.4.4 TF Magnet Power Conversion Module (TFCPWR)

4.4.4.1 Code Description

The TF power conversion code TFCPWR calculates design and cost data for the equipment that interfaces with the TF magnets, which may have resistive (R) water-cooled coils, SC helium-cooled coils, or a combination of R and SC coils. The code uses pertinent input parameter data and computes the design and cost data for the load control centers, power supplies, coil protection equipment, power cables and bussing, and the associated I&C. It also provides an estimate of the building floor space and volume needed for the equipment.

Resistive coils do not require the energy removal protection system that is needed for the SC coils because they do not change state when the operating environment becomes unfavorable because of faulted equipment or operator error. The R coils require much more power than the SC coils, and they must be protected against the loss of coolant. This protection is generally an interruption of power to the R coils when loss of the water flow is detected. The following major categories of equipment are associated with the TF magnets:

1. load control center and power supplies required by the R or SC magnets,

2. power cables and/or electrical bussing between components in the R or SC magnet circuits,

3. local I&C for electrical currents and protection of the R or SC magnet circuits,

4. direct current (dc) circuit breakers and switches to isolate groups of SC coils for efficient transfer of energy to the dump resistors, and

5. energy dump resistors to dissipate most of the energy of the SC magnets during a fast discharge.

Figures 4.7 through 4.9 are general one-line diagrams that show the interconnections among these components for both the SC and R magnets.

The TF coil power conversion system module TFCPWR is based on the one-line diagram shown in Fig. 4.7. One or two low-voltage power supplies provide the current for charging and sustaining the TF coils. Sixteen TF coils are shown in the figure; this corresponds to the present design of the TIBER/ETR, but any even number of coils may be used. The TF coils are assumed to be paired off and connected to dc circuit breakers and dump resistors. A fast coil discharge is initiated by opening the dc circuit breakers (DCBR) and interrupting the power supplies. The SC coils are discharged through both series- and parallel-connected energy dump resistors. Switches (DCSW) are used to initiate a slow discharge of the TF coils.

Extensive local I&C is needed for quench protection of the TF coils, for programmed current control, and for the cryogen system operation. Monitoring of the TF coils requires a large number of instrumentation cables and local I&C as shown in Fig. 4.8. Because of the critical need for this I&C, redundancy is assumed to be necessary. The local I&C is therefore a significant cost item.

When R coils are a part of the design, the TFCPWR code assumes that the one-line diagram of Fig. 4.9 is applicable. Power conversion for R coils is generally more costly than for SC coils because very large controlled current power supplies are needed for hundreds of megawatts. Note that, in the figure, several large power supplies are

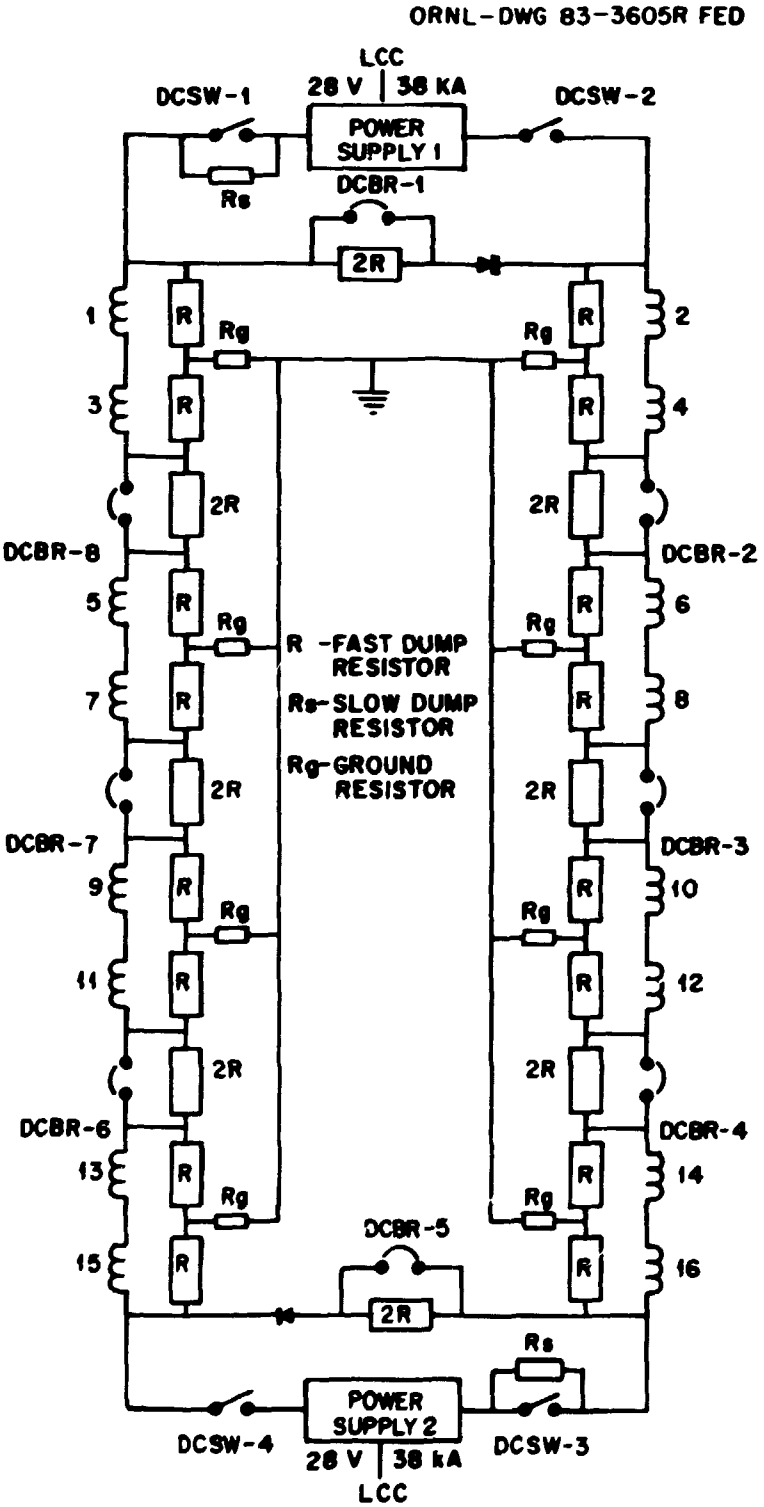

Fig. 4.7. Power conversion and protection system for the toroidal field magnets.

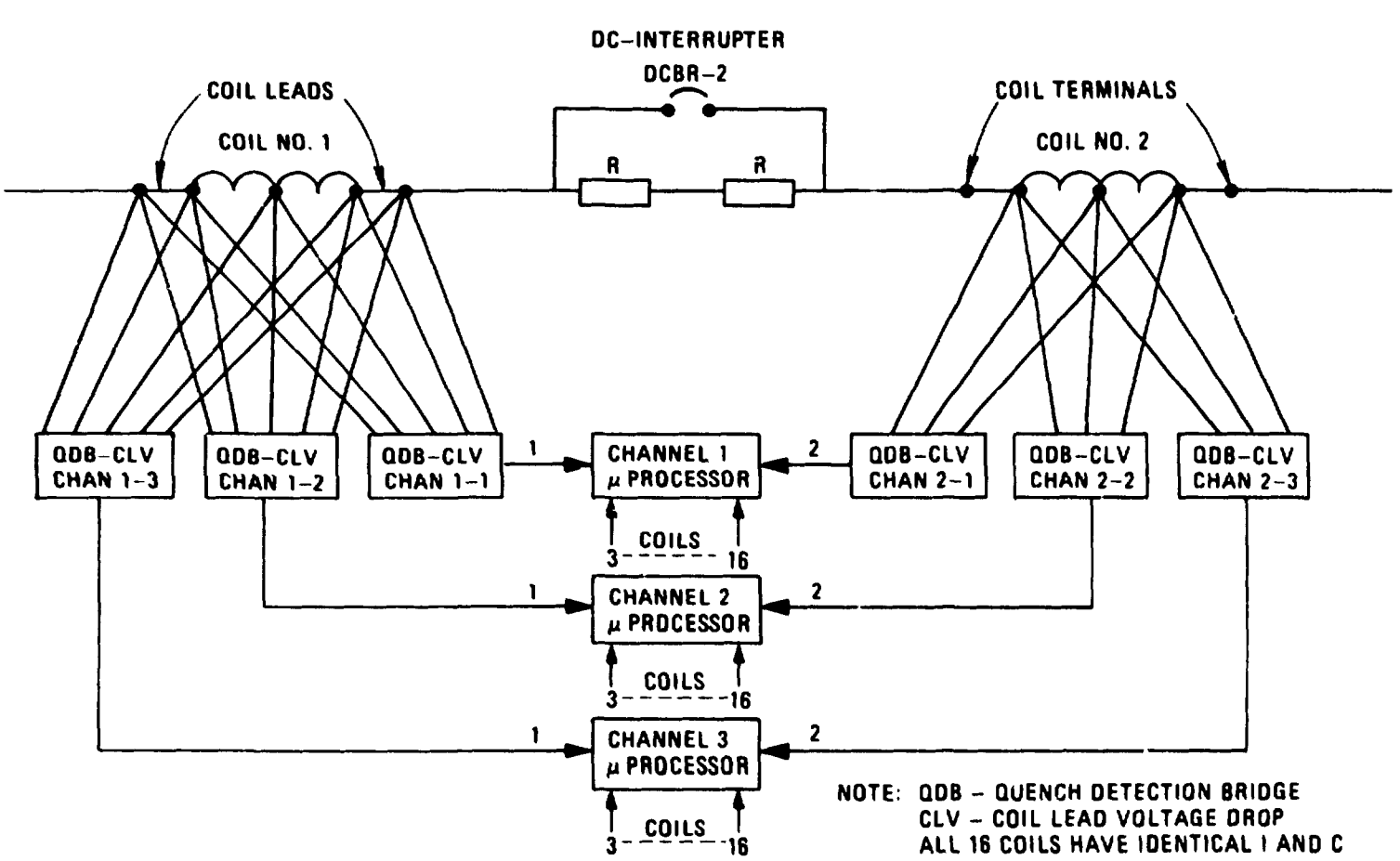

Fig. 4.8. Typical three-channel signal conditioning for the toroidal field coil protection system.

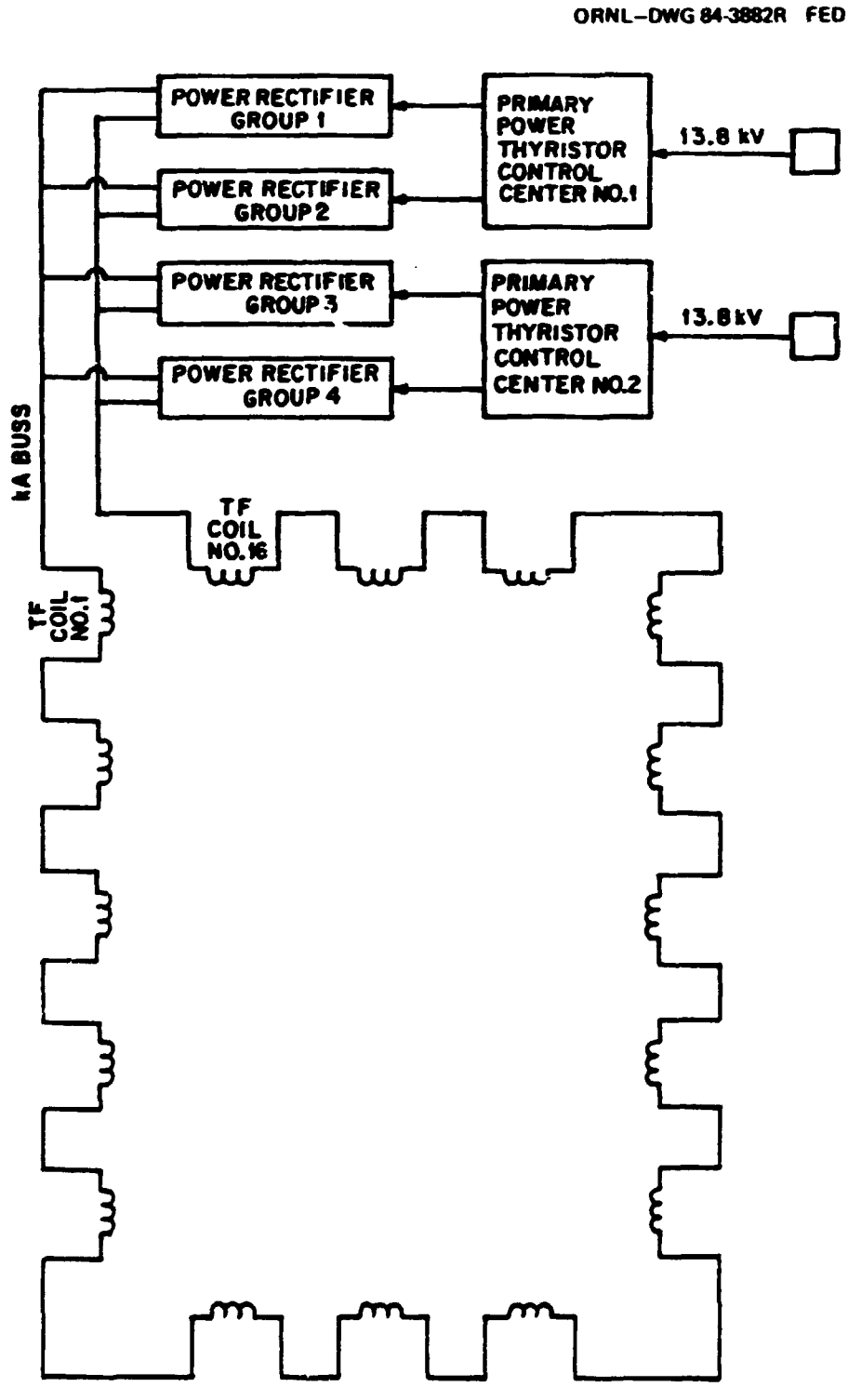

Fig. 4.9. Power conversion system for resistive toroidal field coils.

connected in parallel and controlled to provide the desired current. Large 13.8-kV circuit breakers are needed to provide fault protection.

4.4.4.2 TF coil power conversion input data

The input data needed for the TF power conversion module are given in Tables 4.10 and 4.11. The data in Table 4.10 are stored in a file that is rarely changed. It contains expert input data that should be changed only after consulting with a person knowledgeable about power conversion systems. The first column shows the mnemonic used by the code to identify the data. The second column relates the use of the data to the type of coils or equipment. If the data are related to the type of TF coil, the label SC, R, or SC/R is used to denote SC coils, R coils, or a combination of both. Other data are related to the electrical bussing, load center, power supply, dump resistors, or dc circuit breakers (i.e., BUS, LC, PS, DR, and BKR, respectively). Because the average user may not be familiar with the data range, lower and upper bounds are given in column 3.

Input data from the other code modules are given in Table 4.11, which is arranged in the same format as Table 4.10. An added entry, given in parentheses in column 1, identifies the source of the input data. The use of the parameter is given in column 2. The first and last entries of column 2 apply to both types of coils. In a hybrid system, which has both SC and R coils, all data in this table are used in the power conversion computations.

4.4.4.3 TF coil power conversion output data

The two types of power conversion output data are (1) data used by the other code modules and (2) data printed out for user evaluation.

Table 4.12 lists parameters needed for other TETRA systems code modules for computing the cost of equipment, for designing facilities, and for determining the load on the ac power system. The table has the same format as Tables 4.10 and 4.11. However, the first column contains not only the mnemonic for the parameter but also the output module identification, given in parentheses. The expected range in values, given in column 2, is relatively wide; the lower bound applies to

Table 4.10. User input data (for TFCPWR) from the expert data file

Code mnemonic	Code use	Expected range	Mnemonic description
TFPRT	SC/R	0.0 or 1.0	Print summary output only Print all output data
NCPBKR	SC	1 2	No. of TF coils per circuit breaker
KCOUP	SC/R	0.5 0.9	Coefficient of coupling between the R TF coils and the SC TF coils
TCHRHR	R	0.002 0.200	Ramp time to charge the R TF coils, h
TCHSR	SC	1.0 5.0	Ramp time to charge the SC TF coils, h
DJMKA	BUS	0.1 0.2	Design current density for the air-cooled bussing of the TF coils, kA/cm^2
RTFPS	PS	1.0 2.0	Multiplying factor for obtaining the power supply rating
ALCPKG	BUS	15 25	Cost of assembled aluminum bussing, \$/kg
CPKW1	LC	300 700	Cost coefficient of the TF coil load center, $\$/kW^{0.7}$
CPKW2	PS	1500 3000	Cost coefficient for the TF coil power supplies, $\$/kW^{0.7}$
CPMVA	BKR	0.004 0.008	Cost coefficient for the dc circuit breakers, $\$ \times 10^6/MVA$
CPMJ	DR	30 50	Cost coefficient for the dump resistors, \$/MJ
CPCHAN	I&C	1000 2000	Cost of one instrumentation channel, \$
FSPC1	SC/R	0.10 0.25	Floor area coefficient for the power supplies, $m^2/kW^{0.67}$
FSPC2	SC	0.60 1.00	Floor area coefficient for the dc circuit breakers, $m^2/kW^{0.67}$
FSPC3	SC/R	0.50	Floor area coefficient for the ac power load centers, $m^2/kW^{0.67}$

Table 4.11. Input data (for TFCPWR) from other systems code modules

Code mnemonic[a]	Code use	Expected range	Mnemonic description
NTFC	SC/R	8 16	Number of TF coil groups connected by circuit breakers
ETFRMJ	R	10 1000	Stored energy per R TF coil or TF coil group, MJ
ETFSMJ	SC	200 2000	Stored energy per SC TF coil or TF coil group, MJ
ITFRKA	R	50 500	Electrical current through the R TF coils, kA
ITFSKA	SC	5 50	Electrical current through the SC TF coils, kA
RPTFC	R	1×10^{-5} 2×10^{-3}	Resistance per TF coil, Ω
VTFSKV	SC	1 5	Maximum voltage across a TF coil during a fast discharge, kV
RMAJOR	R/SC	2 6	Major radius of the tokamak plasma, m

[a]All inputs except RMAJOR are from the TFCOIL module.

Table 4.12. Output data (from TFCPWR) to other systems code modules

Code mnemonic[a]	Expected range	Mnemonic description
ETTFMJ (COSTETR)	2000 20000	Maximum stored energy in all TF coils, MJ
ITFKA (COSTETR)	5 500	Maximum current through the TF coils, kA
NTFC (COSTETR)	8 16	Total number of TF coils
VTFSKV (COSTETR)	1 5	Maxium voltage across a TF coil, kV
TFCKW (COSTETR)	1 500	Available dc power for charging the TF coils, MW
TFBUSL (COSTETR)	300 1500	Total bus length of the TF coil system, m
DRAREA (BLDGS)	200 1000	Approximate area needed for the energy dump resistors, m^2
TFCFSP (BLDGS)	200 1000	Approximate floor area needed for the power conversion equipment, m^2
TFTBV (BLDGS)	1200 6000	Approximate building space needed for the power conversion equipment, m^3
TFACPD (ACPOW)	2 600	Approximate steady-state TF coil ac power demand, MW

[a]Parentheses contain the names of the modules to which the output data are sent.

SC TF coil equipment, and the upper bound applies to the R TF coil equipment.

A sample of the data printed out for user evaluation is given in Table 4.13. This table includes parameters passed on to other code modules, pertinent input data, and considerable design data for the user. If the user is not interested in all of these data, he can set the print option flag, TFPRT = 0, and only the summary data at the bottom of the table will be printed. The data in this table apply to one of the versions of the TIBER II tokamak design. Note that both the mnemonic label and a description of the data are given in the table.

4.4.4.4 Flow diagram for the power conversion module

The code flow diagram of the TF magnet power conversion module is given in Fig. 4.10. At the top of the diagram, following the subroutine call, the ITFPSWCH flag determines whether the interactive calculations of the systems code are finished. If they are not finished, ITFPSWCH = 0, and the subroutine calculations continue. Eventually, when the systems code calculations are completed, ITFPSWCH = 1, and the final printout is executed.

Input data are available on demand from the user's data file and from the TF magnet design module TFCOIL. The preliminary data calculations provide the initialization data and the logic data for one or two passes through the main program. The code statements represented by the diamond-shaped block labeled "hybrid option" determine whether one or two passes are needed.

If the TF coils are either all SC or all R, the left branch of the hybrid option decision block in Fig. 4.10 applies. The next decision block determines whether to use the SC coil branch or the R coil branch. If the coils are R, the path to the far left applies. NSPTFC is initially set equal to 1. Then, if ETTFR > 1, the value of NSPTFC is reduced to 0, and the code is initialized for R coil calculations, as shown at the lower right of the diagram. After the power conversion calculations are completed with one pass through the program, the detailed output data will be printed if TFPRT = 1. The value of NSPTFC

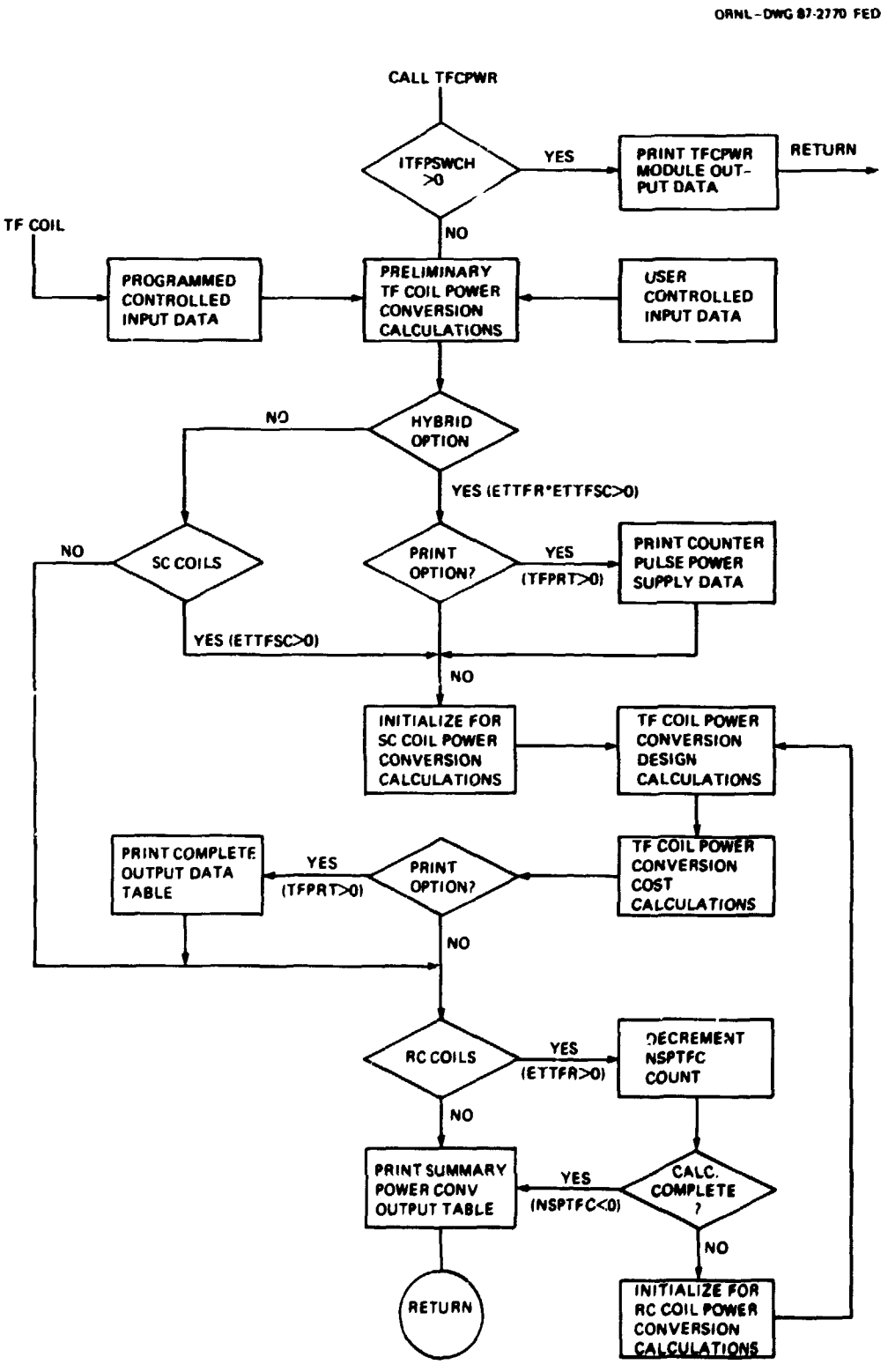

Fig. 4.10. Code flow diagram for the toroidal field magnet power conversion module TFCPWR.

Table 4.13. Toroidal field coil superconducting power conversion data

Variable	Description	Value
#ETTFMJ	Stored energy of TF coils, MJ	5104.0
#ITFKA	TF coil current, kA	38.89
#NTFC	No. of TF coils	16.00
#VTFSKV	Maximum voltage across coil, kV	10.00
TCHGHR	TF coil charge time, h	4.000
LTFTH	Inductance of all TF coils, H	6.749
RCOILS	Resistance of all TF coils, Ω	0
LPTFCS	Inductance per TF coil, H	0.4218
TFCV	TF coil charging voltage, V	85.24
NTFBKR	No. of dc circuit breakers	16.00
CTFBKM	Cost of dc circuit breakers, $ × 10^6	2.639
NDUMPR	No. of dump resistors	64.00
R1DUMP	Resistance of one dump resistor, Ω	0.2571
R1PPMW	Dump resistor peak power, MW	97.22
R1EMJ	Energy to a dump resistor, MJ	79.75
TTFSEC	L/R time constant of TF coils, s	1.640
CTFDRM	Cost of dump resistors, $ × 10^6	0.8966
TFPSC	Power supply voltage, V	89.50
TFPSKA	Power supply current, kA	40.83
#TFCKW	DC power supply rating, kW	3655.0
TFACKW	AC power for charging TF coils, kW	4061.0
RPOWER	TF coil resistive power, MW	2.606
XPOWER	TF coil inductive power, MW	0.7089
CTFPSM	Cost of TF supplies, $ × 10^6	0.7797
DJMKA	Aluminum bus current density, kA/cm^2	0.1250
ALBUSA	Aluminum bus section area, cm^2	311.1
#TFBUSL	Total length of TF bussing, m	2046.0
ALBUSWT	Aluminum bus weight, t	171.9
RTFBUS	Total TF bus resistance, mΩ	1.7232

Table 4.13. (Continued)

Variable	Description	Value
VTFBUS	TF coil bus voltage drop, V	67.02
CTFBSM	Cost of TF bussing, $ \times 10^6$	4.813
CTFLCM	Cost of TF load control center, $ \times 10^6$	0.1559
CTFCIM	Cost of control & instrumentation, $ \times 10^6$	1.010
CTFPCM	Total cost of TF power conversion, $ \times 10^6$	10.58
#DRAREA	Dump resistor area, m^2	598.7
#TFCFSP	TF power conversion floor space, m^2	829.3
TFCBV	TF power conversion building volume, m^3	4976.0
	TF coil power conversion summary	
CTFPCT	Total TF power conversion cost, $ \times 10^6$	10.58
XPWR W	Total TF ac inductive power demand, MW	0.7876
#TFACPD	Total steady-state ac power demand, MW	2.896
TFTSP	TF power conversion floor space, m^2	829.3
TFTBV	TF power conversion building volume, m^3	4976.0

#--Global outputs.

is then decremented to -1, and the decision block at the lower right of the diagram calls for printing out the summary table. If the coils are all SC, the program is initialized by the operations represented by the block in the center of the diagram and the SC coil power conversion calculations are performed. The detailed output table is then printed if TFPRT = 1. In all cases, the summary table is printed out as indicated at the lower part of the diagram.

If the hybrid case exists, both types of coils require power conversion. Counterpulse power supply data, associated with the hybrid case only, are then calculated as shown on the right side of Fig. 4.10. Then, the program is initialized for the SC coil power conversion pass. After these calculations are complete, the R coils decision block (RC) directs the path through the NSPTFC counter, and the R coil calculations are made as described earlier.

4.4.4.5 Fortran listing of the TF power conversion code

A Fortran listing of the TFCPWR code is stored in filem (see Sect. 3.4.6). All of the code mnemonics are identified at the beginning of the TF power conversion module listing, and they are grouped to correspond with the data given in Tables 4.10 through 4.12. Program inputs are followed by preliminary logic and calculations that correspond to those of the flow diagram. Decision statements are at or close to statement reference numbers 30, 35, 45, 105, 180, and 190. The SC coil power conversion initialization begins at statement 185.

4.4.5 PF Magnet Power Conversion Code Module (PFPOW)

4.4.5.1 Code description

The PF power conversion system subroutine PFPOW calculates design and cost data for the equipment that interfaces with the PF magnets, which may have water-cooled R coils, helium-cooled SC coils, or a combination of R and SC coils. The code reads pertinent input parameter data and computes the design and cost data for the load control centers, burn power supplies, pulsed power supplies, coil protection equipment, power cables and bussing, and the associated I&C. It also provides an estimate of the building floor space and volume needed for the equipment.

The R coils do not require the energy removal protection system that is needed for the SC coils because they cannot change their state when the operating environment becomes unfavorable because of faulted equipment or operator error. The R coils require much more power than the SC coils, and they require protection against the loss of coolant.

This protection is generally an interruption of power to the R coils when loss of the water flow is detected. The following major categories of equipment are associated with the PF magnets:

1. load control centers and burn power supplies for the PF magnets,
2. pulsed power supplies for the PF magnets,
3. power cables and/or electrical bussing between components in the R or SC magnet circuits,
4. local I&C for PF coil currents and protection of the R or SC magnets,
5. dc circuit breakers and switches to isolate groups of SC coils for efficient transfer of energy to the dump resistors, and
6. energy dump resistors to dissipate most of the energy of the SC magnets during a fast discharge.

Figure 4.11 through 4.13 are general one-line diagrams that show the interconnections among these components. The first figure shows that a number of power convertor modules must be connected in parallel to provide the required PF coil current. A dump resistor bank is connected in series with the coil that is normally bypassed with the dc circuit breaker and switch. If the power invertors fail to operate when an SC coil quench occurs, the two-way switch changes position, bypassing the power supply. The circuit breaker then opens so that the coil discharge is through the dump resistor bank, which absorbs most of the stored energy. The transient voltage suppressor is considered part of the local I&C that is not otherwise shown in the figure.

Figure 4.12 shows one type of module that may be connected in parallel with others as shown in the first figure. This module represents a two-quadrant power unit with a single-quadrant, low-voltage burn power supply unit in the middle. During the flattop part of the fusion cycle, the two outer pulsed power bridges are bypassed with the commutating thyristors. Some of the PF coils require current flow in both directions in different parts of the fusion cycle. Four-quadrant power supplies, like those shown in Fig. 4.13, are required. The lower part of the four-quadrant module is like that shown for the quadrant power supply in the second figure, but the additional antiparallel

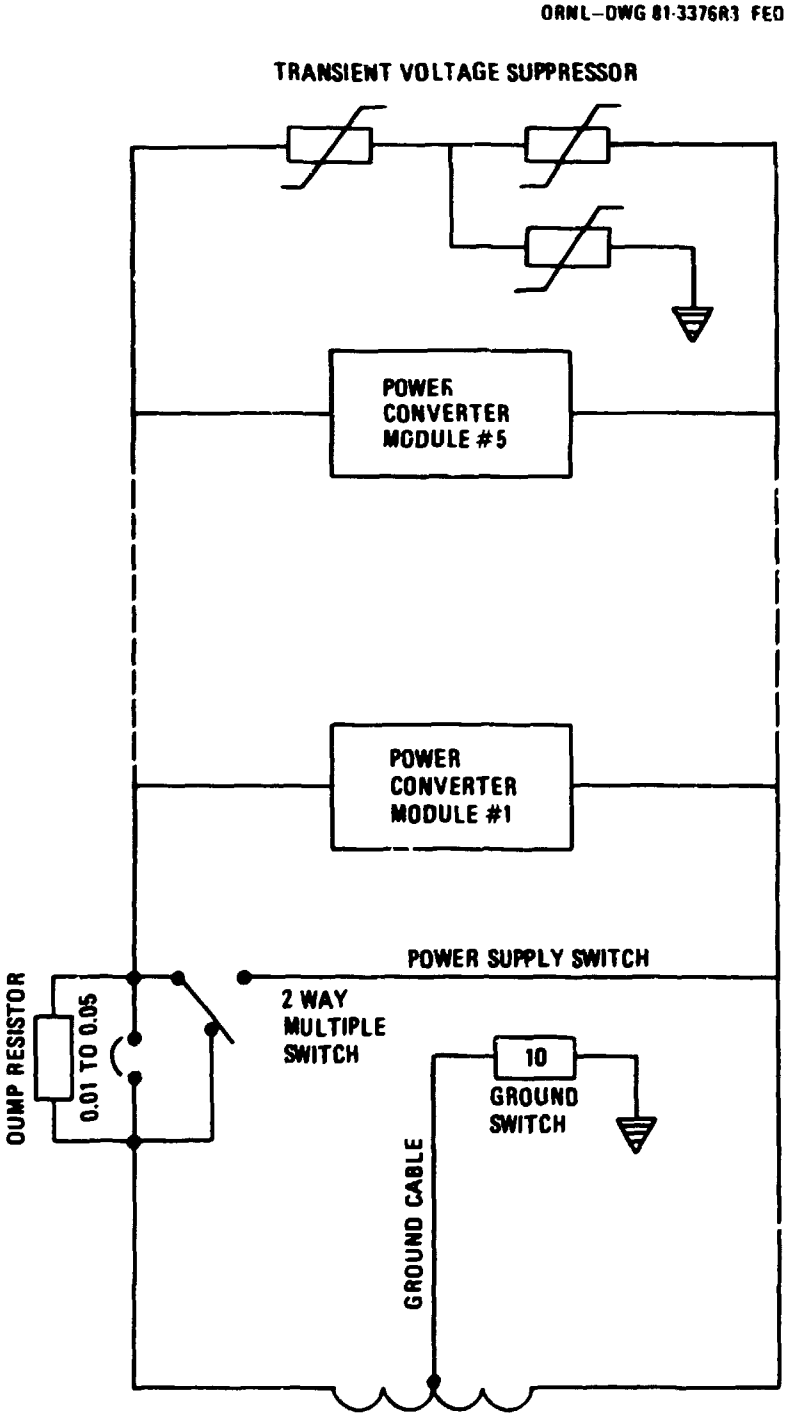

Fig. 4.11. One-line diagram of a superconducting poloidal field coil power conversion and protection system.

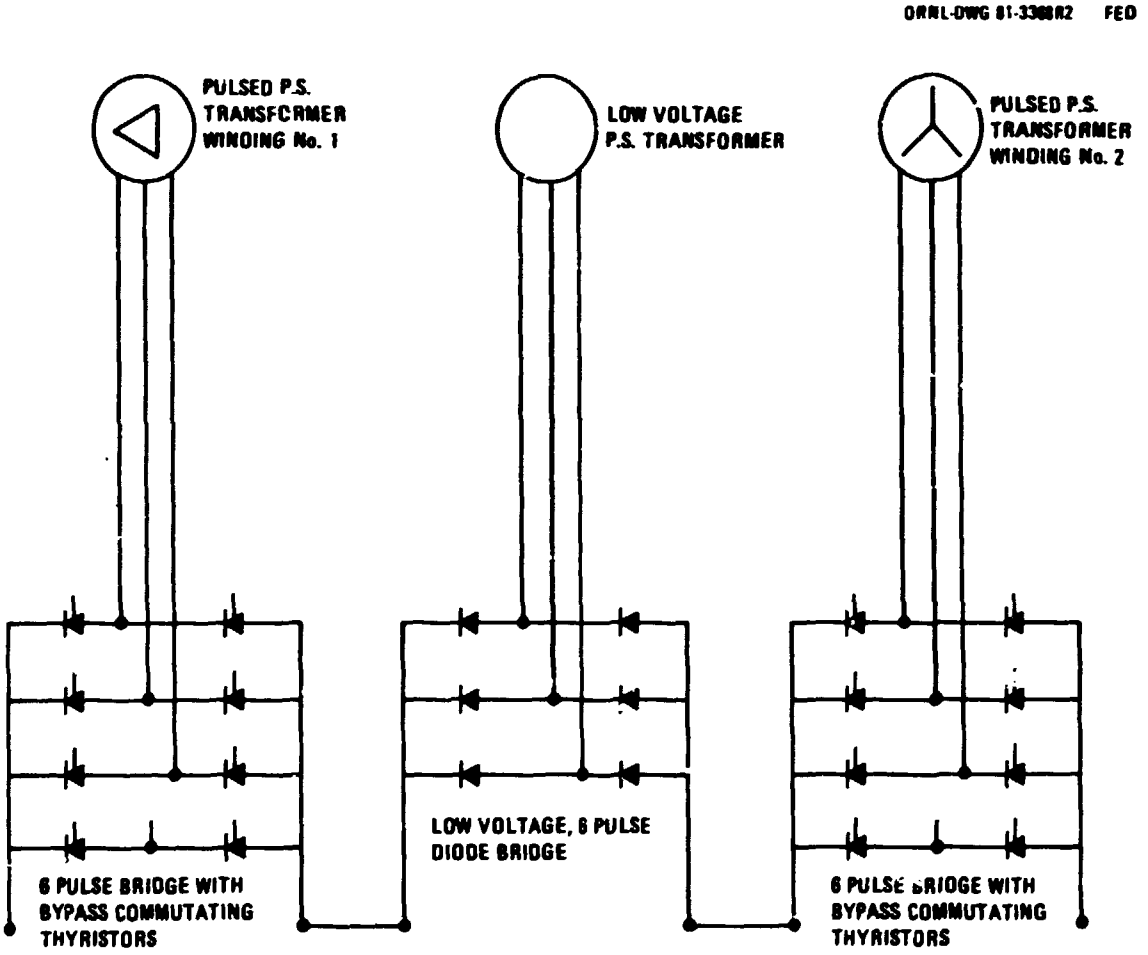

Fig. 4.12. A typical two-quadrant pulsed power supply module integrated with a low-voltage burn power supply unit.

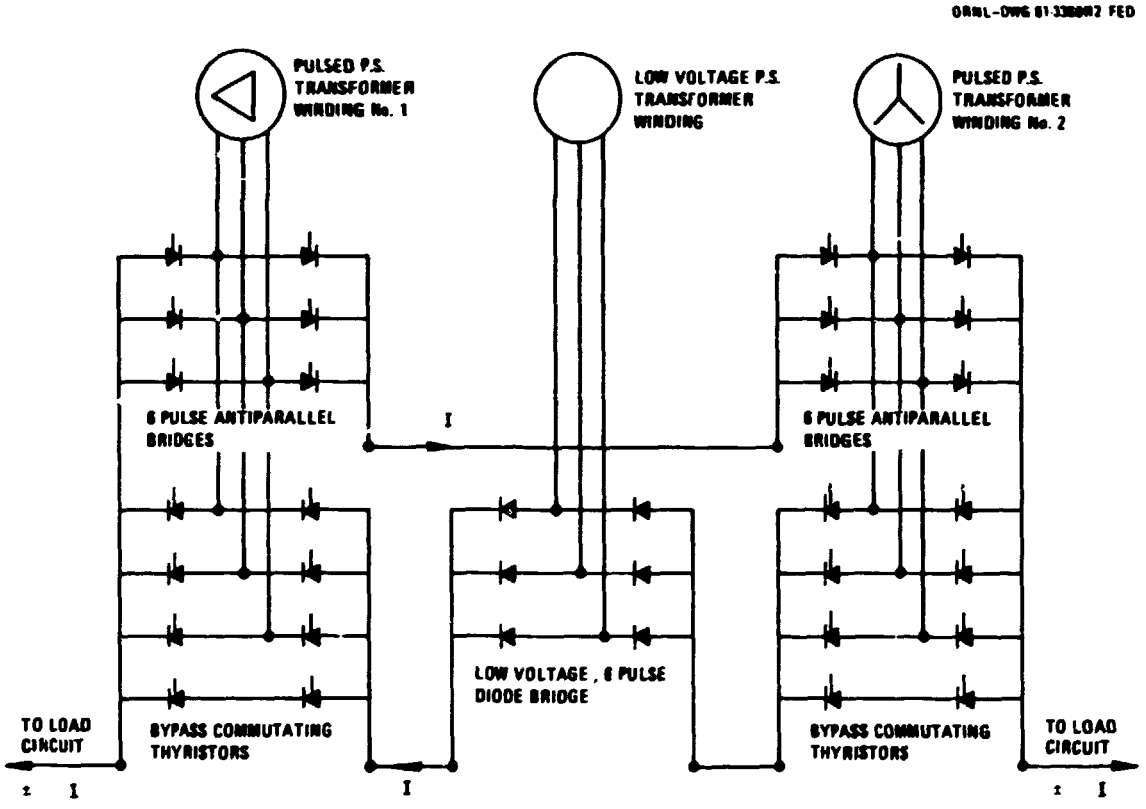

Fig. 4.13. A typical four-quadrant pulsed power supply module integrated with a low-voltage burn supply power unit.

bridges in the upper part of the figure are needed to carry current in the reverse direction.

The PFPOW code module uses the total swing in the power supply MVA to determine the cost of the power supply modules. The total MVA swing for a four-quadrant power supply is obviously more than for a two-quadrant supply. The code also provides a separate cost estimate for the burn power supply even though it will probably be integrated into the pulse power supply as shown in Figs. 4.12 and 4.13. Although the code now uses a power supply for each coil, as shown in Fig. 4.11, only one power supply with twice the voltage would actually be used for two identical symmetrical coils connected in series, as shown in Fig. 4.14. Alternately, the identical symmetrical coils could be connected in parallel to a power supply having the same voltage but twice the current rating, as shown in Fig. 4.15.

4.4.5.2 PF coil power conversion input data

The input data needed for the PF power conversion module are given in Tables 4.14 and 4.15. The input data of Table 4.14 are stored in a file that is changed infrequently by the user. It contains data that change as the tokamak design evolves. In Table 4.14, the first column identifies the mnemonic used by the code for the data, and the second column shows how the data are used. Because some users may not be familiar with the data, lower and upper bounds are given in column 3. The fourth column describes the data in some detail.

Input data from the other code modules are given in Table 4.15 in a format similar to Table 4.14. Column 1 defines the variable in the matrix format used by the code, where (I) and (J) refer to the PF coil circuit number and (K) refers to a time at the end of a current waveform segment. One limitation of the code is that the coil current waveforms must be presented in the form of line segments. The second column identifies the module that provides the input data. The expected ranges of the variables given in column 3 are generally valid but may exceed the limits by small margins. Ranges for coil current values are expressed in terms of positive currents, but the currents should be considered to be absolute values because they may be negative as well as positive.

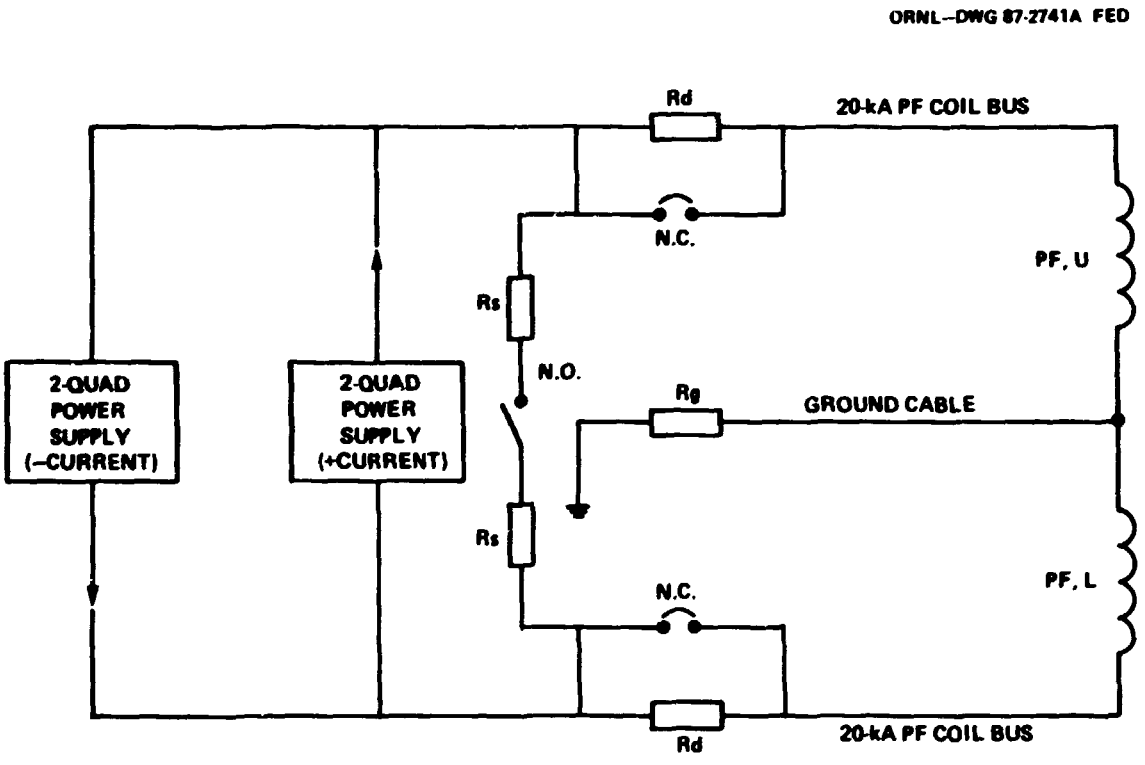

Fig. 4.14. One-line diagram of a poloidal field power conversion circuit with corresponding symmetrical coils connected in series.

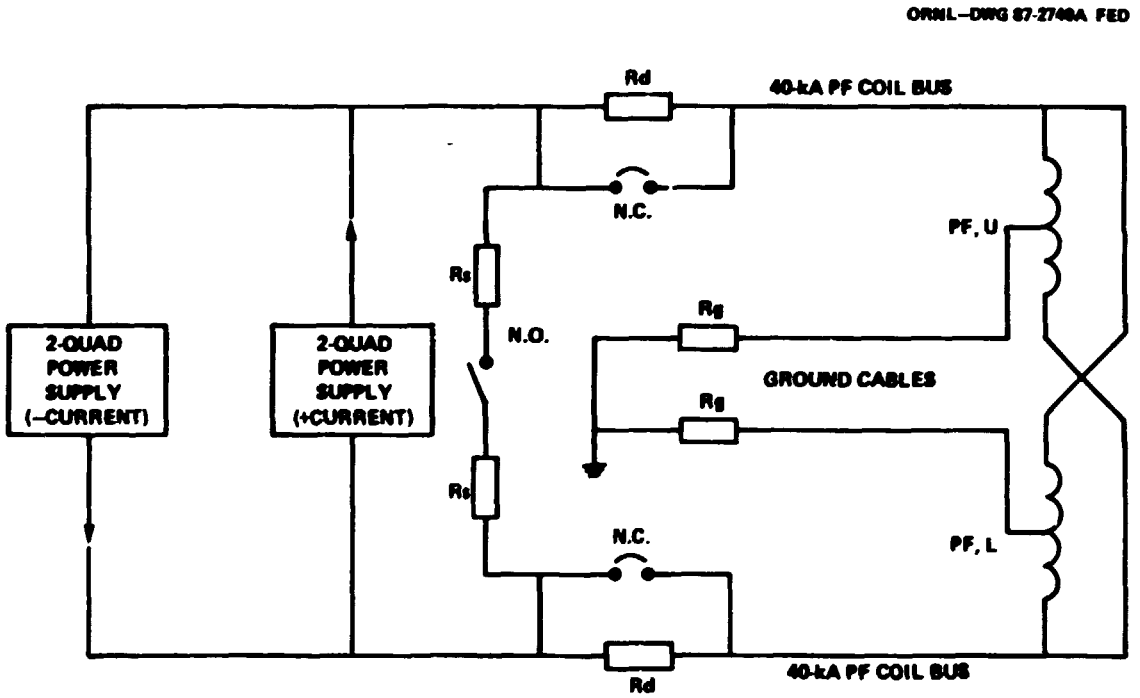

Fig. 4.15. One-line diagram of a poloidal field power conversion circuit with corresponding symmetrical coils connected in parallel.

Table 4.14. Input data (for PFPOW) from the user data file

Code mnemonic	Code use	Expected range	Mnemonic description
PFCR(J)	Compute PF coil circuit resistance	0.0-0.1 Ω	Terminal-to-terminal resistance of PF coil J
TTFRAMP	Compute TIM(2)	5-50 s	Time to complete the first segment of the current waveforms for the PF coils
TRAMP	Compute TIM(3)	5-50 s	Time to complete the second segment of the current waveforms for the PF coils
TOHS	Compute TIM(4)	5-50 s	Time to complete the third segment of the current waveforms for the PF coils
THEAT	Compute TIM(5)	1-20 s	Time to complete the fourth segment of the current waveforms for the PF coils
TBURN	Compute TIM(6)	50-1200 s	Time to complete the fifth segment of the current waveforms for the PF coils
TQNCH	Compute TIM(7)	5-30 s	Time to complete the sixth segment of the current waveforms for the PF coils
TTFQNCH	Compute TIM(8)	5-30 s	Time to complete the seventh segment of the current waveforms for the PF coils
RMAJOR	Compute PFBUS[	1-6 m	Plasma major radius

Table 4.15. Input data (for PFPOW) from other systems code modules

Code mnemonic	Input module	Expected range	Mnemonic description
CPT(I,K)	PFCOIL	0-100 kA	Current per turn of coil I at the end of time period K (A)
CPTD(I)	PFCOIL	20-100 kA	Maximum current per turn of coil I (A)
NCIRT	PFCOIL	5-18	Total number of PF coils, including the OH coils and the plasma. Plasma is # ncirt. OH coil is # ncirt-1
SXLG(I,J)	INDUCT	0-10 H	Inductance between coils I and J. Inductance matrix includes self-inductances (I = J)
WAVES(I,K)	PFCOIL	0-1	Normalized current in coil I at the time K

4.4.5.3 PF coil power conversion output data

The two types of power conversion output data are (1) data used by other code modules and (2) data that is printed out for user evaluation.

Table 4.16 lists parameters needed by other systems code modules for computing the cost of equipment, for designing facilities, and for determining the energy and power load on the energy storage and/or ac power system. The table has the same format as Table 4.15. Output data

Table 4.16. Output data (from PFPOW) to other systems code modules

Code mnemonic	Output module	Expected range	Mnemonic description
PEAKMVA	ESTORE	100 to 1000 MVA	Maximum peak MVA of all PF power supplies combined
ENSXPFM	ESTORE and COSTETR	1000 to 5000 MJ	Maximum stored energy in all PF circuits combined
ENGTPFM	ESTORE	4000 to 20000 MJ	Maximum dissipated energy per cycle for PF circuits combined
TFINAL = TIM(8)	ESTORE	200 to 2000 s	Fusion power pulsed cycle time
ENSRPF(5)	ESTORE	500 to 2500 MJ	Total energy to all PF coil circuits at the beginning of the burn phase
ENSRPF(6)	ESTORE	4000 to 20000 MJ	Total energy to all PF coil circuits at the end of the burn phase
TBURN	ESTORE	200 to 2000 s	Burn phase time interval
PFBLDGM2	BLDGS	500 to 2000 m^2	Required PF coil power conversion equipment floor area
PFBLDGM3	BLDGS	3000 to 12000 m^3	Required PF coil power conversion equipment space
SPSMVA	COSTETR	200 to 1500 MVA	Sum of the required MVA of all PF coil power supplies
PFCKTS	ESTORE and COSTETR	5 to 20	Number of PF coil power supply circuits = NCIRT - 1
SPFBUSL	COST	1000 to 4000 m	Sum of electrical bus length for all PF coil circuits
SRCKTPM	COST	1 to 5 MW	Sum of the maximum resistive power in all PF circuits
ACPTMAX	COST	10 to 50 kA	Average of the maximum current per turn of all PF coils
VPFSKV	COST	2 to 10 kV	Maximum allowable voltage across a PF coil

from the PF power conversion module are passed on to three other code modules; the energy storage system module (ESTORE), the facility module (FAC), and the cost computation module (COST), as shown in column 2.

Typical data printed out for the benefit of the user are given in Tables 4.17 and 4.18. At the top of Table 4.17, the power and the MVA of all of the PF coil circuits are listed at the time segment breakpoints of the coil current waveforms. Two values are given for each break point. One value corresponds to the slope of the current waveform (dI/dt) to the left of the breakpoint, and the other value corresponds to the slope to the right of the breakpoint. The resistive power depends only on the value of the current, not on the current derivative. Therefore, the power is the same on both sides of the breakpoint. Another table, not shown here, can be printed out to list the same data for each of the PF circuits. The data in Table 4.17 apply to one version of the TIBER II tokamak design.

The lower part of Table 4.17 lists the electrical data for each PF coil circuit power supply. Because some power supplies are two quadrant and some are four quadrant, the voltage and current swing data are used to determine power supply ratings and their cost estimates.

Table 4.18 shows additional data used to determine the cost estimate for each major category of equipment. The power conversion system cost estimates and the source data for determining the cost are grouped together for related equipment. The mnemonic is also given with the description of each parameter. The building floor space and volume requirements for the PF power conversion equipment are given in the lower part of the table.

4.4.5.4 Flow diagram for the power conversion module

The PFPOW code flow diagram for the PF coil power conversion module is shown on the three pages of Fig. 4.16. At the top of the first page, the IPRNT flag determines whether the iterative calculations for the module are complete or not. If incomplete, IPRNT = 0 and the subroutine calculations continue. Eventually, when the systems code calculations are complete, IPRNT = 1, and the final printout is executed.

ORNL-DWG 67-2706 FED
PART 1

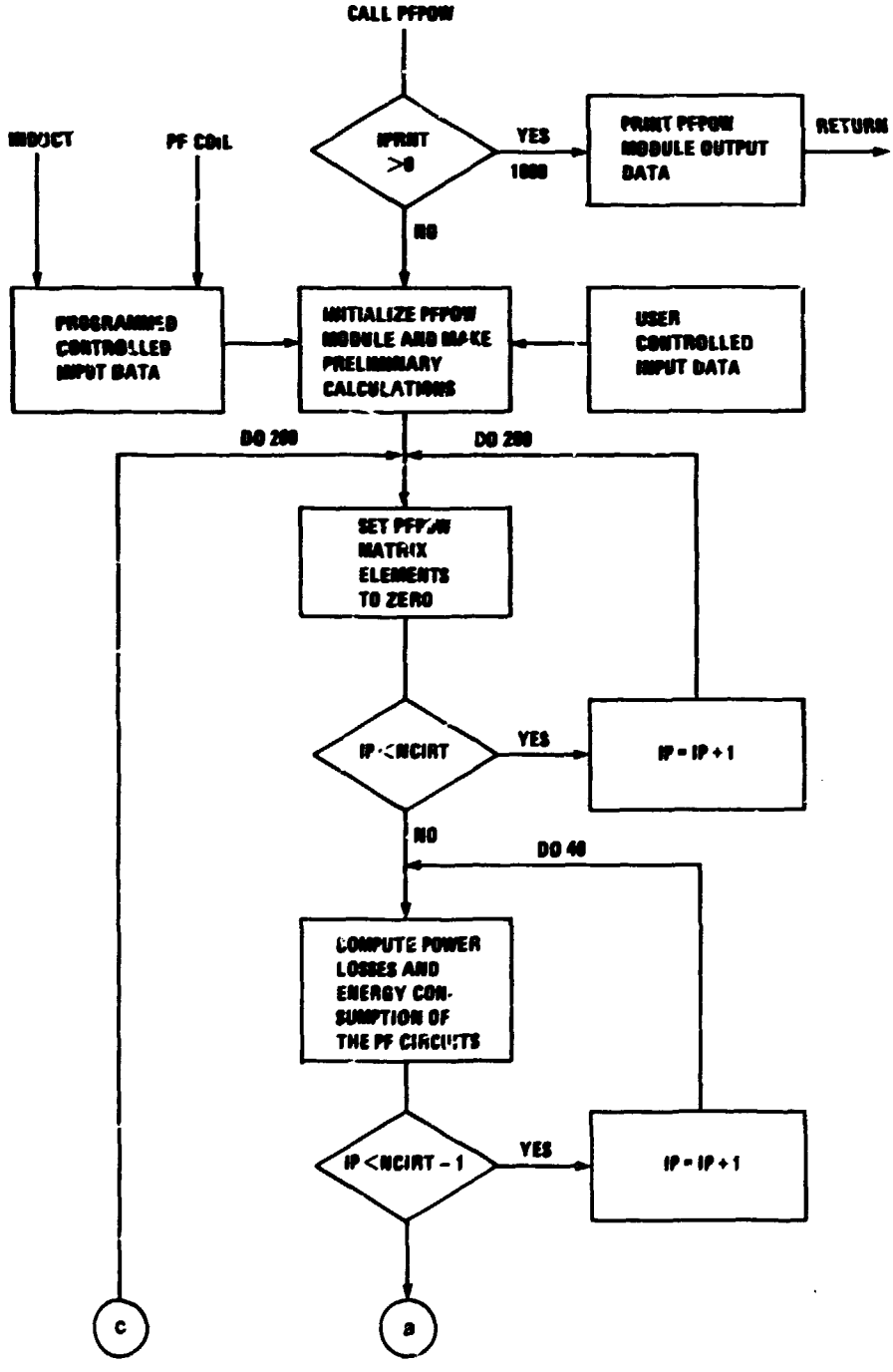

Fig. 4.16. Computer software flow diagram for the PFPOW module.

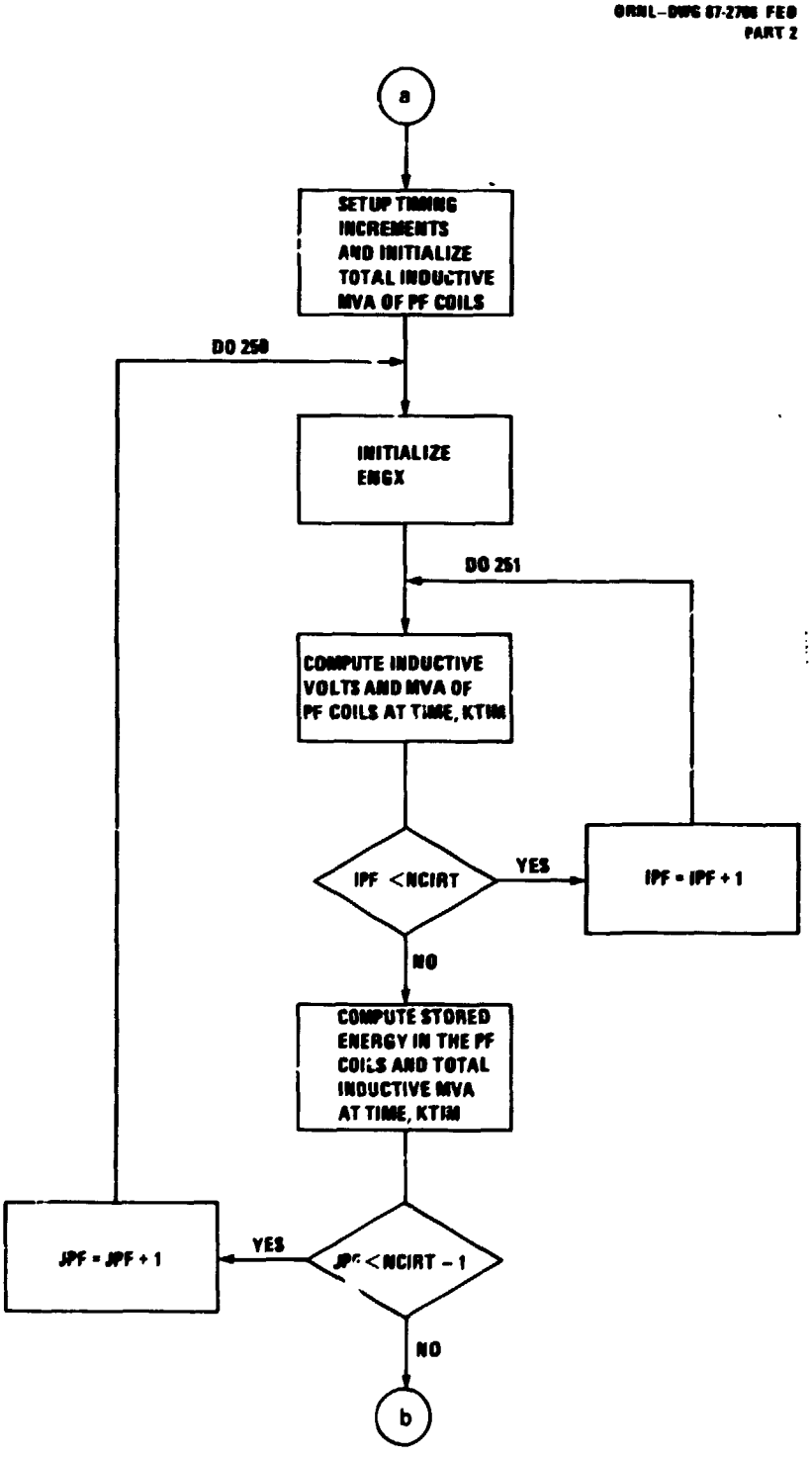

Fig. 4.16. (Continued)

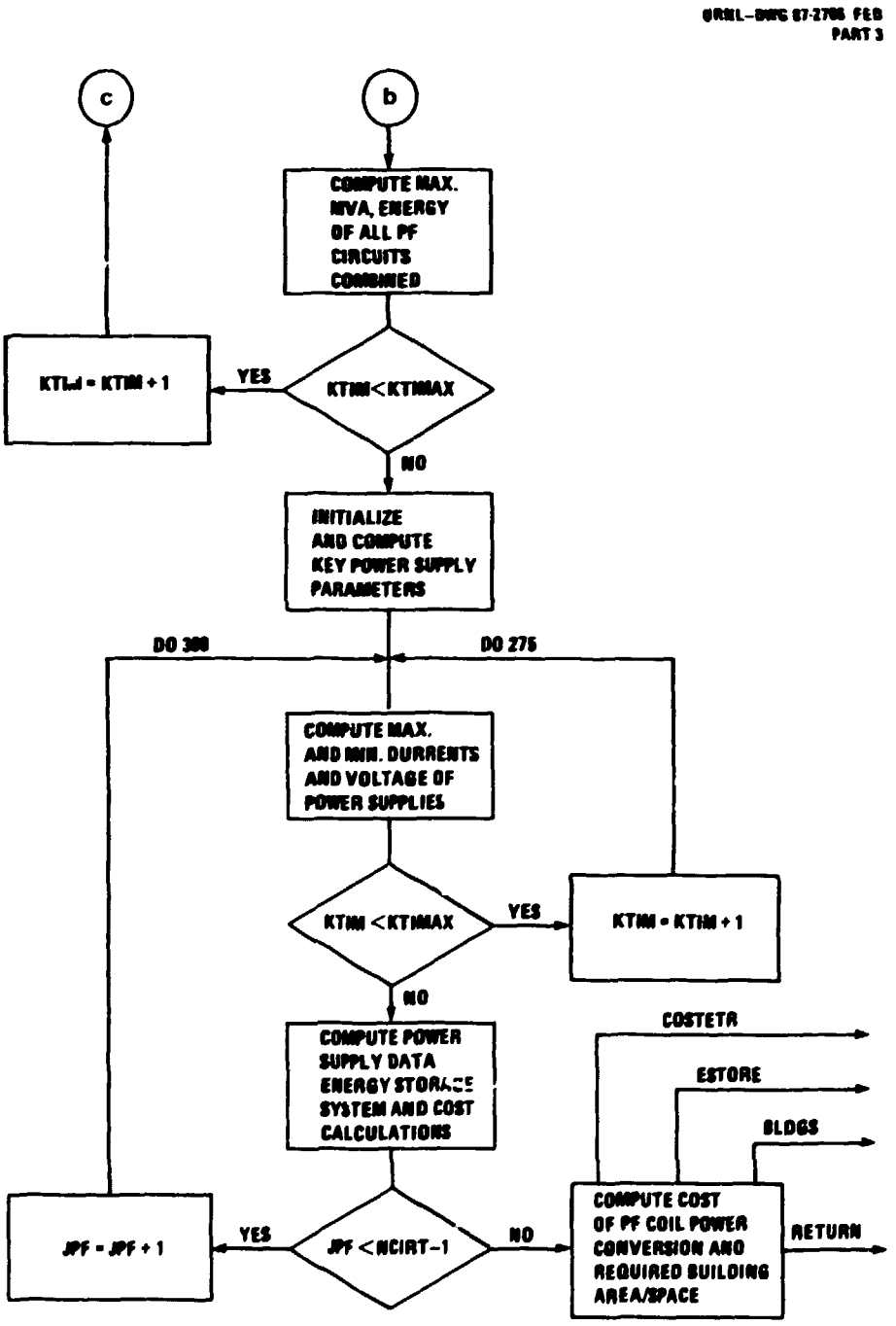

Fig. 4.16. (Continued)

Table 4.17. Poloidal field coil power conversion requirements

Time (s)	Resistive power (MW)	Total MVA
0	0	0
0	0	0
30	1.388	29.07
30	1.388	-30.23
50	1.738	121.1
50	1.738	26.50
56	1.933	28.48
56	1.933	3.526
156	2.148	3.847
156	2.148	-249.2
168	0	0
168	0	0

PF coil circuit No., PFCKT	Maximum voltage, VPFMAX (kV)	Minimum voltage, VPFMIN (kV)	Maximum current, CPTMAX (kA)	Minimum current, CPTMIN (kA)	MVA, PSMVA
1	0.1754	-0.2785	25	0	11.35
2	0.1754	-0.2785	25	0	11.35
3	0.2718	-0.8478	25	0	27.99
4	0.2718	-0.8478	25	0	27.99
5	0.0071954	-0.0060180	10.35	-25	0.4672
6	0.0071954	-0.0060180	10.35	-25	0.4672
7	0.8015	-0.5091	5.467	-25	39.93
8	0.8015	-0.5091	5.467	-25	39.93
9	2.141	-1.241	0	-25	84.53
10	2.141	-1.241	0	-25	84.53
11	0.2390	-0.2745	23.29	-25	24.79
12	0.2390	-0.2745	23.29	-25	24.79
13	1.696	-1.489	9.545	-22.57	102.3

Table 4.18. Additional data used to estimate cost for PFPOW

Variable	Description	Value
PFCKTS	No. of PF coil circuits	13.00
SPSMVA	Sum of PSMVA of all PF coil circuits	480.4
APSMVA	Average PSMVA of all PF coil circuits	36.95
TCPFPPSM	Cost of all pulsed power supplies, $ × 10^6	12.01
TCPFCIM	Cost of all PF circuit I&C, $ × 10^6	3.052
ARCKTPM	Average R power of the PF circuits, kW	199.9
ACPTMAX	Average maximum current/turn of the PF circuits, kA	24.81
SPFBUSL	Sum of the bus lengths of the PF circuits, m	2131.0
SRCKTPM	Sum of resistive power in PF circuits, kW	2598.0
TCPFBSM	Cost of all PF bussing, $ × 10^6	2.644
TCPFBPSM	Cost of burn phase power supplies, $ × 10^6	2.504
VPFSKV	Maximum PF coil voltage, kV	5.000
ENSXPFM	Maximum sum of stored energy in PF circuits, MJ	1508.0
TCPFBKM	Cost of all dc circuit breakers, $ × 10^6	1.899
TCPFDRM	Cost of all energy D-resistors, $ × 10^6	0.2158
TCPFSM	Total cost of PF conversion system, $ × 10^6	22.41
ENGTPFM	Maximum resistive energy of all PF circuits over the entire cycle, MJ	1589.0
BPSFM2	Floor area of the burn power supplies of the PF coils, m^2	444.2
PPSFM2	Floor area for the pulsed power supplies of the PF coils, m^2	576.9
BKRFM2	Floor area for the dc circuit breakers, m^2	323.9
PFBLDGM2	Total building floor area for the PF coil power supplies, m^2	1345.0
PFBLDGM3	Building volume for the PF coil power supplies, m^3	8070.0

During the iterative calculations, the PFPOW subroutine uses the most recent data from the inductance matrix module INDUCT and the PF coil module PFCOIL. Before entering the major DO 200 loop, the program initializes module parameters and performs preliminary time-step calculations. A DO 30 loop, which sets some vector parameters equal to zero, is part of this block.

The PFPOW code module uses many nested DO loops to perform matrix and vector calculations. Calculations are made on both sides of the current waveform breakpoints for each PF coil. The outer DO 200 loop index is therefore KTIM, the time coordinate of the current breakpoints. The inner DO 209 loop sets the pertinent vector and matrix elements to zero before making calculations at each time coordinate. The DO 40 loop computes the power and energy losses in each of the PF circuits at time KTIM. The DO 250 loop, shown on the second page of Fig. 4.16, computes the inductive voltage drop, the inductive MVA, and the energy storage for each PF coil at time KTIM. The first block at the top of the third page of Fig. 4.16 computes the maximum MVA and energy of all PF circuits combined at time KTIM. The DO 200 loop is then incremented, and the process repeats for the next KTIM.

After completing the calculations of the DO 200 loop, the program initializes for the power supply calculations for each of the PF coil circuits. The power supply calculations are then performed by the DO 300 loop, shown on the third page of Fig. 4.16. Nested inside the DO 300 loop is a KTIM DO 275 loop that determines the maximum and minimum voltages and currents that must be provided by the power supplies. The differences between the maximum and the minimum currents and voltages are multiplied together outside the DO 275 loop to provide the maximum swing in the MVA for each circuit. The maximum MVA swing is used to determine the cost of power supplies. Other data needed for the energy storage system module ESTORE are also calculated. Finally, outside the DO 300 loop, cost estimates are computed for the PF power conversion system and the building floor area and space requirements. Flow diagram outputs to other systems code modules are shown in the lower right corner.

4.4.5.5 Fortran listing of the PF power conversion code

The Fortran listing of the PFPOW code is part of a separate document containing the total code listing (see Sect. 3.4.6). This document is available for reference use. The code mnemonics are identified at the beginning of the PFPOW list and are grouped to correspond to Tables 4.14 through 4.16. Program inputs are followed by initialization statements, preliminary logic, and DO loop calculations that correspond to those of the flow diagram described earlier. Comment statements are interspersed between and inside the many DO loops so that one can follow the code and change or add to the program as future needs develop. The inductance matrix module INDUCT of the systems code now provides an output for each coil; therefore, a power supply is required for each PF coil. In the future, it will be desirable for INDUCT to combine like symmetrical coils into one circuit so that the power supply calculations are for one power supply connected in series with two pairs of coils.

4.4.6 Energy Storage System Code Module (ESTORE)

4.4.6.1 Code description

The energy storage system subroutine ESTORE calculates electrical design parameters and the cost of an MGF energy storage system for the pulsed plasma heating and the PF coil loads. Costs of the ac circuit breakers and the power feeders between the energy storage source and the PF coil power supplies are also included in this module. One of the limitations of this code module is that the energy source for cost estimation is MGF units, the utility line, or a combination of both. A software switch labled ISCENR is set by the user to integers 1, 2, or 3, corresponding to the following energy source selections:

1 = MGF units provide energy for all the pulsed power loads;

2 = the utility power line provides energy for all the pulsed power loads; and

3 = MGF units provide energy for the PF coil loads, and the utility power line provides energy for the plasma current drive and burn power supply loads.

The code module uses input data from the PF coil power conversion module PFPOW and the plasma current drive power module CUDRIV. The input data are used to determine the energy storage system requirements for the selected energy source(s). Costs of the MGF units and their support equipment are calculated if the ISCENR switch is set to 1 or 3. The energy storage system module also calculates the pulsed MVA and the MW loads on the utility power line when the ISCENR switch is set to 2 or 3. The total MVA and MW loads are used by the ac power module to calculate the size and cost of the capacitor bank to correct the power factor to about 0.95.

Figure 4.17 is a one-line diagram that shows the energy storage system and its interfaces with the PF power conversion system, the auxiliary heating power system, and the ac power system. The auxiliary heating power system includes power and energy needed for electron cyclotron heating, ion cyclotron heating, LH current drive, NBI, and the PF coils during the burn phase. The two double-pole, double-throw electrical switches, with poles A through H, represent the software switch ISCENR. The insert table in the figure shows the positions of the switch poles corresponding to ISCENR = 1, 2, and 3. Figure 4.18 is a block diagram that describes the functions of the input/output (I/O) interface modules and their relationship to the energy storage system module ESTORE.

4.4.6.2 Energy storage system module input data

Tables 4.19 and 4.20 define the input data needed by ESTORE. The data in Table 4.19 are located in data files or statements that may be changed by the user only. The data in Table 4.20 are provided by other subroutines or modules not directly under user control.

Only the first entry in Table 4.19, the software switch ISCENR, is likely to be changed frequently, and for that reason this entry is placed in a more accessible common file. Other input data in Table 4.19

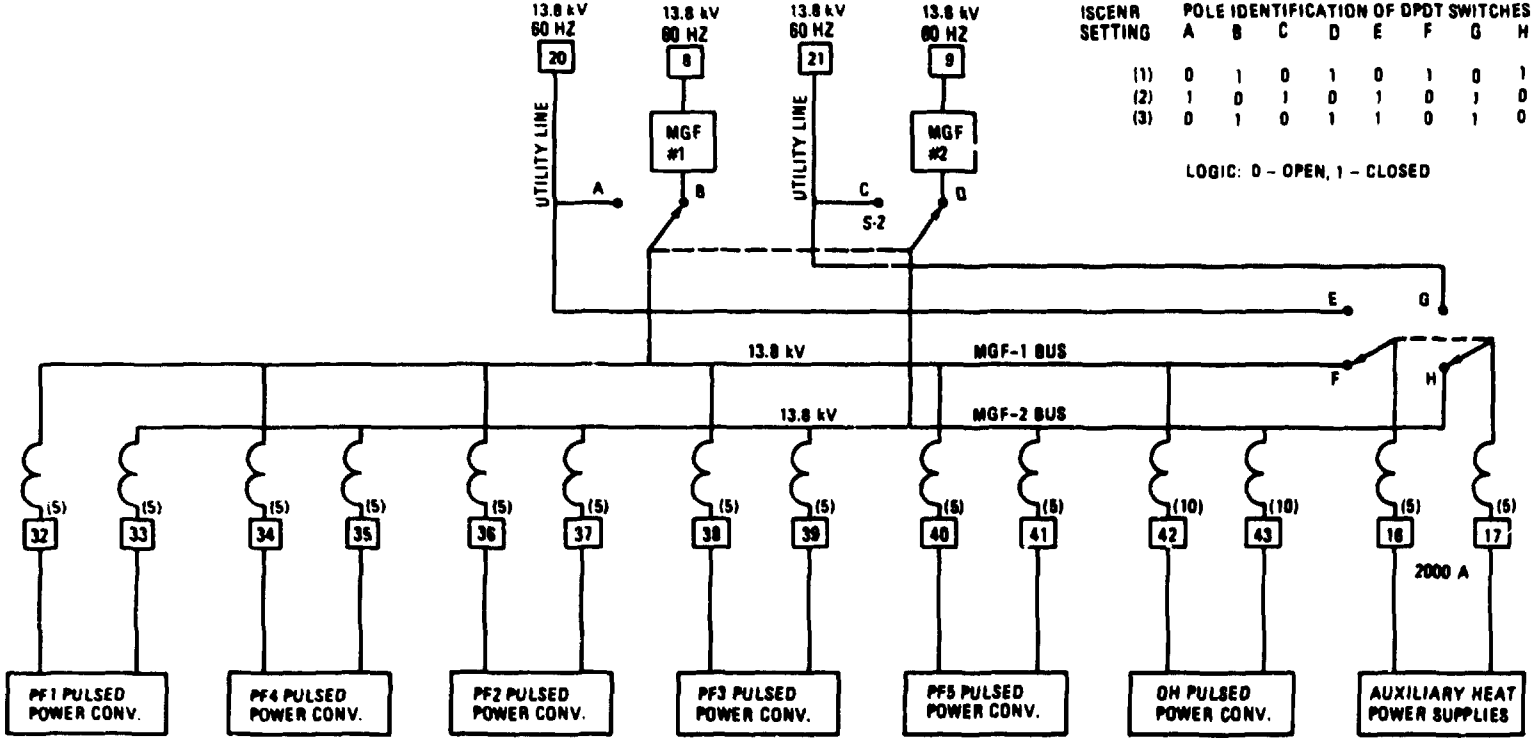

ISCENR SETTING	POLE IDENTIFICATION OF DPDT SWITCHES A	B	C	D	E	F	G	H
(1)	0	1	0	1	0	1	0	1
(2)	1	0	1	0	1	0	1	0
(3)	0	1	0	1	1	0	1	0

LOGIC: 0 - OPEN, 1 - CLOSED

Fig. 4.17. One-line diagram of the energy storage system with the ISCENR switching logic.

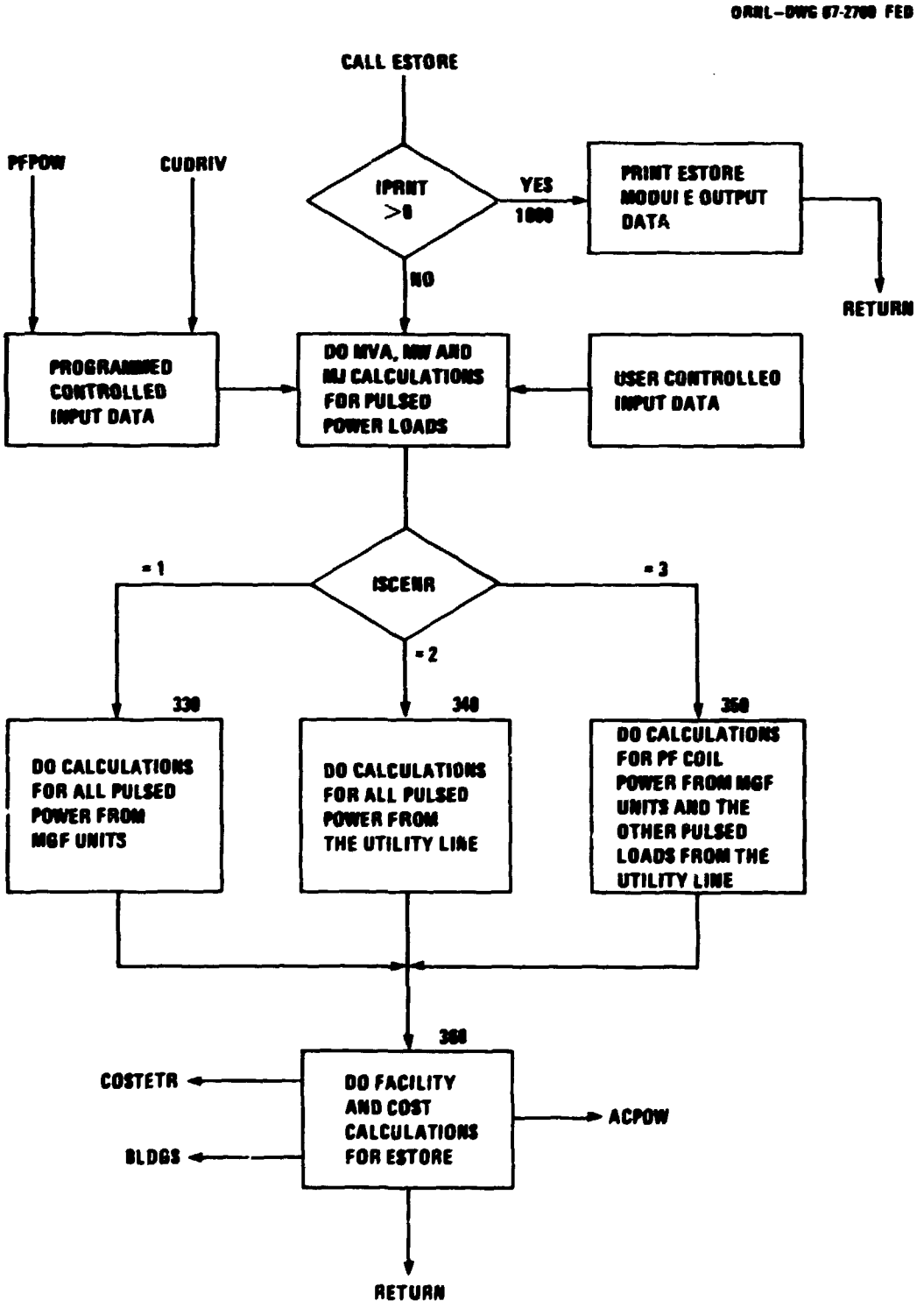

Fig. 4.18. Block diagram of the energy storage module and its interfaces with other code modules.

Table 4.19. User-controlled input data for ESTORE

Code mnemonic	Default value	Expected range	Mnemonic description
ISCENR	None	1, 2, or 3	User-controlled software energy storage source selector switch
PSEFF	0.92	0.88 to 0.95	Average efficiency of the pulsed power supplies
EREFF	0.75	0.60 to 0.80	Average energy recovery efficiency from the PF coils
DMEFF	0.80	0.65 to 0.85	Average efficiency of a variable-speed drive motor for an MGF unit
PWRFAC1	0.60	0.50 to 0.70	Average power factor for the PF coil power conversion
PWRFAC2	0.85	0.80 to 0.90	Average power factor for all power supplies except those for the PF coils
PWRFAC3	0.75	0.70 to 0.80	Average power factor for a variable-speed drive for an MGF unit

are changed very infrequently and thus are placed in data statements that are part of the subroutine. The default values given in column 2 are the recommended values that will be used by the ESTORE subroutine unless the user makes a change in the pertinent data statement.

Input data from two other code modules are identified in Table 4.20. Except for column 2, which lists the acronym of the module providing the input data, this table has the same format as Table 4.19. Only two modules provide input data: the PF coil power conversion module PFPOW and the plasma current drive/heating module CUDRIV. The expected ranges given for the data in column 3 are fairly wide to allow for wide variations in the design optimization of tokamak reactors.

4.4.6.3 Energy storage system module output data

The energy storage module, like most of the other modules or subroutines, computes (1) output data needed as inputs to other modules and (2) other design/cost data that are printed out for user evaluation.

Table 4.20. Input data (for ESTORE) from other systems code modules

Code mnemonic	Input module	Expected range	Mnemonic description
PEAKMVA	PFPOW	100 to 1000 MVA	Maximum peak MVA of all PF power supplies combined
ENSXPFM	PFPOW	1000 to 5000 MJ	Maximum stored energy in all PF coil circuits combined
ENGTPFM	PFPOW	4000 to 20000 MJ	Maximum dissipated energy per cycle for all PF coil circuits combined
TFINAL = TIM(8)	PFPOW	200 to 2000 s	Pulsed fusion power cycle time
ENSRPF(5)	PFPOW	500 to 2500 MJ	Total energy to all PF coil circuits at the beginning of the burn phase
ENSRPF(6)	PFPOW	4000 to 20000 MJ	Total energy to all PF coil circuits at the end of the burn phase
TBURN	PFPOW	200 to 2000 s	Burn phase time interval
PFCKTS	PFPOW	5 to 20	No. of PF coil power supply circuits (NCIRT - 1)
PHEATMW	CUDRIV	50 to 200 MW	Average plasma current drive/ heating power
PHTGMJ	CUDRIV	4000 to 20000 MJ	Plasma current drive/heating energy per fusion power cycle

Table 4.21 lists output parameters needed by other code modules for computing design/cost of the equipment and facilities and for determining the pulsed and steady-state power loads on the ac power system. The output table format is the same as Table 4.20 except for column 2, which identifies the acronyms of the modules receiving output data from the ESTORE modules. The first two entries in Table 4.21 are used by the ac power module ACPOW to determine the electrical parameters and cost of a capacitor bank needed to increase the power factor so that it is between 0.95 and 1.00 during the startup power pulse. Table

Table 4.21. Output data (from ESTORE) to other systems code modules

Code mnemonic	Output module	Expected range	Mnemonic description
ULPMW	ACPOW	100 to 800 MW	Maximum pulsed power from the utility power line
ULPMVA	ACPOW	200 to 1200 MVA	Maximum pulsed MVA from the utility power line
ESBLDGM2	BLDGS	75 to 300 m^2	Building floor space needed for the energy storage system
ESBLDGM3	BLDGS	500 to 2000 m^3	Building volume needed for the energy storage system
ACCKAM	COSTETR	40,000 to 200,000 kA-m	Total kA-m of 13.8-kV power feeder cable
FMGMVA	COSTETR	200 to 1200 MVA	Maximum MVA of the MGF units combined
FMGMJ	COSTETR	2000 to 10,000 MJ	Energy taken from the MGF units per pulsed fusion cycle

entries 3 and 4 are inputs used by the facilities code BLDGS to determine the size and cost of buildings for the energy storage system. The remaining entries are used to determine the cost of power feeder cables, ac circuit breakers, and MGF units.

Typical data, printed out for user evaluation, are given in Table 4.22. At the top of the table are values of the burn time, cycle time, and user-controlled inputs. The second block of data in the table is the total PF coil and plasma current drive/heating power and energy data that are independent of the software switch ISCENR setting. Electrical characteristic data for an energy storage system are given in the third block. This block of data is set equal to zero if the software selector switch is set equal to 2, corresponding to taking all the pulsed load power from the utility line. The last block of data in the table consists of utility line electrical power and energy data and the floor area and building volume data.

4.4.6.4 Flow diagram for the energy storage system module

Figure 4.19 is a code flow diagram for the energy storage system module. At the top of the diagram, following the subroutine call, the

Table 4.22. Additional data used to estimate cost for ESTORE[a]

Variable	Description	Value
	Energy Storage System Parameters	
TBURN	Burn time, s	100.0
TFINAL	Total cycle time, s	168.0
PSEFF	Power supply efficiency	0.9200
EREFF	Energy recovery efficiency	0.7500
DMEFF	MGF drive motor efficiency	0.8000
PWRFAC1	Pulsed power supply power factor	0.6000
PWRFAC2	Plasma heating power supply power factor	0.8500
PWRFAC3	MGF drive motor power factor	0.7500
	Power Supply Energy and Load Data	
ACPFMVA	Peak ac MVA of the PF coil power supply	219.4
ACPHMVA	Peak MVA of the plasma heating power supply	220.9
ACPTMVA	Total peak MVA = ACPFMVA + ACPHMVA	440.3
ACPTMW	Total peak power demand, MW	319.4
PHTGMJ	Plasma heating energy/cycle, MJ	1.7278×10^4
ENGTPFM	Energy to PF coil power supply/cycle, MJ	1589.0
ACPTMJ	Total pulsed energy/cycle, MJ	2.0507×10^4
	MGF Energy Storage Data	
FMGMW	Maximum MGF power output, MW	0
FMGMVA	Maximum MGF MVA output	0
FMGMJ	MGF energy/cycle, MJ	0
FMGRMJ	Energy recovery/cycle, MJ	0
FMGDMW	Average power to MGF motor, MW	0
FMGDMVA	Average MVA to MGF motor	0

Table 4.22. (Continued)

Variable	Description	Value
	Power and Energy from the Utility Line	
ULPMW	Maximum pulsed MW from utility line	319.4
ULPMVA	Maximum pulsed MVA from utility line	440.3
ULPMJ	Pulsed energy from utility line, MJ	2.0507×10^4
FLCCFM2	Floor area needed for the load control center, m^2	69.59
FMGFM2	Floor area needed for MGF units, m^2	0.0
ESBLDGM2	Building floor area for the energy storage system, m^2	69.59
ESBLDGM3	Building volume space for the energy storage system, m^3	417.6
	Energy Storage System Cost Data	
COFFCM	Cost of ac power feeder cables, $\$ \times 10^6$	0.8980
COACPM	Cost of ac power protection circuit breakers and current-limiting reactors, $\$ \times 10^6$	3.226
COFMGM	Cost of MGF energy storage units, $\$ \times 10^6$	0.0
TCESSM	Total cost of energy storage system, $\$ \times 10^6$	4.124

[a]For the option where all pulsed power is taken from the utility grid.

IPRNT flag determines whether the interactive calculations of the systems code are finished. If not, IPRNT = 0, and the subroutine calculations continue. Eventually, when the systems code calculations are completed, IPRNT = 1, and the final printout is executed.

During the interactive calculations, the subroutine uses the most recent data from the PF power conversion module PFPOW and from the plasma current drive/heating module CUDRIV. The electrical parameters of the pulsed loads do not depend on the setting of the ISCENR software

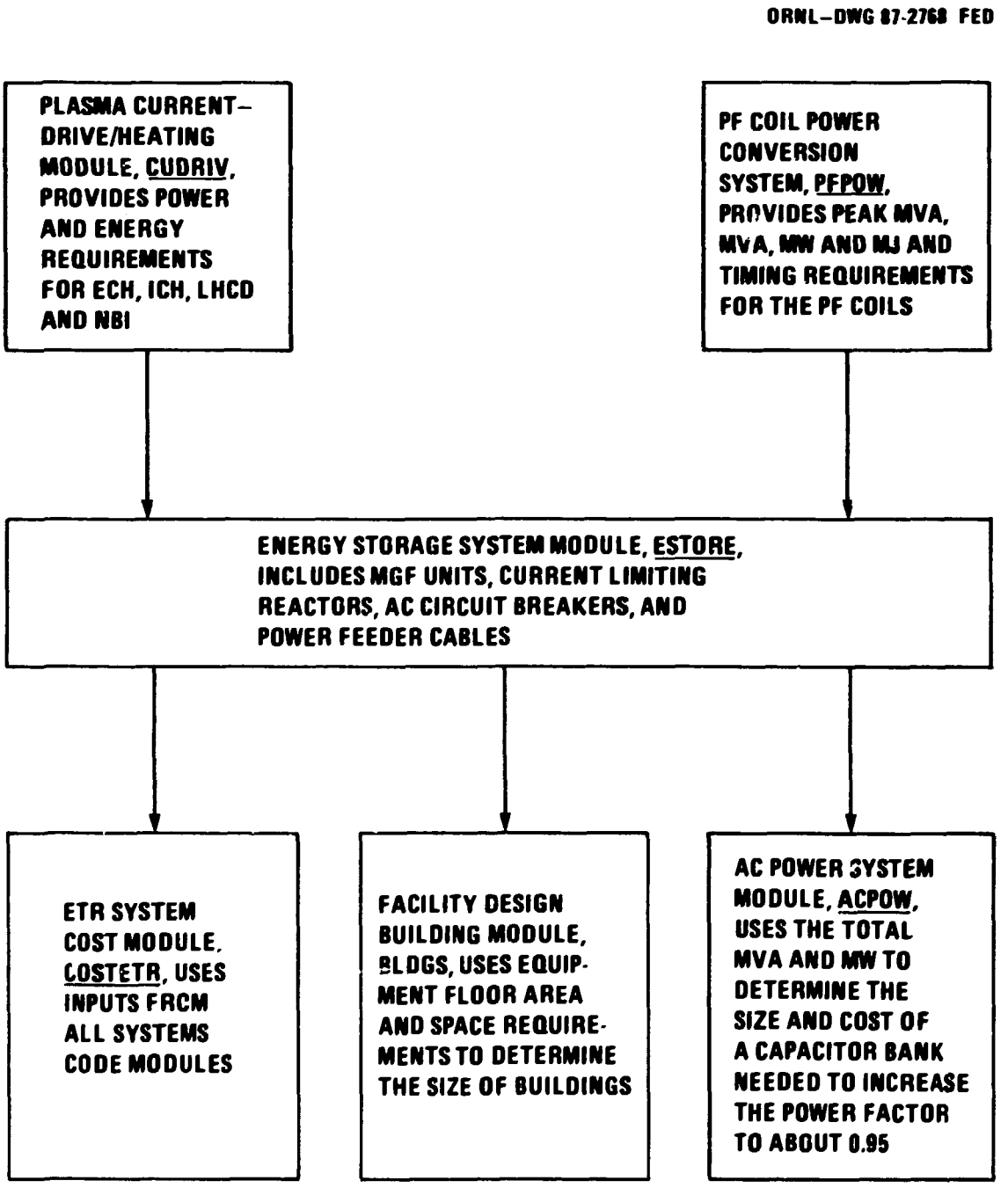

Fig. 4.19. Code flow diagram for the energy storage system module ESTORE.

switch; hence, they are performed before logic decisions are made based on the ISCENR switch settings. Depending on these settings, the subroutine performs computations beginning at statement 330, 340, or 350, as shown in Fig. 4.19. After the branch calculations are completed, the facility and cost calculations are made beginning at statement 360, and the new output data are then available for the ACPOW, BLDGS, and COSTETR modules.

4.4.6.5 Fortran listing of the energy storage system code

The Fortran listing of the ESTORE code is part of the systems code stored in filem (see Sect. 3.4.6). This listing is available for reference use. The code mnemonics are identified at the beginning of the ESTORE list and are grouped to correspond to Tables 4.19 through 4.21. The code contains statements at the beginning that are not dependent on the setting of the software selector switch. The selector switch causes the program to branch to statement 330, 340, or 350 depending on the setting of the switch ISCENR. Pertinent computations are then performed by statements following the selected branch. A final group of computations is then performed following the GO TO statement to 360.

4.4.7 References for Section 4.4

1. L. Reid et al., The Tokamak Systems Code, ORNL/FEDC-84/9, 1984.

2. F. Wu, Ripple-TF Coil Geometry Algorithm, FEDC-M-81-SE-013, 1981.

3. S. S. Kalsi, "Determination of Current Densities for Tokamak Superconducting Toroidal Field Coils," Nucl. Eng. Design/Fusion, 4, 37-48 (1986).

4. M. Wilson, Superconducting Magnets, Clarendon Press, Oxford, England, p. 22 (1983).

5. J. D. Galambos et al., System Studies of Compact Ignition Tokamaks, ORNL/FEDC-86/5, 1987.

6. J. R. Miller et al., High Current Density Magnets for INTOR and TIBER, UCRL-95759, Lawrence Livermore National Laboratory, Jan. 26, 1986.

7. J. W. Ekin, "Strain Scaling Law for Flux Pinning in Practical Superconductors. Part 1: Basic Relationship and Application to Nb_3Sn Conductors," Cryogenics 20, 611 (1980).

4.5 NUCLEAR SYSTEMS

This section contains summaries for the nuclear modules. The function of these modules is to define the performance parameters for each component as a function of the reactor operating conditions. Several design options and cost algorithms are included for each component. Lead authors and affiliations are indicated.

Module	Lead Author	Organization
First wall	Y. Gohar	Argonne National Laboratory (ANL)
Blanket	Y. Gohar	ANL
Bulk shield	Y. Gohar	ANL
Vault shield	Y. Gohar	ANL
Impurity control system	J. N. Brooks	ANL
Tritium systems	P. A. Finn	ANL

4.5.1 First-Wall Module

This module calculates first-wall design parameters, including heating rates, radiation damage parameters, neutron fluences, tritium inventory, tritium permeation rate to the first-wall coolant, and the rate of tile erosion caused by plasma disruptions. The module distinguishes between the inboard and outboard sections of the first wall. Both sections have a prime candidate alloy (PCA) steel structure and a water coolant except for a 1-cm beryllium tile for the inboard section only. The first wall is integrated with the blanket and shield. A multivariable data set generated by several design codes is used to calculate all of the above parameters except the tritium inventory and tritium permeation rates. The tritium parameters are

calculated through a simplified algorithm. This module has three sections to provide neutronics results (energy deposition, neutron fluences, and radiation damage analyses), tritium parameters, and disruption erosion rate.

4.5.1.1 Energy deposition, neutron fluences, and radiation damage analyses

The surface heat load and the nuclear heating were used to calculate the energy deposition rate in the first wall. The surface heat load is obtained from the impurity control module. The nuclear heating is calculated for both sections of the first wall by using a toroidal cylindrical geometry. The one-dimensional discrete ordinates code ONEDANT[1] was used to perform the transport calculations with a P_5 approximation for the scattering cross sections and an S_8 angular quadrature set. A 67-coupled-group nuclear data library (46 neutron and 21 gamma) based on ENDF/B-IV with corrected lithium-7 cross sections was employed for these calculations. The VITAMIN-C[2] and MACKLIB-IV[3] libraries were used to obtain this library. In the geometrical model, it is assumed that the tile material does not have an active coolant and its energy is transmitted to the inboard first wall. The neutron fluence, the atomic displacement, and the helium and hydrogen production rates are calculated based on the number of full-power years of operation used in the analyses. The first-wall coolant is integrated with the main coolant of the blanket and shield.

4.5.1.2 Plasma disruptions

Intense energy fluxes on the plasma chamber wall and impurity control systems are encountered during disruptions. The energy deposited on part of the first wall during a plasma disruption in tokamak devices could exceed several hundred megajoules, and the deposition time is estimated to be in the millisecond range or even shorter. Melting and vaporization of wall materials may then occur.[4,5] An accurate calculation for the amount of vaporization losses

and melt layer thickness resulting from the disruption is very important to fusion reactor design and operation.

The time-dependent heat conduction equation is solved subject to several boundary conditions. These conditions include the surface heat flux and radiation to the surrounding surfaces. Also, possible material phase changes and the vaporization energy of target materials are considered explicitly in the solution. This system of equations is subject to two moving boundaries.[6-9] One boundary is the melt-solid interface because surface heat flux may result in the melting of the surface of the exposed material. Another moving boundary is the receding surface as a result of evaporation of the wall material because of the continuous heating of the melted surface.

The general time-dependent, one-dimensional (1-D) heat conduction, with thermophysical properties κ, ρ, and C_p, which vary with temperature, is given by[9]

$$\rho_s(T)\, C_{p_s}(T)\, \frac{\partial T_s}{\partial t} = \frac{\partial}{\partial x}\left[K_s(T)\, \frac{\partial T_s}{\partial x}\right] , \quad 0 \le x \le L,\ t > 0 , \tag{4.27}$$

$$T(x,0) = f(x) , \quad 0 \le x \le L,\ t = 0 , \tag{4.28}$$

where $f(x)$ is the initial temperature distribution function.

The correct boundary condition requires partitioning of the incident energy into conduction, melting, evaporation, and radiation.

In the solution, to account for a phase change when the temperature of a node reaches the melting temperature of the material T_m, this node temperature is fixed until all heat of fusion is absorbed. Then, the temperature of this node is allowed to change. During the phase change, the material properties of the node are given by a combined value from both solid and liquid properties according to the ratio of the transformation at this time step.

The velocity of the receding surface is a highly nonlinear function of temperature. The model used to calculate the evaporation losses is reviewed in ref. 5. A parametric study was performed to generate a disruption data base as a function of the disruption energy and the

deposition time for the first-wall analyses. The first-wall module interpolates from this data base to calculate the first-wall erosion resulting from vaporization only, assuming no vapor protection of the first-wall material.

4.5.1.3 Hydrogen isotopes permeation and inventory in fusion reactor components

Tritium permeation into the coolant and tritium inventory in the first-wall material and the divertor are key parameters in reactor design scoping studies because of their large impacts on both economic and safety aspects of the fusion device. To compute the permeation and inventory of hydrogen isotopes in fusion reactor components, a steady-state analysis code is used. The permeation model assumes a hydrogen isotope atom implantation flux J_i at a depth δ in the surface, which is less than the surface thickness d. This implantation depth depends primarily on the energy of D-T particles, which is usually in the hundreds-of-eV range.

It is assumed that gas molecules leave either wall surface (front or back) by recombination-limited desorption according to

$$J = 2K_r C^2 \quad , \tag{4.29}$$

where C is the dissolved hydrogen isotope concentration near the surface and K_r is the recombination coefficient given by[10]

$$K_r = \frac{4\alpha}{K_{so}^2 \sqrt{\pi K MT}} \exp\left(\frac{2E_s - E_x}{KT}\right) \quad , \tag{4.30}$$

where

α = sticking coefficient (= 1 for clean surfaces),
K_{so} = pre-exponential Sievert's solubility constant,
K = Boltzmann constant,
M = mass of the molecule formed by recombination,

T = absolute temperature,

E_s = energy of solution for hydrogen in metal,

$E_x = E_s + E_d$ (E_d = diffusion energy),

and

$$E_x = \begin{cases} E_s + E_d , & \text{if } E_s + E_d > 0 , \\ 0 , & \text{otherwise.} \end{cases} \tag{4.31}$$

The governing equations for the surface currents can then be written as

$$J_1 = 2 K_{r_1} C_1^2 = \frac{D(C_m - C_1)}{\delta} , \tag{4.32}$$

$$J_2 = 2 K_{r_2} C_2^2 = \frac{D(C_m - C_2)}{(d - \delta)} , \tag{4.33}$$

$$J_i = J_1 + J_2 , \tag{4.34}$$

where the subscripts 1 and 2 refer to the front (plasma) and back (coolant) surface, respectively. The value C_m refers to the maximum concentration obtained at the implantation depth δ from the surface. The total sample thickness is assumed to be d, and J_i is the implantation flux. The surface current J_2 then represents the net flux going to the coolant (i.e., the permeation flux). The preceding equations are solved numerically by using efficient iteration techniques to yield accurate solutions.[11] The steady-state tritium inventory is calculated from the established concentrations at both surfaces along with the maximum concentration at depth δ. The physical properties of the candidate materials are stored in a separate subroutine in the code.

4.5.2 Blanket

The tritium breeding function of the blanket is integrated in the bulk shield by using an aqueous solution of a lithium compound in the water coolant of the shield. The other blanket function of producing recoverable heat in suitable conditions for power generation is accomplished only in the blanket test module of the device. The first-wall, blanket, and shield are cooled by room-temperature water (20-40°C) at low pressure. The coolant flow rate is adjusted to achieve a 20°C increase in the coolant temperature. The aqueous solution has 16 g $LiNO_3$/100 cm^3 based on neutronics considerations to maximize the tritium breeding ratio. A beryllium zone behind the first wall in the outboard section of the reactor is also employed as a neutron multiplier to enhance the tritium breeding ratio.[12] The neutron transport code and data library described in the first-wall section are employed for the calculations. It should be noted that the results of the first-wall, blanket, and shield modules assume a 100% coverage of the plasma by the first wall. An adjustment should be considered to account for different penetrations in the first wall resulting from plasma heating options and impurity control systems.

The first-wall, blanket, and shield parameters included in this version of the code are based on the TIBER design as given in Table 4.23. A parametric study was performed to generate a three-dimensional (3-D) data set to provide the blanket performance parameters as a function of the zone thickness of the inboard blanket and shield, the beryllium neutron multiplier, and the outboard blanket and shield. This module first calculates the beryllium zone thickness to achieve the required tritium breeding ratio by interpolation in the data set. A normalized bicubic spline algorithm is used to perform the interpolation. Also, the nuclear heating and the coolant mass flow rate for both sections of the reactor are calculated based on a 20°C increase in the coolant temperature.

If the required tritium breeding ratio is zero, the blanket module eliminates the beryllium multiplier zone and the $LiNO_3$ salt from the water coolant by using a different data set.

Table 4.23. First-wall, blanket, and shield parameters

Zone description	Zone thickness[a] (cm)	Zone composition (vol %)			
		PCA steel	H_2O[b]	W	Be
Inboard blanket and shield	x	10	20	70	
Inboard first wall	1	50	50		
Inboard tile	1				100
Inboard scrapeoff layer	6				
Plasma	86				
Outboard scrapeoff layer	11				
Outboard first wall	1	50	50		
Neutron multiplier	y	5	35		60
Outboard blanket and shield	z	65	35		

[a] x, y, and z are variables.

[b] 16 g $LiNO_3$/100 cm^3. A 90% lithium-6 enrichment is used.

4.5.3 Bulk Shield

The nuclear responses in the SC TF coils and the dose equivalent in the reactor vault one day after shutdown are calculated in this module for the input shield thicknesses. These responses should be used to define the allowable D-T neutron wall loading for a specific operating scenario, the total D-T neutron fluence, or the required shield thicknesses to satisfy the design goals.

Irradiation of SC coils tends to lower their performance.[13,14] For SC materials, neutron irradiation reduces the critical current density J_c and the critical temperature T_c. For Nb_3Sn material, it has been shown that J_c generally increases, reaching a maximum, and then decreases as the fast neutron fluence increases.[15] Irradiation experiments[14,16] at 6 K with a fast neutron fluence of 4×10^{18} n/cm^2 show that the maximum value and the increased rate of J_c increase with the magnetic field. At a magnetic field of 5 T, the 6 K experiment

resulted in a 16% increase in J_c at a fast neutron fluence of 2 x 10^{18} n/cm^2 without reaching a peak.

Irradiation experiments at higher temperatures (~350 K) show the same behavior for J_c. The J_c peak, however, was lower than the corresponding value at lower temperature for the same magnetic field. For example, the 350 K irradiation gave only an 8% increase compared with the 16% mentioned before at 6 K. Other experiments at 400 K and a 10-T field[17] resulted in a 90% increase for J_c at a fast neutron fluence of 4.4 x 10^{18} n/cm^2 and dropped to the original value of J_c as the fast neutron fluence increased to 10^{19} n/cm^2. Based on these experimental results[14,15,17] and a comparison between the room-temperature and the 6 K irradiation results and based on a maximum field of ~11 T, it is possible to achieve a fast neutron fluence above 10^{19} n/cm^2 for Nb_3Sn without a decrease in the critical current density. At this fluence, the T_c value is ~0.9 times the original value.[18] The module calculates the fast neutron fluence in the Nb_3Sn transfer conductor to help define the lowest J_c value for the TF coils.

The SC coil is designed to remove the generated I^2R heat so that the normal region does not propagate. The resistance R of the copper stabilizer is the key parameter for this process. The total resistivity ρ of the copper stabilizer can be described as the sum of three components: initial resistivity ρ_0, magnetoresistivity ρ_μ, and irradiation-induced resistivity ρ_{irr}. Magnetoresistance is a function of ρ_0, ρ_{irr}, and the magnetic field, which complicates the evaluation of ρ. Few experimental studies[19-23] have focused on the change of the copper resistivity as a function of magnetic field, neutron fluence, and number of cycles of alternate neutron irradiation at 4 K and annealing at 300 K. The change in the copper resistivity can be (1) accommodated by using more copper stabilizer, which increases the thickness of the coils, (2) partially annealed out by warming the coils, or (3) reduced by improving the shielding performance through an increase in shielding thickness or through the use of better materials. The module calculates the maximum induced resistivity in the copper stabilizer for the TF magnet design module.

The most sensitive component in the coils is the insulator material because the radiation damage is irreversible and this damage limits the operating life of the coils. The properties of interest for the coil designs are electrical resistivity, dielectric strength, mechanical strength, and thermal insulation. Experimental results[24,25] from neutron irradiation at 5 K suggest that polyimides can withstand a radiation dose of 10^{10} rad and retain high resistivity and mechanical strength. Glass-cloth-reinforced, epoxy-type G10-CR or G11-CR shows a serious degradation at 2×10^{9} rad. The module calculates the maximum insulator dose based on the D-T full-power years of operation.

The nuclear energy deposited in the coils impacts the refrigeration power required because ~500 W of electrical power is consumed to remove 1 W from the SC coils at 4 K. This low removal efficiency calls for minimizing the nuclear energy deposited in the SC coils. The module calculates the total nuclear heating in the SC coils and the maximum value for the magnet design module. For personnel protection, the module calculates, for the input configuration, the dose equivalent in the reactor hall one day after shutdown based on the neutron flux at the outer shield surface.[26]

4.5.4 Vault Shield

The shield system of a fusion reactor consists of two parts: the different materials around the vacuum chamber and the concrete walls of the reactor building. The first part of the shield is designed to reduce the neutron and photon leakage intensities at the outer shield surface. This reduction ensures several design criteria: (1) the different reactor components are protected from radiation damage and excessive nuclear heating, (2) the neutron reaction rates in the reactor components that produce undesirable radioactive isotopes are reduced, and (3) the workers are permitted in the reactor vault one day after shutdown. The second part of the shield must protect the workers and the public from radiation exposure during the reactor operation. This part of the shield is calculated in this module.

Recommendations of the International Commission on Radiological Protection and U.S. federal regulations limit occupational exposure to

5 rem/year with a maximum of 3 rem/quarter. The occupational exposure based on regular working hours is 2.5 mrem/h. However, the current practice in the nuclear industry, the exposure policy of the U.S. Department of Energy (DOE), and the national laboratories' guidelines are to keep radiation exposure as low as reasonably achievable. Specifically, DOE Order 5980.1, Chapter XI, states: "Exposure rates in work areas should be reduced as low as reasonably achievable by proper facility design layout. Design efforts to consider are: occupancy time, source terms, spacing, processes, equipment, and shielding. On-site personnel exposure level less than one-fifth of the permissible dose equivalent limits, prescribed in this chapter should be used as a design objective." This guideline limits on-site workers to <1 rem/year (0.5 mrem/h).

The calculation of this module is concerned with the total dose equivalent outside the reactor building during operation to satisfy the 0.5 mrem/h design criterion. A parametric study was performed to define the dose equivalent outside the reactor building as a function of the roof thickness including the contribution from neutrons and photons scattered back by collision with air nuclei (skyshine). A 3-D model was employed to generate a data set for this module.[27] The MCNP general Monte Carlo code[28] for neutron and photon transport was used to perform all the calculations. Variance-reduction schemes were employed for the calculations. The energy distribution of the neutron source was used explicitly in the calculations with a nuclear library based on ENDF/B-V data.

The reactor wall and roof thicknesses are defined in this module based on 0.5 mrem/h outside the reactor building during operation, including the skyshine contribution by interpolation from the stored data set.

4.5.5 Impurity Control Module

The impurity control module models plasma/material interactions related to a divertor. The module provides estimates of divertor plate design and heat load, limits on divertor plate lifetime resulting from

erosion by sputtering and disruptions, sputtered impurity content in the core plasma, and tritium permeation through the divertor plate into the coolant. Inputs to the module are the reactor geometry, frequency of disruptions, plasma edge temperature, and plasma heating powers.

The code is based on extensive analysis of impurity control issues for tokamak fusion reactors, particularly for the INTOR design.[29] Because of the complexity of most impurity control analyses, the intent of the module is to provide approximate parameter estimates for reactor design scoping purposes and to identify general trends (e.g., how erosion might vary with plasma edge temperature).

Sputtering erosion of the divertor plate is computed by applying a simplified version of the REDEP erosion/redeposition code[30] to the divertor plate center. The divertor model is a single or double null type operated in the high or medium recycling regime. Erosion is computed for plate materials of beryllium, carbon, vanadium, molybdenum, and tungsten, with plasma edge temperatures (near the plate center) in the range of 10 to 150 eV. Sputtering caused by hydrogen, helium, and oxygen and self-sputtering are computed. Self-sputtering and associated redeposition are modeled as arising from ionization and transport in the scrapeoff zone and plasma. The general features of sputtered impurity transport identified in ref. 31 for a high recycling divertor are used for the module. The disruption model is based on the disruption results of the TIBER design[32] using disruption parameters of 1-ms energy deposition time and 5-MJ/m^2 thermal load. The default assumption is that the melt layer is not lost; erosion is the result of vaporization only.

The sputtering calculation predicts both gross and net (sputtering minus redeposition) erosion rates. Because this calculation depends on uncertain estimates of redeposited material properties (e.g., adhesion), the results must be cautiously applied whenever high gross erosion rates are predicted. This is particularly true for carbon surfaces.

The divertor plate lifetime calculation uses a design thickness in the range c. 0.5 to 2.0 cm, depending on the plate material and on the disruption and net sputtering erosion rates. Plate design information

(e.g., area) is scaled from the INTOR and TIBER designs for single and double null divertors, respectively, and for different major radii.

The core plasma impurity content caused by sputtering depends on the net sputtering rates, transport through the scrapeoff zone, and transport in the core plasma. Data for the latter are taken from 1-D transport calculations[33] for a tokamak fusion reactor, under the assumption of non-neoclassical impurity particle transport. In this case, the core impurity content is approximately equal to one-fourth of the effective edge D-T sputtering coefficient (ratio of the impurity current entering the plasma edge to the D-T current leaving the edge).

The heat and particle loads to the divertor and adjacent first wall (necessary estimates for the tritium permeation calculations) are based primarily on scaling of data from the analysis for INTOR. Charge exchange flux to the first wall is modeled as occurring in a small region adjacent to the divertor and about equal to the divertor area. The total charge exchange current is equal to half of the ion current to the divertor. Energy of the charge exchange neutrals is scaled from the edge temperature, based on the INTOR analysis. The tritium permeation calculations use the particle fluxes as inputs in a manner similar to that discussed for the first-wall tritium permeation module (see Sect. 4.5.1.3).

4.5.6 Tritium Module

A magnetic fusion reactor fueled with tritium and deuterium has four main tritium processing systems: the plasma processing system, the blanket processing system, the water processing system, and the atmospheric processing system. A computer module was developed to provide information on costs, tritium inventory, power requirements, and sizes for these systems. The tritium module has a main section and two subroutines. The subroutines provide detailed information on the plasma processing system and the water processing system.

4.5.6.1 Main section

The main section of the tritium module has six functions:

1. It determines the tritium and deuterium feed rates for the plasma processing units by summing the flow rates computed in the relevant systems code modules.
2. It determines the tritium inventory and capital cost for blanket options other than the aqueous lithium salt.
3. It determines the tritium inventory in the tritium processing components and in all major units in the fusion plant; this includes tritium in storage or in high-heat components.
4. It determines the tritium supply needed at startup and for each year.
5. It determines the total capital cost, operating cost, size, and power requirements for all tritium systems by using information supplied by the two subroutines.
6. It assesses the tritium loss to the environment as a function of cleanup time and base tritium concentration.

The gas feed rate is the sum of plasma exhaust, fueler exhaust, and blanket exhaust. The magnitude of the plasma exhaust depends on the plasma fractional burn. The fueler options are a neutral beam system, a pellet fueler system, a combination of these two systems, or an alternate system.

The blanket options are FLIBE, lithium-lead, solid oxide, lithium, and lithium salt/water. Generic algorithms are used to determine the tritium inventory in the breeding blanket, the tritium inventory in the blanket processing system, and the capital cost of the blanket processing system. The blanket inventory is a function of blanket mass.

The tritium inventory for plasma processing units or water processing units is calculated in the two subroutines. Inventories in other areas are calculated in the main section of the module.

The tritium supply needs are defined as a function of breeding ratio, processing losses during a year, and decay losses for the on-site tritium inventory.

Capital costs of the plasma processing and water processing systems are determined in the two subroutines. A multiplicative factor of 4 is used with specific plasma processing support equipment (monitors, inventory control instrumentation, secondary containment, etc.) to account for needed equipment in the tritium area, the hot cell area, the reactor hall area, and the neutral beam area or the heat exchanger area. In addition, excess storage beds are needed to handle the reserve storage of a 24-h/d input to the plasma. An algorithm[34] is used to determine the capacity of the needed atmospheric processing systems in the four areas.

Tritium losses in the four areas are assessed as a function of cleanup time, in-leakage rate, amount of tritium release, and tritium base concentration.

The input variables are burn time, dwell time, ramp time, fractional burn-up, fueler options, fuel cleanup option, cost of tritium, type of blanket, blanket mass, water processing option, cleanup time for the four areas, in-leakage rate for the four areas, tritium release for the four areas, and tritium base concentration in the four areas.

The major assumptions are (1) the reactor runs continuously or is pulsed; (2) the pump regeneration times are <2 h; (3) the cost of tritium is <$3 per Curie (U.S. dollars); (4) the breeding ratio is 0-1.5; and (5) a day is a 24-h operational day.

The output is total tritium and total deuterium flow rates, tritium inventory, capital costs, operating costs, size of equipment, power requirements, and tritium cleanup for unplanned releases.

4.5.6.2 Plasma processing system

The first subroutine (TSTA), which is based on the operating experience at the Tritium Systems Test Assembly, provides information on units in the plasma processing system. The processing units included are a palladium diffuser or a molecular sieve unit for fuel cleanup, a cryogenic distillation unit, storage beds, gas analysis instrumentation,

monitors, secondary containment units, a gas effluent unit, emergency air cleanup units, data acquisition units, a solid waste unit, and an inventory control unit.

The TSTA subroutine calculates tritium inventory, power requirements, size, and capital cost (1986 U.S. dollars) for a given plasma processing unit as a power function of the tritium and deuterium feed rate. Based on the experience of the chemical process industry,[35] the power function used is 0.6 for large units and 0.3 to 0.5 for very small installations or for processes employing extreme conditions of temperature or pressure.[36] For certain fixed costs, the power function is 0.

The original capital and installation costs of the subsystems at TSTA have been published;[37] these costs are summarized in Table 4.24. For the gas analysis system, the cost was increased $500,000 to include a mass spectrometer. For the gas effluent system, a recombiner was added for $120,000.

The tritium inventory in each component at TSTA is given in Table 4.25.

The input variables to the TSTA subroutine are the mass flow rate of tritium and deuterium, reactor hall volume, and time to clean the reactor hall.

The major assumptions made are (1) the emergency room cleanup (ERC) unit is sized for the reactor hall; (2) flow through the ERC is greater than the in-leakage rate; (3) cleanup time with the ERC is less than 5 d; (4) the ERC decontamination factor is greater than 10,000; (5) the target concentration after decontamination is 20 MCi/m^3; (6) the volume needed for the plasma processing equipment is an independent parameter; (7) power functions are useful algorithms for modeling the plasma processing units; and (8) a storage bed holds 100 g of tritium.

4.5.6.3 Water processing system

The second subroutine (TWCS) is based on the operating experience at Ontario Hydro. It provides tritium inventory, capital cost, size,

Table 4.24. Capital cost summary for TSTA plasma processing units

Subsystem	Cost ($ × 10^3)		Year of capital expenditure	Design variable[a]	Power function
	Capital	Installation			
Transfer pumps	111	112	77	F	0.3
Fuel cleanup	1000	70	80	F	0.3
Cryogenic distiller	1237	63	78	F	0.3
Storage beds	60	10	81	T	0.6
Gas analysis	469	26	79	-	0.0
Tritium monitor	193	33	78-82	V	0.3
Secondary containment	182	30	78-82	F	0.3
Gas effluent detritiation	443	60	80-81	F	0.6
Emergency cleanup	382	357	79-80	Complex, see program	
Data acquisition/ control	1379	531	79-81	-	0.0
Uninterruptible power source	95	44	80	Complex, see program	
Emergency generator	100	168	80	Complex, see program	
Solid waste discharge	23	0	80	F	0.3
Inventory control	25	13	--	-	0.0

[a] F = flowrate (2.08×10^{-5} kg D-T/s); T = tritium inventory at TSTA (0.130 kg); V = test cell volume at TSTA (3000 m^3).

Table 4.25. Summary of TSTA tritium inventory data

Subsystem	Tritium inventory (g)	Design variable[a]	Power
Isotope separator	100	F	0.6
Fuel cleanup			
Diffuser	3	F	0.3
Molecular sieve	30	F	0.3
Gas effluent detritiation	2	F	0.3
Other	1	F	0.3

[a]F = flowrate (2.08×10^{-5} kg D-T/s); a diffuser is the only option if turbomolecular pumps are used.

and power requirements for several options used to process water or an aqueous lithium salt breeder.

The two main processing options for extracting tritium from water are vapor phase catalytic exchange coupled with cryogenic distillation (VPCE/CD) and direct electrolysis coupled with cryogenic distillation (DE/CD). Other processing options available for specific purposes are water distillation to pre-enrich the tritiated water; flashing to separate the lithium salt from the water; and ion exchange to remove neutron activation products from the water (this last option has not yet been added to the subroutine).

System cost, size, and power consumption are calculated as a function of feed concentration and flow rate. Cost correlations are based on published data.[37,38] The costs are calculated by upgrading known costs to 1987 Canadian dollars and then converting to 1987 U.S. dollars.

The input variables to the Ontario Hydro subroutine include tritiated water feed, tritium concentration in the feed, pre-enrichment choice, front end choice (VPCE or DE), lithium salt concentration as a fraction of solubility limit, and mole fraction of light water (1 or 0).

The major assumptions made are (1) water distillation is only economical for light-water cleanup; (2) water is either light or heavy water (no intermediate mixtures); (3) separate correlations are used for

light and heavy water; (4) lithium salt solutions are flashed to leave the lithium concentration in the remaining liquid at 90% of the lithium salt solubility limit; (5) in VPCE, five stages are used to achieve a detritiation factor of 10; (6) in DE, 25-kA electrolytic cell modules are used; (7) in an electrolysis cell, the tritium concentration in the electrolyte is 12 times higher than the feedwater concentration for hydrogen-tritium (H-T) and 2 times higher than that for D-T; (8) above 70 Ci/kg, double containment of the electrolysis cells is recommended but not included in the cost correlation; (9) the largest cost component in CD is the first column, and its cost is correlated to the cryogenic hydrogen refrigeration requirement; (10) the CD contains a catalytic equilibrator to break up H-T and D-T; and (11) the water concentration is between 0.01 and 34 Ci/L.

4.5.7 References for Section 4.5

1. R. D. O'Dell, F. W. Brinkley, Jr., and D. R. Marr, User's Manual for ONEDANT: A Code Package for One-Dimensional, Diffusion-Accelerated Neutral Particle Transport, LA-9184-M, Los Alamos National Laboratory, February 1982.

2. R. W. Roussin et al., The CTR Processed Multigroup Cross Section Library for Neutronics Studies, ORNL/RSIC-37, Oak Ridge National Laboratory.

3. Y. Gohar and M. A. Abdou, MACKLIB-IV: A Library of Nuclear Response Functions Generated with MACK-IV Computer Program from ENDF/B-IV, ANL/FPP/TM-106, Argonne National Laboratory, 1978.

4. A. M. Hassanein, G. L. Kulcinski, and W. G. Wolfer, J. Nucl. Mater. **103&104**, 321 (1981).

5. A. M. Hassanein, G. L. Kulcinski, and W. G. Wolfer, Nucl. Eng. Design/Fusion, 1(3), 307-324 (July 1984).

6. A. M. Hassanein and G. L. Kulcinski, J. Heat Transfer **106**, 486-490 (August 1984).

7. A. M. Hassanein, J. Nucl. Mater. **122&123**, 1453-1458 (1984).

8. A. M. Hassanein, J. Nucl. Mater. **122&123**, 1459-1465 (1984).

9. A. M. Hassanein, "Numerical Solutions of Two Proving Boundary Problems by Both Finite Difference and Finite Element Methods, with Application," presented at the 5th International Conference on Numerical Methods in Heat Transfer, June 29-July 3, 1987, Montreal, Canada, to be published in International Journal of Numerical Methods in Heat Transfer.

10. M. I. Baskes et al., Tritium and Blanket, FED-INTOR/TRIT/82-5, 1982.

11. A. Hassanein and D. K. Sze, Fusion Technol. 10, 1355-61 (November 1986).

12. Y. Gohar, "Nuclear Data Needs for Fusion Reactors," presented at the International Conference on Nuclear Data for Basic and Applied Science, May 13-17, 1985, Santa Fe, N.M.

13. Y. Gohar and S. Yang, "Energy Deposition and Shielding Requirements for All Concepts of the Blanket Comparison and Selection Study," Fusion Technol. 8, 2010 (1985).

14. B. S. Brown, "Radiation Effects in Superconducting Fusion Magnet Materials," J. Nucl. Mater. 97, 1 (1981).

15. B. S. Brown and T. H. Blewitt, "Critical Current Density Changes in Irradiated Nb_3Sn," J. Nucl. Mater. 103&104, 18 (1979).

16. M. Soell, "Influence of Radiation Damage on the Maximum Attainable Magnetic Field for Toroidal Fusion Magnet Systems," J. Nucl. Mater. 72, 168 (1978).

17. C. L. Snead, Jr., et al., "High-Energy-Neutron Damage in Nb_3Sn: Changes in Critical Properties, and Damage-Energy Analysis," J. Nucl. Mater. 103&104, 749 (1981).

18. R. A. Van Konynenburg et al., "Fusion Neutron Damage in Superconductors and Magnet Stabilizer," J. Nucl. Mater. 103&104, 739 (1981).

19. C. E. Klabunde et al., "The Effects of Irradiation on the Normal Metal of Composite Superconductor: A Comparison of Copper and Aluminum," J. Nucl. Mater. 85&86, 385 (1979).

20. J. M. Williams et al., "The Effects of Irradiation on the Copper Normal Metal of a Composite Superconductor," IEEE Trans. Magn. 15, 731 (1979).

21. S. Tokamura and T. Kato, "The Effects of Low Temperature Irradiation and Other Materials for Superconducting Magnets," J. Nucl. Mater. 103&104, 729 (1981).

22. M. W. Guinan, Radiation Effects Limits on Copper in Superconducting Magnets, UCID-19800, Lawrence Livermore National Laboratory, 1983.

23. R. R. Coltman, Jr., "Organic Insulators and the Copper Stabilizer for Fusion Reactor Magnets," in Proc. Int. Mtg. Neutron Irradiation Effects, Argonne, Illinois, November 9-12, 1981, U.S. Department of Energy, 1981.

24. R. R. Coltman, Jr., et al., Radiation Effects on Organic Insulators for Superconducting Magnets, ORNL/TM-7077, Oak Ridge National Laboratory, 1979.

25. R. H. Kernohan et al., Radiation Effects on Organic Insulators for Superconducting Magnets, ORNL/TM-6708, Oak Ridge National Laboratory, 1978.

26. F. W. Clinard, Jr., and G. F. Hurley, "Ceramic and Organic Insulators for Fusion Applications," J. Nucl. Mater. 103&104, 705 (1981).

27. Y. Gohar and S. Yang, "Skyshine Study for Next Generation of Fusion Devices," in Proceedings of the Topical Conference on Theory and Practices in Radiation Protection and Shielding, April 22-26, 1981, Knoxville, Tennessee.

28. LASL Group X-6, MCNP--A General Monte Carlo Code for Neutron and Photon Transport, Version 2B, LA-7396-M, Los Alamos National Laboratory, revised April 1981.

29. International Atomic Energy Agency, INTOR--Phase Two A, Part 11, STI/PUB714, International Atomic Energy Agency, Vienna, 1986.

30. J. N. Brooks, Nucl. Technol./Fusion 4, 33 (1983).

31. J. N. Brooks, J. Nucl. Mater. 145-147, 837 (1987).

32. C. D. Henning et al., TIBER II Tokamak Ignition/Burn Experimental Reactor, 1986 Status Report, UCID-20863, Lawrence Livermore National Laboratory, October 1986.

33. W. K. Terry et al., Fusion Technol. 7, 158 (1985).

34. R. L. Reid et al., The Tokamak Systems Code, ORNL/FEDC-84/9, Oak Ridge National Laboratory, March 1985.

35. M. S. Peters and K. D. Timmerhaus, Plant Design and Economics for Chemical Engineers, 3rd Edition, McGraw-Hill, New York, Chapter 5, 1980.

36. R. S. Aries and R. D. Newton, Chemical Engineering Cost Estimation, McGraw-Hill, New York, p. 7, 1955.

37. J. R. Bartlit, J. L. Anderson, and V. G. Rexroth, "Subsystem Cost Data for the Tritium Systems Test Assembly," in Proceedings of the 10th Symposium on Fusion Engineering, Vol. 2, p. 1186, 1983.

38. A. H. Dombra, Estimates for the Recovery of Tritium from LiD_2O Breeder in a 1000 MW Fusion Reactor, TTF-N-1, Atomic Energy of Canada Ltd., Chalk River Nuclear Laboratories, August 1986.

4.6 MISCELLANEOUS SYSTEMS

This section contains summaries for the following modules. Lead authors and affiliations are indicated.

Module	Lead Author	Organization
Facilities	S. L. Thomson	FEDC/Bechtel
Heat transport system	S. L. Thomson	FEDC/Bechtel
Maintenance equipment	P. T. Spampinato	FEDC/Grumman
Cost	S. L. Thomson	FEDC/Bechtel

4.6.1 Facilities

The buildings module, BLDGS, calculates the volume of the plant buildings based on input from other modules and user-defined input. The reactor building is sized based on the dimensions of the tokamak, using as the characteristic size the maximum extent of the PF coil, cryostat, or TF coil outer leg. The width of the building is set to permit removal of a TF coil or shield sector horizontally with user-defined clearances. The specification of these clearances gives the user the option of selecting the maintenance design. The length of the building is then set so that a PF coil or cryostat dome can be laid down in a corner with clearances. The building height allows the lifting of a

TF coil over the dome and includes a full basement. The crane clearance is determined from the crane capacity, which can be input or can be calculated based on the weight of the heaviest component.

The tritium building volume is scaled with the equipment volume provided by the tritium module. The cryogenic building volume is scaled with capacity based on a reference design. The electrical building volumes are provided by those modules. The administration and control building and the general shops areas are input by the user.

Output from the BLDGS module includes the effective floor area of the plant, the internal volumes of the buildings, the distance of the building walls from the reactor, and the specification of external volumes for costing.

4.6.2 Heat Transport System

The function of the heat transport system module, HTS, is to account for the plant thermal loads and specify the water cooling system to reject the heat. The module is a revision of that contained in the tokamak systems code, and the model is described in the documentation for that code (ORNL/FEDC-84/9). The primary nuclear heat loads are input from the first-wall, shield, and divertor modules. Primary heat exchangers are sized to transfer these loads to an intermediate water cycle. The other plant heat loads are input or calculated from other module parameters and are transferred to the cooling tower through intermediate heat exchangers. All components are assumed to be cooled with low-pressure, low-temperature water, with an outlet temperature of less than 373 K. The auxiliary loads are the plasma heating system (calculated from injected power and overall efficiency), the cryogenic system (calculated from power at 4.2 K and efficiency), the vacuum system (input), the tritium plant (input), and the facilities. The facility heat load is calculated based on the electrical power requirements, the building load based on floor area, and a fixed base load. Output from the HTS module is the number of primary and intermediate heat exchangers and the listing of circuit loads; the output is sent to the cost module.

4.6.3 Maintenance Equipment

4.6.3.1 Summary and background

The maintenance equipment module is a compilation of the equipment used for remote maintenance operations in the test cell, hot cell, and mock-up cell. Modifying the use of this module for different tokamak configurations is accomplished by changing the input data, either by adjusting the equipment unit costs or by changing the required number of equipment units needed in the test cell and hot cell. The module output consists of a listing of 26 equipment items, their unit cost, an estimate of the required usage, and the total cost for each. An additional 10% of the total cost is estimated to account for equipment that will be installed in the warm cell to maintain components that have no activation or are only mildly activated or contaminated. Table 4.26 shows the maintenance equipment output.

At present, this module does not contain algorithms to adjust the equipment requirements as a function of component size and weight or facilities design. In general, the module also assumes nonparallel maintenance operations that require one-of-a-kind equipment needs. The exception to this is the estimate of through-the-wall manipulators and shielded windows. Availability requirements, if they can be factored into the maintenance equipment module, could have an impact on the quantity of equipment needed for certain operations.

The mock-up equipment is representative of the operations that occur in the test cell and, in most cases, these are estimated to have the same cost as the test cell equipment. Where a 0.5 quantity is indicated, the equipment cost for the mock-up is assumed to be half of that in the test cell. For example, the bridge-mounted servomanipulator in the test cell costs $2.6 million but is assumed to cost $1.3 million for the mock-up. This is because the overhead transport system for the manipulator can be scaled down to reflect the smaller span and reach requirements in the mock-up cell.

Some future additions to this module will be made to portray more accurately the costs associated with remote maintenance operations. Among these are the following:

Table 4.26. Sample output of the maintenance equipment module

Equipment item	Unit cost ($ × 10^3)	Cost Factor: Test cell	Cost Factor: Hot cell	Cost Factor: Mock-up	Total ($ × 10^3)
Servomanipulator (bridge-mounted)	2600	1.0	1.0	0.5	6500
Power manipulator (bridge-mounted)	500	1.0	1.0	0.5	1250
Robot arm (floor-mounted)	100	1.0	1.0	1.0	300
Mechanical manipulator (through-the-wall)	100	0.0	5.0	1.0	600
Mobile manipulator	1000	1.0	0.0	1.0	2000
In-vessel manipulator system	1300	2.0	0.0	1.0	3900
Leak detection system	800	1.0	0.0	0.0	800
Small "hand" tools	500	1.0	1.0	1.0	1500
Lifting fixtures, slings, etc.	250	1.0	1.0	0.0	500
Shielded windows	250	4.0	5.0	1.0	2500
Transporter for large components	500	1.0	0.0	0.0	500
Welders--structural	100	1.0	1.0	0.0	200
Welders--piping	150	1.0	1.0	0.0	300
Cutters--structural	100	1.0	1.0	0.0	200
Cutters--piping	150	1.0	1.0	0.0	300
Sector module transporter	500	1.0	0.0	0.0	500
Manipulator end-effectors	500	1.0	1.0	1.0	1500
Decontamination (decon cell)	1000	1.0	0.0	0.0	1000
Decontamination (hot cell)	100	0.0	1.0	0.0	100
Rad-waste handling (hot cell)	1000	0.0	1.0	0.0	1000
Waste handling casks	500	0.0	1.0	0.0	500
Transfer lock (into test cell)	1000	1.0	0.0	0.0	1000
Cell lighting and audio	100	1.0	1.0	0.5	250
Closed-circuit television	100	1.0	1.0	0.5	250
Blanket module handling	500	1.0	0.0	0.0	500
					28450
Warm cell (10% of above)					2845
Total					31295

1. Algorithms to adjust equipment cost or quantity as a function of the machine configuration, the auxiliary components, and the facilities design.

2. In-vessel inspection system. One or more such systems will be needed to evaluate the plasma chamber for wear or damage prior to starting in-vessel related maintenance operations. Data for these are available from the experience of the Joint European Torus and Tokamak Fusion Test Reactor, as well as the concept design for the CIT.

3. Machine tools in the hot cell and maintenance repair shop. A number of machine tools (e.g., lathes, mills, grinders, and inspection tools) will be required in the hot cell and in the "warm" maintenance shop. Those used in the hot cell will be designed with special features for remote operation and maintenance of the machine tools.

4.6.3.2 Assumptions

The unit costs used in the maintenance equipment module are based on the cost estimating data used for the CIT. In general, these numbers reflect a 1986 basis. The unit costs should be periodically reviewed and compared to actual CIT costs as that program becomes a capital funded project.

The following items are not included in the maintenance equipment module: overhead crane systems, which are included in the facility costs; transfer flasks to minimize the spread of contamination; and development costs for the equipment.

4.6.4 Cost Accounting

The cost accounting module calculates the total constructed cost of the plant based on design parameters generated by the code. The constructed cost includes direct cost, indirect cost, and contingency. Direct cost consists of equipment and materials, installation labor, and

first-of-a-kind component engineering. Equipment cost is the purchase price for the component delivered to the site. The equivalent purchase price is estimated as the build-to-print cost if the component is not commercially available. The component engineering cost, or cost of generating the design for a build-to-print contract, is also estimated for first-of-a-kind equipment. This accounts for the nonrecurring design costs but not for the systems design cost for the specific application, which is included in indirect cost. Indirect cost includes the plant engineering, procurement, construction services, and construction management. It is assumed that these services are provided by the managing organization or by a subcontractor with a total project scope, so that the costs are recorded as indirect, rather than as direct, costs to specific components or systems. A process contingency allowance is included to account for uncertainties in the design, and an overall project contingency is used to provide for cost increases during construction. Costs of the research and development program and of the blanket test modules are excluded.

In this version of the code, an attempt has been made to show all cost calculations explicitly to simplify review and revision. Detailed descriptions of the cost scaling factors (with default values) and of the required design parameters are included in the cost module and in ref. 1. The scaling factors are controlled through the code input, and the factors used in a run are listed in the output. All costs reported in the cost output are calculated in the cost module. Some cost calculations are performed in design modules, but these are for the information of experts in those modules and are not reported in the cost output. In many cases, the cost module calculations repeat those of design modules. In others, a simpler algorithm is selected so that exact agreement is not obtained.

The default cost factors are primarily based on the TIBER II design of September 1987. However, the cost calculated by the code for the TIBER II design model does not duplicate the project estimated cost. The code cost factors are in some cases more general than those selected for the project so that a wider range can be considered by the code. The factors should be carefully reviewed for applications to designs

that differ significantly from TIBER II. The primary reason for the difference between project and code costs is that the level of detail developed in a project is considerably greater than that generated by the code. This greater detail leads in turn to larger quantities of equipment and higher costs. The systems code output should accordingly be used for the relative cost comparison of cases and not for absolute cost. The selection of cost factors should similarly ensure that the proper relative balance between major system costs is achieved.

4.6.5 Reference for Section 4.6

1. S. L. Thomson, "Systems Code Cost Accounting," FEDC-M-88-SE-004, Oak Ridge National Laboratory, Feb. 19, 1988.

5. TIBER BENCHMARK
(Sample execution)

A sample run of the TETRA1 code is included in this section. The input file used to generate this output, itetra1, is stored in filem in the global read directory .TETRA as discussed in Sect. 3 of this document. This input file is consistent with the TIBER II configuration. Because this was a benchmark run, the nonlinear equation solver (HYBRID) without optimization was used to generate this point (see Sect. 3).

```
TETRA:  Superconducting Tokamak
Systems Code, Developed at the FEDC
 for TIBER - ETR studies


 code run 03:02:59  10/08/87 on machine d
 code loaded 10/08/87  00:16:25
 user 001057   account 560etg   dropfile +xtetrae channel a
 input  file called   itetral
 output file called   otetral
 namelist file called outnam
 summary file called  summary



 icase = TIBER 100% -TF

 the following are always variables

    i     ixc      label

    1       2     betap
    2      14     beta
    3      17     fdene
    4      26     fcpttf
    5      33     fcptoh
    6       5     ftfport
    7      36     fefac
    8      21     rjcontf
    9      16     fbeta
   10      25     fvs
   11      36     ftfsts
   12      24     fwalld
   13       9     rmajor
   14      10     rnbeam
   15      34     fqval
   16      27     fohsts
   17      42     ffwlrad
   18      43     ffwladd
   19      44     ffwlht
   20      48     feptf
   21      49     fepoh

the following are only optimization variables

    i     ixc      label

   22      15     dene
   23      18     soltx
   24      19     boresol
   25      30     tfthkl
   26       8     aspect
   27      12     te
   28       1     bt
   29      20     coheof
   30       3     thwcndut
   31       6     thkcas
   32       7     vftf
```

143

33	41	fcutf
34	45	twcdtoh
35	46	vfohc
36	47	fcuoh

the following are the equations used

i	icc	label
1	1	poloidal beta
2	3	total beta
3	4	power balance
4	21	tf port size
5	7	density limit
6	8	beta limit
7	22	oh max. cpt
8	23	tf max. cpt
9	10	B at tf coil
10	18	v-s capability
11	17	TF Coil stress
12	9	radial build
13	13	wall loading
14	2	hot beam ion den
15	27	Q-value
16	16	OHC stress
17	19	ins. rad. dose
18	20	shut. dose rate
19	25	TFC nuc. heating
20	28	TFC cond. stab.
21	29	OHC cond. stab.

****

namelist variables used to obtain the first solution vector

```
fcase = TIBER 100% -TF
icc     =  1  3  4 21  7
           8 22 23 18 10
          17  9 13  2 27
          16 19 20 25 28
          29  0  0  0  0
           0  0  0  0  0
ixc     =  2 14 17 26 33
           5 30 31 16 28
          36 24  9 10 34
          27 42 43 44 40
          49 15 10 19 30
           8 12  1 20  3
           6  7 41 45 46
          47  0  0  0  0
           0  0  0  0  0
           0  0  0  0
boundl  =  0.100000e-01  0.100000e+00  0.           0.100000e-01  0.100000e+00
           0.300000e-01  0.           0.250000e+01  0.240000e+01  0.100000e-05
           0.500000e+00  0.100000e+01  0.100000e-02  0.500000e-02  0.100000e+19
           0.100000e-01  0.100000e-01  0.100000e-02  0.100000e-02  0.100000e+01
           0.100000e+01  0.100000e-02  0.100000e-02  0.900000e+00  0.100000e-08
           0.100000e-02  0.100000e+01  0.100000e-08  0.300000e+01  0.300000e+00
           0.100000e-02  0.100000e-02  0.100000e+00  0.100000e-02  0.100000e-02
           0.           0.           0.100000e+01  0.100000e+01  0.
           0.100000e-02  0.100000e-02  0.100000e-02  0.100000e-02  0.100000e-02
```

```
          0.100000e+00  0.100000e+00  0.100000e-02  0.100000e-02
boundu    = 0.200000e+02  0.100000e+02  0.300000e+01  0.100000e+02  0.104000e+01
            0.900000e+00  0.100000e+01  0.100000e+02  0.100000e+02  0.300000e+01
            0.300000e+01  0.500000e+02  0.992000e+00  0.100000e+01  0.100000e+23
            0.030030e+00  0.100000e+01  0.100000e+02  0.100000e+02  0.900000e+09
            0.100000e+10  0.100000e+02  0.100000e+01  0.300000e+01  0.101300e+01
            0.000000e+00  0.125000e+01  0.100000e+02  0.300000e+10  0.100000e+02
            0.100000e+02  0.200000e+00  0.111500e+01  0.212000e+00  0.100000e+02
            0.172000e+01  0.100000e+02  0.100000e+03  0.100100e+01  0.
            0.100000e+01  0.100000e+01  0.100000e+01  0.100000e+01  0.100000e+01
            0.100000e+01  0.100000e+01  0.100000e+01  0.100000e+01
boundl    = 1. 6.1 0. 1. 0.1 3.e-02 0. 2.5 2.4 9.99999999999997e-07 0.5 1. 1.e-03 5.e-03 1.e+10 1.e-02 1.e-02 1.e-03 1.e-03 1. 1.
            1.e-03 1.e-03 0.95 1.e-09 1.e-03 1. 1.e-09 3. 0.3 1.e-03 1.e-03 0.1 1.e-03 1.e-03 0. 0. 1. 1. 0. 1.e-03 1.e-03 1.e-03
            1.e-03 1.e-03 0.1 0.1 1.e-03 1.e-03
boundu    = 20. 10. 3. 10. 1.04 0.9 1. 10. 10. 3. 3. 50. 0.902 1. 1.e+22 0.03 1. 10. 10. 999999999. 1999999999. 10. 1. 3. 1.013 0.0
            1.25 10. 3000000000. 10. 10. 0.2 1.116 0.212 10. 1.72 10. 100. 1.001 .. 1. 1. 1. 1. 1. 1. 1. 1. 1.
epsfcn    = 1.01e-03
epsvmc    = 1.e-05
factor    = 0.1
ftol      = 1.e-05
icase     = 607345043798384268B 34692144678103342480 0 0 0 0
icc       = 1 3 4 21 7 0 22 23 18 19 17 9 13 2 27 16 19 20 26 28 29 0 0 0 0 0 0 0 0 0 0
ioptimz   = -2
ixc       = 2 14 17 26 33 5 30 21 16 25 36 24 9 10 34 27 42 43 44 48 49 15 18 19 30 0 12 1 20 3 6 7 41 45 46 47 0 0 0 0 0 0 0 0 0 0
            0 0 0
maxcal    = 100
minmax    = 1
neqns     = 21
nineqns   = 0
nvar      = 36
0
alap      = 16.
alphan    = 1.02
alphat    = 0.50
aspect    = 3.594
beta      = 6.020868129881616-02
betap     = 1.0909882737166
bt        = 5.55
capa      = 1.2
carea     = 1.
cmur      = 1.5
csawth    = 1.
currin    = 0.
cvol      = 1.
dene      = 1.06e+20
dign      = 1.
dnbeta    = 4.
dpreqr    = 0.4
falpha    = 1.
fbeta     = 0.69741817217124
fdene     = 0.18773671654819
fefac     = 1.4958453861368
flfac     = 0.1
fractn    = 0.2
ftr       = 0.5
fvsef     = 1.
gamma     = 0.5
ibetin    = 2
icurr     = 2
ideni     = 2
idivrt    = 2
ilnvqd    = 0
imprf     = 1
ipinjc    = 6
```

```
iout     = 1
ires     = 0
isc      = 3
iscrp    = 1
kappa    = 2.4
plasind  = 0.
pohc     = 0.
q        = 2.3
ralpne   = 3.7570000000000001e-02
recycle  = 0.75
rli      = 1.1
rmajor   = 2.995
rminor   = 0.83333333333334
rnbeam   = 2.9e-02
sbar     = 0.
scrapli  = 0.17000000100000001e-02
scraplo  = 0.14170000000001
taupre   = 2.
te       = 15.7
ti       = 21.25
tratio   = 1.02
triang   = 0.4
trial    = 0.1
zeff     = 2.005
zimp     = 8.
$
bmax0    = 11.115
fbcbkl   = 0.16702449207972
fbcbr    = 0.69325084463775
fbmax    = 1.
fcptoh   = 7.7035905069343 5e-02
fcpttf   = 1.0001615754107
fdshi    = 1.1036195352520
fdsho    = 2.0310561611015
fepoh    = 1.
feptf    = 1.
ffigmr   = 0.
ffwiht   = 1.
ffwirad  = 1.
ffwisdd  = 1.
fgmrin   = 0.
fohsts   = 1.
fqval    = 1.
ftfsts   = 0.98137738560640
ftfport  = 1.
fwalld   = 1.
fvs      = 3.3339344020003
itiber   = 1
walalw   = 1.3
$
avall    = 0.3
cordh    = -5.e-02
cordho   = 0.
ddweq    = 2.e-02
dfwi     = 2.e-02
dfwo     = 2.e-02
di2      = 0.
dido     = 0.
dosemax  = 4770000000.
do2      = 0.
dshi     = 0.40
dsho     = 1.25
freqdie  = 100.
fwoeq    = 2.e-02
```

```
htfmax   = 5.e-03
ioptsh   = 1
obdpc    = 0.75
portsz   = 1.2
ribdpc   = 0.
sddrmax  = 2.5
split    = 0.75
tburn    = 600.
tdwell   = 100.
theat    = 6.
tlife    = 10.
tohs     = 5.
tqnch    = 12.
tramp    = 30.
ttfqnch  = 0.
ttframp  = 0.
voifrc   = 0.25
$
acndut   = 5.1e-04
ajcmtf   = 1143000000.
bcylth   = 0.
casfact  = 1.55
csutf    = 1500000000.
csytf    = 1000000000.
dagi     = 2.e-02
dago     = 1.e-02
dcase    = 7000.
dcond    = 6500.
ddwex    = 5.e-02
ddwi     = 0.
dpstf    = 0.
dstrdtf  = 1.02e-03
ebuck    = 220000000000.
ecase    = 207000000000.
fcfbuc   = 1.
fcutf    = 0.41
fstndut  = 3.e-03
rhotf    = 0.
rjcontf  = 120021621.81927
ripple   = 1.
rmubuck  = 0.34
tfthkl   = 0.49
tfno     = 16.
tftmp    = 4.5
thkcas   = 6.2000000000001e-02
thlcndut = 5.000000000001le-04
thwcndut = 3.e-03
vftf     = 0.4
vgaptf   = 0.75
vtfskv   = 10.
ysbuck   = 414000000.
$
acdtoh   = 2.9e-04
alfapf   = 0.
aref     = 0.834
asaclpf  = 0.2
boresol  = 0.55
cfxl     = -3060000., -3060000., -3060000., -3060000., -3060000., -3060000., 0., 0., 0., 0., 0., 0., 0., 0., 0., 0., 0., 0., 0., 0., 0., 0.,
           0., 0., 0., 0., 0., 0., 0., 0., 0., 0., 0., 0., 0., 0., 0., 0., 0., 0., 0., 0., 0., 0., 0., 0., 0., 0., 0., 0., 0., 0., 0., 0., 0., 0.,
cohbop   = 11000000.,
coheof   = 27500000.,
cptdin   = 25000., 25000., 25000., 25000., 25000., 25000., 25000., 25000., 25000., 25000., 25000., 25000., 25000., 25000., 25000., 25000.,
           25000., 25000., 25000.,
ecasoh   = 207000000000.,
```

```
fcuoh     = 0.35
fsigax    = 0.20
fsigtan   = 0.3
gapboh    = 0.
ibias     = 1
ncls      = 2 2 2 2 2 2 0 0 0 0 0 0 0 0 0 0 0 0 0 0 0 0 0 0 0 0 0 0 0 0 0 0
nfxfh     = 7
nfxl      = 6
ngrp      = 6
ngrp0     = 0
ohhghf    = 0.24
rbcdtoh   = 1.72e-03
refbetp   = 1.04
refli     = 1.03
rfxl      = 0.0 0.0 0.0 0.0 0.0 0.0 0. 0. 0. 0. 0. 0. 0. 0. 0. 0. 0. 0. 0. 0. 0. 0. 0. 0. 0. 0. 0. 0. 0. 0. 0. 0. 0. 0. 0. 0. 0. 0.
            0. 0. 0. 0. 0. 0. 0. 0. 0. 0. 0. 0. 0. 0. 0. 0. 0. 0. 0. 0. 0. 0. 0. 0. 0. 0.
rlcref    = 7.91 3.99 0.796 -1.93 -3.70 -7.65 0. 0. 0. 0. 0. 0. 0. 0. 0. 0. 0. 0. 0. 0.
rlphbr    = 10.
rjconpf   = 25000000. 25000000. 25000000. 25000000. 25000000. 25000000. 10000000. 10000000. 25000000. 25000000. 25000000. 25000000.
            30000000. 30000000. 30000000. 30000000. 30000000. 30000000. 30000000. 30000000.
routr     = 5.14
roref     = 3.
rref(1,1) = 0.0 2. 4. 6.2 6.2 0.0 0. 0.
rref(1,2) = 0.0 2. 4. 6.2 6.2 0.0 0. 0.
soltx     = 0.52
tfhtr     = 3.270
thkcoh    = 5.e-02
tlcdtoh   = 1.e-03
tmpoh     = 4.5
twcdtoh   = 2 4e-03
vf        = 0.35 0.35 0.35 0.35 0.35 0.35 0.35 0.35 0.35 0.35 0.35 0.35 0.44 0.35 0.35 0.35 0.35 0.35 0.35 0.35
vfohc     = 0.44
vltoh     = 10000.
zref(1,1) = 2.4 4.25 4.25 2.5 1. 1.2 0. 0.
zref(1,2) = -2.4 -4.25 -4.25 -2.5 -1. -1.2 0. 0.
zfxl      = -0.625 -0.375 -0.125 0.125 0.375 0.625 0. 0. 0. 0. 0. 0. 0. 0. 0. 0. 0. 0. 0. 0. 0. 0. 0. 0. 0. 0. 0. 0. 0. 0. 0. 0. 0.
            0. 0. 0. 0. 0. 0. 0. 0. 0. 0. 0. 0. 0. 0. 0. 0. 0. 0. 0. 0. 0. 0. 0. 0. 0. 0. 0. 0. 0. 0. 0.
$
befblkt   = 0.
blnkti    = 0.
blnkto    = 0.
gapblki   = 0.
gapblko   = 0.
tbrmin    = 1.
vbz       = 0.6
vfblkt    = 0.25
$
bscfmax   = 0.99
enbeam    = 500.
echdat    = 50.
echfrq    = 240000000000.
ftritbm   = 0.5
iefrf     = 0
irfcd     = 1
$
ajsource  = 60.
ppsource  = 1.33
ppneut    = 1.93449999999999e-02
pptorus   = 1.33e-04
ab        = 80.
pmax      = 25000000.
nsource   = 2
tshield   = 0.25
efolda    = 0.69
```

148

```
lduct    = 0
ucost    = 1.690
$
pdiv     = 0.12
pbase    = 2.6e-06
tn       = 300.
rat      = 1.3e-08
ntype    = 0
nflag    = 0
cvalve   = 300000.
cduct    = 32500.
cshield  = 30.
ctpumpt  = 0.
ccpump   = 300000.
clc      = 1000000.
cbpump   = 225000.
$
ti       = 20. 40. 60. 80.
to       = 100. 110. 120. 130.
tm       = 0. 10. 20. 30. 40.
dpd      = 2.
dtc      = 10.
clt      = 40.
$
iscenr   = 2
$
iz       = 4
te0      = 20.
$
rxcl     = 1.
trcl     = 1.
row      = 4.
atcl     = 3.
clh1     = 3.
clh2     = 10.
fndt     = 2.
wgt      = 200000.
wgt2     = 100000.
shmf     = 0.5
hcwt     = 1.5
hccl     = 5.
plbv     = 20000.
conv     = 20000.
admv     = 50000.
shov     = 100000.
$
con      = 0.
peff     = 0.2
geff     = 0.2
tff      = 0.
dff      = 0.
regen1   = 1.
regen2   = 1.
regen3   = 1.
darea    = 10.
ctrit    = 1.5
br       = 0.99
tb       = 3.
bblm     = 0.
wc0n     = 10.
wvol     = 200000.
tdiv     = 10.
fco      = 1.
fa       = 1.
```

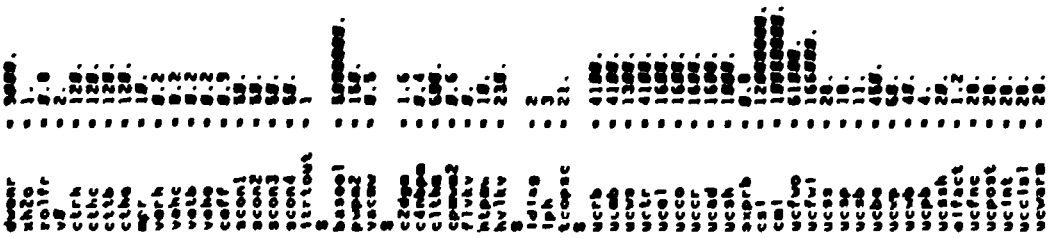

```
ucfp2     = 92000000.
ucfp3     = 363000000.
ucfs1     = 7070000.
ucfs2     = 12400000.
ucfs3     = 770.
ucmon     = 91.
ucscu     = 3000000.
ucgen1    = 1000000.
ucgen2    = 2000000.
ucflu1    = 116000.
ucflu2    = 2440000.
ucenr     = 15200000.
uccd1     = 2000000.
uccd2     = 2610000.
uccd3     = 3030000.
ucvp1     = 1160000.
ucvp2     = 36600000.
ucvp3     = 24400000.
eltlpr    = 1.2
uctac     = 1000000000.
ucme      = 60000000.
ucpp      = 0.33
ucacp     = 4.
uc2dg     = 1600000.
uc4mb     = 400000.
ucofe1    = 0.
ucofe2    = 60100000.
uclvd     = 6.000000000000001e-07
elacp     = 1.3
ucmisc    = 25000000.
uchrs     = 1.4
exphrs    = 0.8
cfind     = 0.35
cont1     = 0.2
cont2     = 0.1
$
*************************************************************************

***** starting point section *****



***** found a feasible starting point *****


estimate of the constraints (sqsumsq) =   0.1329e-04

the following are the   21 components  of the solution vector:

  i                 xce          xcm          residue      scafc        scale

  1   betap        0.1222e+01   0.1121e+01   0.2404e-04   0.1091e+01   0.9167e+00
  2   beta         0.7163e-01   0.1100e+01   0.9102e-06   0.6820e-01   0.1659e+02
  3   fdene        0.4127e+00   0.2190e+01   0.1344e-04   0.1077e+00   0.5327e+01
  4   fcpttf       0.8516e+00   0.8515e+00   0.8650e-06   0.1000e+01   0.9990e+00
  5   fcptoh       0.1115e+01   0.1440e+02   0.3940e-04   0.7704e-01   0.1290e+02
```

6	ftfport	0.9977e+00	0.9977e+00	0.1940e-06	0.1000e+01	0.1000e+01
7	fafac	0.1251e+01	0.0362e+00	0.3651e-04	0.1496e+01	0.6687e+00
8	rjcontf	0.1271e+09	0.1052e+01	0.4077e-06	0.1200e+09	0.8277e-08
9	fbeta	0.0269e+00	0.1106e+01	0.2006e-05	0.6974e+00	0.1434e+01
10	fvs	0.1013e+01	0.5430e+00	0.1729e-04	0.3334e+01	0.2999e+00
11	ftfsts	0.1692e+01	0.1724e+01	0.1220e-05	0.9814e+00	0.1019e+01
12	fwalld	0.9402e+00	0.9402e+00	0.2926e-06	0.1000e+01	0.1000e+01
13	rmajor	0.2995e+01	0.1000e+01	0.1947e-04	0.2995e+01	0.3339e+00
14	rnbeam	0.2927e-01	0.1009e+01	0.2821e-06	0.2900e-01	0.3448e+02
15	fqval	0.2121e+00	0.2121e+00	0.3716e-07	0.1000e+01	0.1000e+01
16	fohsts	0.1253e+01	0.1253e+01	0.2420e-06	0.1000e+01	0.1000e+01
17	ffwlrad	0.9902e+00	0.9902e+00	0.1037e-05	0.1000e+01	0.1000e+01
18	ffwladd	0.7407e+00	0.7407e+00	0.1097e-06	0.1000e+01	0.1000e+01
19	ffwlht	0.3203e+00	0.3203e+00	0.3400e-05	0.1000e+01	0.1000e+01
20	feptf	0.6868e+00	0.6865e+00	0.1067e-06	0.1000e+01	0.1000e+01
21	fepoh	0.7843e+00	0.7843e+00	0.2001e-06	0.1000e+01	0.1000e+01

the following are the 21 constraints:

		rcm
1	poloidal beta	-0.5683e-05
2	total beta	0.1542e-05
3	power balance	-0.1868e-05
4	tf port size	0.1883e-06
5	density limit	0.4039e-05
6	beta limit	-0.4017e-06
7	oh max. cpt	0.2201e-06
8	tf max. cpt	0.9916e-06
9	B at tf coil	0.3037e-06
10	v-s capability	-0.1140e-04
11	TF Coil stress	0.3420e-07
12	radial build	-0.4017e-06
13	wall loading	-0.4471e-07
14	hot beam ion den	-0.1013e-05
15	Q-value	0.1247e-05
16	OHC stress	0.0531e-00
17	ins. rad. dose	-0.4271e-06
18	shut. dose rate	-0.7847e-06
19	TFC nuc. heating	-0.1752e-05
20	TFC cond. stab.	0.2650e-05
21	OHC cond. stab.	-0.5114e-06

********** END OF STARTING POINT **********

****

****

***** final feasible point output *****

*** summary of values used in equation evaluation

betap = 0.122238e+01 beta = 0.716296e-01 bt = 5.55000 bp = 0.134388e+01

beta = 0.716296e-01

```
palp =   8.642723e+00 pohmpv =   8.345388e-02 ptri =   8.674488e+00ptre =   8.673489e+00 prad =   8.761477e-01
tf coil port size (m) =    1.32594required port size =    1.32982
dene =   8.186888e+21 dnellmt =   8.288868e+21
beta =   8.716296e-01  betalim =   8.885241e-01
peak solenoid cpt (A) =  -8.2257e+06 allowable solenoid cpt(A) =   8.2823e+06
TFC current/turn (a) =   8.3889e+05 allowable TFC current/turn(a) =   8.4886e+05
 tatf1 =   8.488162e+01 artf1 =   8.488162e+01
v-s requirement =   8.894827e+02 v-s cap. =  -8.493578e+02
 tf coil stress (Pa)) =     8.8452e+09 alowable stress (Pa) =     8.4998e+09
rbld =   8.299585e+01 rmajor =   8.299584e+01
wall load =   8.123269e+01 walalw =   8.138888e+01
dnbeam =    3.182e+18   dnbeam2 =    3.182e+18
fusion power (Mw) =    3.878e+02 inj. power (w) =   6.524e+07
  OHC stress =    6.259e+08  allowable str. =    4.998e+08
insulator dose (rad)=   4.7614e+09 max alw.=  4.7788e+09
 shut down dose rate in vault (mrem/hr) =     1.8516e+08 alowable =     2.5888e+08
 max TFC nuclear heating (w/cc) =   1.642e-03 allowable rate =    8.888e-03
 TF cond stab parameter =  8.946e+06 min TF cond stab    parameter =  3.888e+06

OHC cond. stab. parameter =  3.977e+08min OHC          stab. parameter =  3.888e+06

 end of equation info. summary
```

********** Start of Cost Output (M$) **********

211	Site improvements and facilities	12.00
212	Reactor building	34.05
213	Turbine building	0.00
2141	Reactor maintenance building	27.00
2142	Warm shop	4.55
215	Tritium building	16.94
216	Electrical equipment building	6.99
2171	Adminstration building	5.19
2172	Control room	4.52
2173	Shop & Warehouse	10.00
2174	Cryogenic building	3.02
2175	Miscellaneous buildings	10.00
21	total account 21 cost	141.02

********** Reactor Systems **********

22111	Inboard first wall	11.19
22112	Outboard first wall	8.00
2211	Total first wall	19.20
2212	Blanket	0.00
22131	Bulk shield	103.20
22132	Penetration shielding	0.00
2213	Total shield	103.20
22141	PF fence	1.00
22142	Center post	0.17
22143	Intercoil support structure	4.02
22144	Cold island support structure	1.51
22145	Warm support structure	7.40
2214	Total structure	17.90
2215	Divertor	50.32
221	Total account 221 cost	190.05

********** Magnets **********

22211	Conductor	56.95
22212	Winding	24.47
22213	Case	37.29
2221	TF Magnet assemblies	118.70
22221	conductor	21.13
22222	winding	28.79
22223	case	2.76
2222	PF Magnet assemblies	44.68
2223	Cryostat assembly	11.72
222	Total account 222 cost	175.10

********** Power Injection **********

22311	Source	0.00
22312	Distribution waveguide	0.00
22313	Ancillary equipment	0.00
22314	Power supplies	0.00
2231a	Equipment cost for one module	0.00
2231	Ech System cost	0.00
2232	Lower hybrid cost	54.23
2233	Neutral beam cost	157.70

223	Total account 223 cost	222.81
	********** Vacuum Systems **********	
2241	High vacuum pumps	5.44
2242	Backing pumps	7.20
2243	Vacuum duct	2.29
2244	Valves	4.91
2245	Duct shielding	0.00
2246	Instrumentation	1.00
224	Total account 224 cost	27.09
	********** Power Conditioning **********	
22511	power supplies	0.94
22512	breakers	3.17
22513	dump resistors	0.46
22514	I&C	1.04
22515	bussing	4.30
2251	total, tf power	12.97
22521	power supplies	22.37
22522	I&C	5.12
22523	bussing	2.62
22524	burn power supplies	2.50
22525	breakers	0.02
22526	dump resistors	0.07
22527	ac breakers	0.97
2252	Total, pf power	43.00
2253	Total, energy storage	0.00
225	Total account 225 cost	86.00
	********** Heat Transport System **********	
cpp	Pumps and piping system	7.12
chx	Primary heat exchanger	7.03
2261	total, reactor cooling system	18.39
cppa	pumps, piping	3.42
chxa	Heat exchanger	0.02
2262	total, auxiliary cooling system	10.91
2263	total, cryogenic system	21.05
226	Total account	50.37
	********** Fuel Handling System **********	
2271	fueling system	30.00
2272	Fuel processing and purification	6.17
2273	Storage and receiving systems	6.30
2274	Atmospheric recovery systems	19.00
2275	Water recovery systems	0.00
2276	Blanket recovery systems	28.13
227	Total account 227 cost	89.39
	********* Instrumentation and control *********	
228	Instrumentation and control	166.00

********** Maintenance equipment **********

229	Maintenance equipment	60.00

****

22	Total Account 22	976.67

********** Turbine plant equipment **********

23	Turbine plant equipment	0.00

********** Electric plant equipment **********

241	pulsed power system	9.35
242	Facility, ac power system	1.53
243	Two diesel generatos	1.60
244	Four no-break power supplies	0.40
245	Low voltage distribution	2.70
24	Account 24	20.25

******** Miscellaneous plant equipment ********

25	Miscellaneous plant equipment	25.00

********** Heat rejection system **********

26	Heat rejection system	15.86

********** Plant direct cost **********

2	Plant direct cost	1179.59

********** Process contingency **********

ccont'	Process contingency	196.33

********** Indirect cost **********

c9	Indirect cost	481.22

********** Project contingency **********

ccont2	Project contingency	185.61

********** Total contingency **********

ccont	Total contingency	388.95

********** Constructed cost **********

```
concost Constructed cost                                      2041.76

************* End of Cost Output ****************



************ START OF PLASMA OUTPUT **********


Plasma Geometry :

major radius (m)                        (rmajor)           2.995
minor radius (m)                        (rminor)           0.833
aspect ratio                            (aspect)           3.594
elongation                              (kappa)            2.400
triangularity                           (triang)           0.400
plasma sur. area (m**2)                 (sarea)        1.699e+02
plasma volume (m**3)                    (vol)          9.573e+01

plasma configuration = double null divertor


Current and Field :

plasma current (MA)                     (plascur/1.e6)    10.016
field on axis (T)                       (bt)               5.550
poloidal field (T)                      (bp)               1.343
edge safety factor                      (q)                2.300
q-star                                  (qstar)            2.067
q-star (no triang.)                     (qstar2)           2.171
 mean safety factor , q-bar, used for q

Beta Information:

plasma beta                             (beta)            0.0716
poloidal beta                           (betap)           1.2224
fast alpha beta                         (betaft)       1.402e-02
beam ion  beta                          (betanb)       7.327e-03
beta limit                              (betalim)      8.662e-02
Troyon beta scaling used with the coefficient        4.000

Temperature and density (volume averaged):

electron temperature (keV)              (te)              15.700
ion temperature (keV)                   (ti)              16.014
electron density (m**3)                 (dene)         1.060e+20
ion density (m**3)                      (dnitot)       8.864e+19
fuel density (m**3)                     (deni)         7.964e+19
high Z impurity n (m**3)                (dnz)          1.912e+18
cold alpha ash (m**3)                   (dnalp)        3.982e+18
hot beam density (m**3)                 (dnbeam)       3.102e+18
density limit (m**3)                    (dnelimt)      2.569e+20
```

effective charge	(zeff)	2.000e+00
mass weighted effective charge	(zeffai)	4.219e-01
density profile factor	(alphan)	1.020e+00
temperature profile factor	(alphat)	5.000e-01

Greenwald density limit used

Fusion power:

fusion power (MW)	(powfmw)	3.076e+02
alpha power (MW)	(alpmw)	6.153e+01
alpha power from nb (MW)	(palpnb)	0.934e+00
neutron wall load (MW/m**2)	(wallmw)	1.233e+00
fraction of pow to elec.	(falpe)	6.6233e-01
fraction of pow to ions	(falpi)	3.3767e-01

Plasma power balance terms :

ohmic heating power (MW)	(pohmpv*vol)	3.385e-01
Brehm. rad. power (MW)	(prad *vol)	7.389e+00
ion transport (MW)	(ptri*vol)	5.499e+01
electron transport(MW)	(ptre*vol)	6.447e+01
injected power to ions (MW)	(pcdssi)	4.383e+07
injected power to elec (MW)	(pcdsse)	2.141e+07

ion and electron confinement times =
modified Kaye-Glodston scaling
H-factor = 1.251
no inverse quadrature included

global confiment time (sec)	(taueff)	7.289e-01
ion energy conf.time (sec)	(tauei)	7.289e-01
elec energy conf time (sec)	(tauee)	7.289e-01
n-tau (sec/m**3)	(dntau)	7.727e+19

Volt-sec information :

total volt-sec req. (Wb)	(vsstt)	89.403
inductive volt-sec (Wb)	(vsind)	52.715
startup resistive (Wb)	(vsres)	10.367
flat-top resistive (Wb)	(vsbrn)	26.401
plasma resistance (ohm)	(rplas)	3.295e-09
plasma inductance (H)	(rlp)	5.263e-06
sawteeth coefficient	(csawth)	1.000e+00

Auxiliary information :

convective loss rate (A)	(qfuel)	6.992e+01
burnup fraction	(burnup)	5.000e-01
vertical field (T)	(bv)	1.060e+00

Ignition margins with various scalings

ion confinement = electron confinement

scaling law	conf. time (sec)	lg. margin
Neo-alcator	1.92864	2.41655
Mirnov	1.93963	2.42839
kaye-goldston - L	0.58358	0.00981
kaye-goldston - H	1.16788	1.54737
asdex - H	1.66478	2.12638
JAEA ASDEX-H	2.99985	3.48878

********** end of plasma output **********

******* START OF CURRENT DRIVE SECTION *****

ss rf efficiency (a/w)	0.17958
ss nb efficiency (a/w)	0.07776
cur. dr. eff. model #	0
s.s. cd power req (w)	6.5237e+07
bootstrap fraction	2.7688e-01

lower hybrid and neutral beam current drive used
lower hybrid fraction of current drive = 0.53000

neutral beam energy (kev)	500.00000
neutral beam current (A)	87.65564
neutral beam power (w)	4.3928e+07
ech power	0.
lower hybrid power (w)	2.1489e+07

******** end of Current Drive output *******

1

MODULE: NBEAM -- NEUTRAL BEAMS

pinj = 4.383e+01 total injected power requirement (MW)

```
ebeam    = 5.000e+02 beam energy requirement (keV)
aibeam   = 8.766e+01 total injected current requirement (A)
nlines   = 2          no. of beamlines
effcy    = 3.372e-01 overall efficiency -- inj. power / wall-plug power
pwp      = 1.300e+02 total wall-plug power (MW)
ucost    = 1.698e+00 neutral beam unit cost -- $/W of wallplug power norm. to 500 keV energy ($/W)
cost     = 2.207e+08 total cost of beamlines and power supplies ($)

nsource  = 2          no. of source arrays/beamline
ajsource = 6.000e+01 av. source current density (A/m2)
a        = 1.183e-01 source array width (m)
b        = 9.465e+00 source array height (m)
asource  = 4.479e+00 total area of all sources (m2)

psource  = 1.000e-02 source pressure (torr)
paccl    = 1.000e-04 accelerator pressure (torr)
pneut    = 1.455e-04 neutralizer inlet pressure (torr)
pnout    = 1.455e-05 neutralizer outlet pressure (torr)
plast    = 1.455e-05 final line pressure (torr)
ptorus   = 1.000e-06 torus vacuum pressure (torr)
qtorus   = 9.071e+19 room temp gas load to torus from all beamlines (D2 molecules/sec)

ep       = 9.500e-01 power supply efficiency
ea       = 8.499e-01 accel (current) efficiency (power efficiency = ea/2 + 0.5)
en       = 5.000e-01 neutralizer efficiency
el       = 9.045e-01 final line efficiency
es       = 6.721e-01 collimator skimmer efficiency
effcyi   = 3.262e-01 beamline current efficiency
effcy    = 3.372e-01 overall (power) efficiency

plossp   = 6.490e+00 total loss in power-supplies (MW)
plossa   = 4.633e+00 accelerator loss per beamline (MW)
plossn   = 2.398e-01 neutralizer loss per beamline (MW)
plossl   = 5.138e-01 final line loss per beamline (MW)
plosss   = 1.069e-01 collimation skimmer loss per beamline (MW)

zsrcaccl = 3.200e+00 source/accel. length (m)
zneut    = 3.000e-01 neutralizer length (m)
zlast    = 5.000e+00 final line length (m)
zsrcplsm = 4.571e-01 total line length from source to plasma (m)
zfocus   = 4.110e+01 distance from source to min focus between outer TF coil legs (m)
zext     = 3.020e+01 length of beamline external to vacuum vessel (m)

efolds   = 6.900e-01 collimator width in narrow direction (beam e-folds)
wduct    = 4.119e-01 width of duct at min focus between outer tf coil legs (m)
hduct    = 8.420e-01 height of duct at min focus (m)
wtf      = 1.326e+03 minimum permissible separation of of outer TF coil legs -- case to case (m)
zduct    = 4.607e+00 distance from min focus to tangential intercept at plasma axis (m)
```

OUTPUT FROM FUELING MODULE

Plasma Parameters:

ra(cm)	Te0(keV)	alpt	ne0(cm**-3)	alpn

83.33	24.81	0.58	0.214e+15	1.02

Pellet Size and Composition:

rp@(mm)	%D2	%T2	mass(mg)
2.00	0.500	0.500	0.67

Speed and Rep-Rate Requirement:

penetration(cm)	req speed(km/s)	rep-rate(1/s)
33.33	22.83	0.16

Injector Scheme:

injector	speed ok?	# port	launcher(m)
laser-jet	yes	1	59.9

Gas Load, Power, and Cost Estimates:

D,T gas load(g/hr)	power(kW)	Cost(M$)
23.33	3.06	30.0

****** RADIAL BUILD ********
(m)

	Thickness	Radius
Device Centerline	0.0	0.000
Bore	0.550	0.550
O. H. Solenoid	0.520	1.070
Gap	0.000	1.070
Bucking Cylinder	0.000	1.070
TF Coil	0.490	1.560
Cryostat	0.000	1.560
Gap	0.020	1.580
Shield - inboard	0.480	2.060
Gap	0.000	2.060
Inboard Blanket	0.000	2.060
Gap	0.000	2.060
First Wall - inboard	0.020	2.080
Scrape Off	0.082	2.162
Plasma C/L	0.833	2.995
Plasma Edge	0.833	3.828
Scrape Off	0.142	3.970
First Wall - outboard	0.020	3.990
Gap	0.000	3.990
Outboard Blanket	0.000	3.990
Gap	0.000	3.990
Shield - outboard	1.250	5.240
Lead	0.000	5.240
Gap	0.010	5.250
Cryostat	0.000	5.250
TF Coil	0.490	5.740

Cryostat 0.850 5.790

********** Start of Divertor Output **********

**********INPUT**********

Atomic number of div. plate surface material	4
Number of divertor nulls	2
Peak plasma temperature at divertor plate, ev	20.000
major radius, m	2.995
fusion power, Mw	387.631
auxilliary power, Mw	65.237
Number of disruptions per full power year	100.000
Helium fraction	0.030
Oxygen fraction	0.010

**********OUTPUT**********

Gross erosion rate due to sputtering, cm/yr	411.189
Net erosion rate due to sputtering, cm/yr	6.295
Average impurity fraction in plasma	0.014
Heat load to divertor, Mw	31.691
Divertor plate area, m2	71.881
Heat load to first wall, Mw	95.072
Tritium permeation rate (divertor), gm/day	0.002
Tritium permeation rate (first wall), gm/day	0.110
Divertor plate life based on erosion, yrs	0.149
Charge-exchange tritium current to wall,atom/s	0.618e+24
Wall area receiving tritium current, m2	25.353

********** End of Divertor Output **********

******* Start of First Wall Blanket Shield **********

ainwl	: Average Inboard Neutron Wall Loading.....	MW/m**2	1.2327e+00
aonwl	: Average Outboard Neutron Wall Loading.....	MW/m**2	1.2327e+00
tbr	: Tritium Breeding Ratio.....	t/DTn	1.0000e+00
fpys	: DT Full Power Years of Operation.....	y	2.5157e+00
ifwa	: Inboard First Wall Surface Area.....	m**2	6.7427e+01
ofwa	: Outboard First Wall Surface Area.....	m**2	1.3258e+02
aishl	: Average Inboard Surface Heat Load.....	MW/m**2	4.7553e-01
aoshl	: Average Outboard Surface Heat Load.....	MW/m**2	4.7553e-01
ifwbstm	: Inboard Tile, First Wall, Blanket, and Shield thickness....	m	5.0000e-01
ofwbstm	: Outboard First Wall, Blanket, and Shield thickness.....	m	1.2700e+00
tfwl	: Total Inboard first wall length in The Z-Direction.....	m	5.1593e+00
nod	: Number of Disruption per Full Power Year.....	#/fpy	1.0000e+02
dpd	: Disruption Power Density.....	MJ/m**2	2.0000e+00
dtc	: Disruption Time Condtsnt.....	ms	1.0000e+01
cit	: Coolant Inlet Temperature.....	celsius	4.0000e+01
tc	: Tritium Current to First Wall.....	t/s/cm2	2.4302e+10
fwotc	: First Wall Area With Tritium current.....	m**2	2.5353e+01
tmr	: Outboard Beryllium Zone Thickness.....	m	1.6000e-01
tip	: Total Inboard Power.....	MW	1.4026e+02

ptop	Total Outboard Power	MW	3.1021e+02
pt	Total Power	MW	4.5847e+02
psh	Tile Surface Heating	MW/m**2	4.7553e-01
pth	Tile nuclear Heating	MW/m**3	7.8938e+00
pfwsh	Outboard First Wall Surface Heating	MW/m**2	4.7553e-01
pfwnh	Outboard First Wall Nuclear Heating	MW/m**3	2.1971e+01
pfwdpa	Outboard First Wall Atomic Displacement	dpa	3.9788e+01
pfwfnf	Outboard First Wall Fast Neutron Fluence	n/cm**2	2.3887e+22
pfwtnf	Outboard First Wall Total Neutron Fluence	n/cm**2	3.5222e+22
pfwhep	Outboard First Wall Helium Production	appm	2.3821e+03
pfwhp	Outboard First Wall Hydrogen Production	appm	6.7884e+02
coolt	Coolant Outlet Temperature	celsius	6.0000e+01
ifcfr	Inboard Coolant Flow Rate	g/s	2.0587e+06
ofcfr	Outboard Coolant Flow Rate	g/s	4.3076e+06
tfcfr	Total Coolant Flow Rate	g/s	6.3662e+06
fwe	First Wall erosion for Steel Structure	cm	1.1172e-15
fwtor	First Wall Tritium Permeation Rate (steady state)	g/d	1.2912e-01
fwtl	First Wall Tritium Inventory (steady state)	g	4.6547e+02
mcch	Maximum Coil Case Heating	W/cm**3	3.1028e-03
mwch	Maximum Coil Winding Heating	W/cm**3	1.6416e-03
tcch	Total Coil Case Heating	W	6.4067e+03
twch	Total Coil Winding Heating	W	1.2855e+04
mcfnf	Maximum Fast Neutron Fluence in the Coil Winding	n/cm**2	8.2216e+18
mcdad	Maximum Atomic Atomic Displacement in the Cooper Stablizer	dpa	4.0781e-03
mcdir	Maximum Induced Resistivity in the Copper Stablizer	nohm.cm	4.3650e+02
mcld	Maximum Electrical Insulator Dose	rads	4.7614e+09
dmasirv	Dose equivalent One Day After Shutdown Inside Reactor Vault	mrem/h	1.8516e+00

********** End of First Wall Blanket Shield ********

********** START OF TF COIL OUTPUT **********

----- Superconducting TF coils -----

number of TF coils (tfno) = 16.00000

tf coil ripple:
reqd. ripple = 1.000
cal. ripple = 0.370

outboard midplane inter-tf-coil spacing (m)
(case to case)

outer tfcoil clearance = 0.1329e+01
minimum clearance = 0.1326e+01

Current Density :
cond current density (a/m2) = 0.127889e+09
winding pack current den. = 0.439289e+08
overall current density = 0.287697e+08

```
   tf coil area (m2)=   8.2501
    inner thickness =          0.498
    inside half width =   0.300   outside half width =   0.289   corner cut =0.092
    tma turns =     83.112
    ripple (%) =     0.378
    max field(t) =  11.096

    stored energy/coil (gJ) =   0.319
    mean coil circum. (m) =    18.712

 coil geometry :

    * inner leg radius, r1 (m)          =  1.315
    * outer leg radius, rtotl (m)       =  5.495
    * max hight, hmax (m)               =  3.250
    * radius to max hight, rhmax (m)    =  2.570
    * clear bore (m)                    =  3.690
    * clear vertical bore (m)           =  6.500
 * (measured from torroidal axis to inside of TF Coil)
 * (measured from toroidal axis to middle of coil)

   weight per coil (kg) =0.4884e+05
                cond weight =0.1158e+05   density (kg/m3) = 8986.66   vftf = 0.40
                case weight =0.2842e+05   density          = 7866.66
                tcas weight = 0.1582e+06


     weight per coil (lbs) =0.8821e+05
                cond weight =0.2554e+05   density (lb/in3) =   0.32   vftf = 0.40
                case weight =0.6267e+05   density          =   0.28

the TF Coil shape is approximated by arcs between the    following points:

point          x (m)          y (m)

  1              1.560          6.000
  2              1.660          2.700
  3              2.570          3.250
  4              3.460          2.190
  5              5.250          0.000


center of arcs between  the points are:

arc #          x-center (m)   y-center (m)
  1              4.939          1.231
  2              2.503          2.329
  3              2.394          1.001
  4              1.850          0.000


Conductor Information :
   conduit cond. + void area (m**2)   5.1000e-04
   conduit case thickness (m)         3.0000e-03
   conduit insulation thickness (m)   5.0000e-04
   outer coil case thickness (m)      6.2000e-02
   outer coil case area (m**2)        1.2563e-01

   conductor area/coil (m**2)         4.8873e-02
   stucture area/condutor area        1.0352e+00
   insulation area/condutor area      1.9120e-01
```

```
  void area/conductor area              6.6667e-01

  tensile stress (Pa)                   2.0219e+08
  compress. stress (Pa)                 6.4388e+08
  total tresca stress (Pa)              8.4519e+08
  allowable stress (Pa)                 4.9958e+08
  case tensile strain                   9.7677e-04

  tf turns / coil                       1.3357e+02
  current per turn (a)                  3.8889e+04

********** Start of TF Superconducting Analysis ******

Peak field at the winding, T  (bm       ) =    11.1
Ampere-turns/coil , A-turns   (at       ) =   5.195e+06
Operating Current,A           (aio      ) =   3.889e+04
Conduit corner bend radius,m  (rb       ) =   3.000e-03
Conduit wall thickness,m      (tw       ) =   3.000e-03
Condutor insulation thick,m   (tl       ) =   5.000e-04
He fraction inside conduit    (fhe      ) =   0.400
Area inside the conduit,m2    (acs      ) =   5.100e-04
Jopt over cable space,A/m2    (ajo      ) =   7.625e+07
Jopt over conduit     ,A/m2   (ajw      ) =   4.393e+07

Jmax in bronz, Bm, T=0 ,A/m2  (ajcm     ) =   1.143e+09
Dia of supercondutor strand,m (dr       ) =   1.020e-03
Winding bulk temperature,K    (tba      ) =    4.50
Fraction of Cu in SC strand   (fcu      ) =   0.410
Non-Cu fract.  in SC strand   (fnoncu   ) =   0.590
Thermal cont.- conduit,(m/m)  (strsh    ) =  -1.740e-02
Thermal cont.- filament,(m/m) (strfil   ) =  -7.300e-03
Yield stress of copper,Pa     (cusy     ) =   6.000e+07
Yield stress of bronz,Pa      (bzsy     ) =   1.190e+08
Youngs modulus of filament,Pa (efil     ) =   1.650e+11
Number of strands             (ns       ) =   64
Area inside conduit,m2        (acs      ) =   5.100e-04
Area of all NbSn films.,m2    (tfila    ) =   5.236e-05
Area of conduit wall,m2       (acl      ) =   2.059e-04
Millers empirical factor      (ffhe     ) =   6.622e-02
Init cooldown strain,T=1000-4K(eint     ) =  -4.966e-03
Dilation strain in cond wall  (esh      ) =   9.760e-04
Net strain in the SC filament (eof      ) =  -4.097e-03
Jc of non-cu @T&B,A/m2        (ajc      ) =   5.465e+08
Jc of non-cu @ Bm,A/m2        (ajco     ) =   9.764e+08
Tc @ zero strain and @ B=0    (tcmo     ) =   18.0
Tc @ zero strain and @ Bm     (tcm      ) =   18.0
Tc @ operating strain and @ Bm(tco      ) =   18.2
Ratio Io/Ic                   (aiol     ) =   0.394
JWDG-LTD by B,T & Strain, A/m2(ajcwdg   ) =   1.115e+08

----- stability output -----

Stability Parameter ,         (eta      ) =   0.226
He heat cap.in conduit,J/m3-K (she      ) =   5.110e+05
Heated cond.length-1/2 turn,m (hl       ) =    9.36
Resistivity of Cu,ohm-m       (curho    ) =  6.925e-10
Duration of heat pulse,s      (th       ) =   1.000e-03
Current sharing temperature,K (tcs      ) =    7.97
J LTD by heat transfer A/m2   (ajht     ) =   0.954e+07
JWDG-LTD by heat trans., A/m2 (ajwht    ) =   5.150e+07
```

```
 J LTD by stability,A/m2          [ajstab  ] =   9.692e+07
 JWDG-LTD by stability,A/m2       [ajwstab ] =   5.583e+07
 Stability margin,j/m3            [ep      ] =   4.946e+05
 Min stability margin,j/m3        [epmin   ] =   3.000e+05
 Recovery time,s                  [tr      ] =   2.523e-02
 Temperature margin (tcs-tb),K    [tmarg   ] =    3.47
 Helium inlet pressure ,Pa        [pr      ] =   6.000e+05


 ----- protection output -----

 J LTD by protec. reqmnts,A/m2    [ajcp    ] =   4.814e+08
 JWDG LTD by protec. reqmnts,A/m2 [ajw     ] =   2.773e+08
 Length of the cooled channel,m   [al      ] =    115.
 Maximum quench pressure,Pa       [pmax    ] =   1.010e+08
 Maximum wdg temperature,K        [tmax    ] =    160.

 J LTD by quench pressure,A/m2    [ajprot  ] =   1.296e+08
 JWDG LTD by quench pres.,A/m2    [ajw     ] =   7.466e+07

 PERMISSIBLE CURRENT DENSITY , (A/m2) (WDG )    5.150e+07
PERMISSABLE CURRENT , (A)  [CPTTF0] =           4.566e+04


************ End of TFC Supercondutor ************
```

TF Coil SC power conversion data

```
 #ettfmj,stored energy of tf coils, mj          5104.
 #itfka, tf coil current,ka                     38.00
 #ntfc, number of tfcoils                       16.00
 #vtfskv, max. voltage across coil, kv          10.00
 tchghr, tf coil charge time, hours             4.000

 ltfth, inductance of all tf coils, h           6.749
 rcoils, resistance of all tf coils,ohms        0.
 lptfcs inductance per tf coil, henries         0.4218
 tfcv, tf coils charging voltage, volts         85.24
 ntfbkr, number of dc circuit breakers          16.00
 ctfbkm, cost of dc circuit breakers, $m        2.639

 ndumpr, number of dump resistors               64.00
 rldump, one dump resistor, ohms                0.2571
 rippmw, dump resistor peak power, mw           97.22
 rlemj, energy to a dump resistor, mj           79.75
 ttfsec, 1/r time constant of tf coils,s        1.640
 ctfdrm, cost of dump resistors, $m             0.0966

 tfpsc, power supply voltage, volts             89.50
 tfpska, power supply current, ka               40.03
 #tfckw, dc power supply rating, kw             3595.
 tfackw, ac kw for charging tf coils, kw        4061.
 rpower, tf coil resistive power, mw            2.686
 xpower, tf coil inductive power, mw            0.7009
 ctfpsm, cost of tf supplies, $m                0.7797

 djmka, al bus current density, ka/sq.cm        0.1250
 albusa, al bus section area, sq. cm            311.1
 #tfbusl, total length of tf bussing, m         2946.
 albuswt, al bus weight, metric tons            171.9
```

rtfbus, total tf bus resistance, ohms		8.1723e-02
vtfbus, tf coil bus voltage drop, volts		67.02
ctfbsm, cost of tf bussing, $m		4.813
ctflcm, cost of tf load control ctr, $m		8.1559
ctfclm, cost of control & instr, $m		1.010
ctfpcm, total cost of tf power conv, $m		10.50
#drarea, dump resistor area ,sq.m		598.7
#tfcfsp, tf power conv floor space,sq.m		829.3
tfcbv, tf power conv bldg volume, cu.m		4976.

tf coil power conv. summary

ctfpct, total tf power conv. cost, $m		10.50
spwrmw, total tf ac xpower demand, mw		8.7076
#tfacpd, total s.s. ac power demand, mw		2.096
tftsp, tf pwr conv. floor space, sq.m		829.3
tftbv, tf pwr conv. bldg. volume, cu.m		4976.

--global outputs

********** START OF PF COIL OUTPUT **********

OH Coil Stress

tresca stress (MPa)	(sigoh)	6.259e+02
tang. stress (MPA)	(sigohtan)	5.864e+02
axial stress (MPa)	(sigohax)	1.196e+02
tang. fudge factor	(fsigtan)	3.000e-01
axial fudge factor	(fsigax)	2.000e-01
bmax in OHC (T)	(bmaxoh)	13.784

structure-to-conductor ratio =	1.169
cond current density (a/m2) =	1.390e+08
winding pack current den.	3.950e+07
overall current density =	2.790e+07

Superconductor information :

condult cond. + void area (m**2)	2.900e-04
condult case thickness (m)	2.400e-03
condult insulation thickness (m)	1.000e-03
outer coil case thickness (m)	5.000e-02
outer coil case area (m**2)	2.000e-01
conductor area/coil (m**2)	8.162870e+00
stucture area/condutor area	8.116857e+01
insulation area/condutor area	8.918885e-01
void area/conductor area	8.785714e+00
case tensile strain	8.244632e-02
OHC # turns	8.188290e+04

current per turn (a) -0.225673e+05

edge locations of pf coils, OH coil and plasma
ra(b) is inner (outer) radius
zh(l) is the high (low) vertical location

ra	rb	zl	zh	turns	index
0.51	1.00	2.09	2.66	367.00	1
0.51	1.00	-2.09	-2.66	367.00	1
1.75	2.25	3.97	4.47	200.00	1
1.75	2.25	-3.97	-4.47	200.00	1
4.03	4.19	4.14	4.38	20.00	1
4.03	4.19	-4.14	-4.38	20.00	1
6.17	6.45	2.33	2.51	87.00	1
6.17	6.45	-2.33	-2.61	87.00	1
6.12	6.50	0.70	1.16	160.00	1
6.12	6.50	-0.70	-1.16	160.00	1
0.56	1.03	0.94	1.48	241.00	1
0.56	1.03	-0.94	-1.48	241.00	1
0.55	1.07	-0.70	0.70	1002.90	1
2.16	3.03	-2.00	2.00	1.00	2

pf coils

coil	circuit	current (ma)	current/turn (a)	turns	j (amp/m 2)	* r (m)	** zpf (m)	wtc (kg)	wts (kg)	field (T)
pf coil	1	9.17	24997.49	367.00	0.279e+00	0.00	2.37	7685.11	1537.02	10.09
pf coil	2	9.17	24997.49	367.00	0.279e+00	0.00	-2.37	7685.11	1537.02	10.09
pf coil	3	6.99	24955.53	280.00	0.279e+00	2.00	4.22	14681.10	2936.22	7.16
pf coil	4	6.99	24955.53	280.00	0.279e+00	2.00	-4.22	14681.10	2936.22	7.16
pf coil	5	-0.68	-24184.17	28.00	0.279e+00	4.11	4.22	2938.00	586.02	1.04
pf coil	6	-0.68	-24184.17	28.00	0.279e+00	4.11	-4.22	2938.00	586.02	1.04
pf coil	7	-2.16	-24791.39	87.00	0.279e+00	6.31	2.47	14328.29	2865.66	3.31
pf coil	8	-2.16	-24791.39	87.00	0.279e+00	6.31	-2.47	14328.29	2865.66	3.31
pf coil	9	-3.98	-24862.54	160.00	0.279e+00	6.31	0.97	26426.50	5285.30	4.67
pf coil	10	-3.98	-24862.54	160.00	0.279e+00	6.31	-0.97	26426.50	5285.30	4.67
pf coil	11	-6.02	-24961.99	241.00	0.279e+00	0.00	1.17	5039.46	1007.89	8.19
pf coil	12	-6.02	-24961.99	241.00	0.279e+00	0.00	-1.17	5039.46	1007.89	8.19
OH Coil	13	-22.63	-22567.33	1002.90	0.279e+00	0.81	0.00	15300.60	5276.05	13.75
		80.11						157481.66	33712.27	

* r is measured from the toroidal axis
** zpf is measured from horizontal mid-plane

********** end of pf coil output **********

********** Start of OHC Supercondutor Analysis ** **********

Peak field at the winding, T	[bm	] =	13.8
Ampere-turns/coil , A-turns	[at	] =	2.263e+07
Operating Current,A	[aio	] =	2.257e+04
Conduit corner bend radius,m	[rb	] =	1.720e-0[illegible]
Conduit wall thickness,m	[tw	] =	2.400e-03
Condutor insulation thick,m	[ti	] =	1.000e-03
He fraction inside conduit	[fhe	] =	0.440
Area inside the conduit,m2	[acs	] =	2.900e-04
Jopt over cable space,A/m2	[ajo	] =	7.702e+07
Jopt over conduit ,A/m2	[ajw	] =	3.959e+07
Jeax in bronz, Bm, T=0 ,A/m2	[ajcm	] =	1.143e+09
Dia of supercondutor strand,m	[dr	] =	7.000e-04
Winding bulk temperature,K	[tba	] =	4.50
Fraction of Cu in SC strand	[fcu	] =	0.350
Non-Cu fract. in SC strand	[fnoncu	] =	0.650
Thermal cont.- condult,(m/m)	[strsh	] =	-1.740e-02
Thermal cont.- filament,(m/m)	[strfil	] =	-7.300e-03
Yield stress of copper,Pa	[cusy	] =	6.000e+07
Yield stress of bronz,Pa	[bzsy	] =	1.190e+08
Youngs modulus of filament,Pa	[efil	] =	1.650e+11
Number of strands	[ns	] =	79
Area inside conduit,m2	[acs	] =	2.900e-04
Area of all NbSn films.,m2	[tfila	] =	3.061e-05
Area of conduit wall,m2	[acl	] =	1.752e-04
Millers empirical factor	[ffhe	] =	5.360e-02
Init cooldown strain,T=1000-4K	[eint	] =	-4.572e-03
Dislation strain in cond wall	[esh	] =	2.446e-03
Net strain in the SC filaments	[eef	] =	-2.394e-03
Jc of non-cu @T&B,A/m2	[ajc	] =	6.184e+08
Jc of non-cu @ Bm,A/m2	[ajco	] =	1.054e+09
Tc @ zero strain and @ B=0	[tcmo	] =	10.0
Tc @ zero strain and @ Bm	[tcm	] =	9.09
Tc @ operating strain and @ Bm	[tco	] =	8.85
Ratio Io/Ic	[aioic	] =	0.412
JWDG-LTD by B,T & Strain, A/m2	[ajcwdg	] =	9.677e+07

----- stability output -----

Stability Parameter ,	[ats	] =	0.227
He heat cap.in conduit,J/m3-K	[shc	] =	5.110e+05
Heated cond.length-1/2 turn,m	[hl	] =	2.54
Resistivity of Cu,ohm-m	[curho	] =	0.215e-10
Duration of heat pulse,s	[th	] =	1.000e-03
Current sharing temperature,K	[tcs	] =	7.06
J LTD by heat transfer A/m2	[ajht	] =	6.977e+07
JWDG-LTD by heat trans., A/m2	[ajwht	] =	3.841e+07
J LTD by stability,A/m2	[ajstab	] =	9.911e+07
JWDG-LTD by stability,A/m2	[ajwstab	] =	4.822e+07
Stability margin,j/m3	[ep	] =	3.977e+05
Min stability margin,j/m3	[epmin	] =	3.000e+05
Recovery time,s	[tr	] =	1.392e-02
Temperature margin (tcs-tb),K	[tmarg	] =	2.56
Helium inlet pressure ,Pa	[pr	] =	6.000e+05

----- protection output -----

```
 J LTD by protec. reqmnts,A/m2   (ajcp   ) =   9.783e+07
 JWDG LTD by protec. reqmnts,A/m2 (ajw   ) =   4.924e+07
 Length of the cooled channel,m  (al     ) =    21.9
 Maximum quench pressure,Pa      (pmax   ) =   1.854e+08
 Maximum wdg temperature,K       (tmax   ) =    150.

 J LTD by quench pressure,A/m2   (ajpres ) =   3.778e+08
 JWDG LTD by quench pres.,A/m2   (ajw    ) =   1.918e+08

 PERMISSIBLE CURRENT DENSITY , (A/m2) (JWDG )   3.541e+07
PERMISSABLE CURRENT , (A)  (CPTTF=1) =          2.823e+04

********** End of OHC Superconductor Analysis ********

1


          MODULE: STRUCT  --  TORUS SUPPORT STRUCTURE
          -------------------------------------------


 MASSES:
 ------
 fncmass = 3.578e+04   mass of outer pf coil fence (kg)
 postmass= 6.248e+03   mass of center post (kg)
 aintmass= 1.722e+05   mass of intercoil support (kg)
 cislmass= 9.356e+04   mass of cold island support (incl struts) (kg)

 coldmass= 3.077e+05   total mass of cold support structure (kg)
 warmmass= 2.672e+05   total mass of warm support structure (shield support + warm struts) (kg)

 sprtmass= 5.749e+05   total mass of torus support structure (warm + cold) (kg)


 COSTS  (structure unit cost= 28.0 $/kg)
 ------
 fnccost = 9.995e+05   cost of outer pf coil fence ($)
 postcost= 1.749e+05   cost of centerpost ($)
 aintmass= 4.820e+06   cost of intercoil support structure ($)
 cislcost= 2.620e+06   cost of cold island support ($)

 coldcost= 8.614e+06   total cost of cold support structure ($)
 warmcost= 7.483e+06   total cost of warm support structure ($)

 sprtcost= 1.610e+07   total cost of torus support structure ($)



********** START OF VOLT-SEC OUTPUT **********

                  total volt-second summary
```

	volt-sec start-up	volt-sec burn	volt-sec total
ef :	-35.82	-1.89	-37.70
oh :	-11.07	-0.58	-11.65
total:	-46.89	-2.47	-49.36

summary of volt-sec by circuit during start-up

circuit	
1	-0.38
2	-0.38
3	1.13
4	1.13
5	1.25
6	1.25
7	-5.90
8	-5.90
9	-10.61
10	-10.61
11	-3.49
12	-3.49
OHC	-11.07
total	-46.89

wave forms
current per coil (a)

circuit	time (sec) 0.00	0.00	30.00	36.00	42.00	842.00	851.00	854.00
1	0.	0.	0.917e+07	0.707e+07	0.708e+07	0.773e+07	0.	0.
2	0.	0.	0.917e+07	0.707e+07	0.708e+07	0.773e+07	0.	0.
3	0.	0.	0.469e+07	0.676e+07	0.607e+07	0.699e+07	0.	0.
4	0.	0.	0.469e+07	0.676e+07	0.607e+07	0.699e+07	0.	0.
5	0.	0.	-0.677e+06	0.108e+06	0.233e+06	0.208e+06	0.	0.
6	0.	0.	-0.677e+06	0.108e+06	0.233e+06	0.208e+06	0.	0.
7	0.	0.	0.472e+06	-0.189e+07	-0.283e+07	-0.216e+07	0.	0.
8	0.	0.	0.472e+06	-0.189e+07	-0.283e+07	-0.216e+07	0.	0.
9	0.	0.	-0.945e+06	-0.359e+07	-0.378e+07	-0.398e+07	0.	0.
10	0.	0.	-0.945e+06	-0.359e+07	-0.378e+07	-0.398e+07	0.	0.
11	0.	0.	0.868e+07	-0.485e+07	-0.543e+07	-0.682e+07	0.	0.
12	0.	0.	0.868e+07	-0.485e+07	-0.543e+07	-0.682e+07	0.	0.
13	0.	0.	0.957e+07	-0.194e+08	-0.218e+08	-0.226e+08	0.	0.
plasma(a)	0.	0.	0.	0.188e+08	0.188e+08	0.188e+08	0.	0.

********** end of volt-sec output **********

********** START OF INDUCTANCE OUTPUT ********

Inductance matrix (H*turn**2)

circuit	1	2	3	4	5	6	7	8	9	10
1	0.1733e+00	0.9654e-03	0.2451e-01	0.1548e-02	0.2373e-02	0.4886e-03	0.6362e-02	0.3148e-02	0.1886e-01	0.8819e-02
0.1871e-01	0.1418e-02	0.2018e-01	0.7993e-04							
2	0.9654e-03	0.1733e+00	0.1548e-02	0.2451e-01	0.4886e-03	0.2373e-02	0.3148e-02	0.6362e-02	0.8819e-02	0.1886e-01
0.1418e-02	0.1871e-01	0.2018e-01	0.7993e-04							
3	0.2451e-01	0.1548e-02	0.4811e+00	0.3817e-02	0.1681e-01	0.1196e-02	0.2775e-01	0.9814e-02	0.3918e-01	0.2589e-01
0.6852e-02	0.1777e-02	0.1488e-01	0.1452e-03							
4	0.1548e-02	0.2451e-01	0.3817e-02	0.4811e+00	0.1196e-02	0.1681e-01	0.9814e-02	0.2775e-01	0.2589e-01	0.3918e-01
0.1777e-02	0.6852e-02	0.1488e-01	0.1452e-03							
5	0.2373e-02	0.4886e-03	0.1681e-01	0.1196e-02	0.1698e-01	0.4313e-03	0.1288e-01	0.3632e-02	0.1897e-01	0.9669e-02
0.1885e-02	0.4648e-03	0.3109e-02	0.3858e-04							
6	0.4886e-03	0.2373e-02	0.1196e-02	0.1681e-01	0.4313e-03	0.1698e-01	0.3632e-02	0.1288e-01	0.9669e-02	0.1897e-01
0.4648e-03	0.1885e-02	0.3109e-02	0.3858e-04							
7	0.6362e-02	0.3148e-02	0.2775e-01	0.9814e-02	0.1288e-01	0.3632e-02	0.2418e+00	0.3277e-01	0.1712e+00	0.8992e-01
0.4838e-02	0.2778e-02	0.1497e-01	0.2054e-03							
8	0.3148e-02	0.6362e-02	0.9814e-02	0.2775e-01	0.3632e-02	0.1288e-01	0.3277e-01	0.2418e+00	0.8992e-01	0.1712e+00
0.2778e-02	0.4838e-02	0.1495e-01	0.2054e-03							
9	0.1886e-01	0.8819e-02	0.3918e-01	0.2589e-01	0.1897e-01	0.9669e-02	0.1712e+00	0.8992e-01	0.7848e+00	0.2668e+00
0.6683e-02	0.7807e-02	0.3286e-01	0.4681e-03							
10	0.8819e-02	0.1886e-01	0.2589e-01	0.3918e-01	0.9669e-02	0.1897e-01	0.8992e-01	0.1712e+00	0.2668e+00	0.7848e+00
0.7807e-02	0.6683e-02	0.3286e-01	0.4681e-03							
11	0.1871e-01	0.1418e-02	0.6852e-02	0.1777e-02	0.1885e-02	0.4648e-03	0.4838e-02	0.2778e-02	0.7807e-02	0.6683e-02
0.8598e-01	0.2768e-02	0.7143e-01	0.7613e-04							
12	0.1418e-02	0.1871e-01	0.1777e-02	0.6852e-02	0.4648e-03	0.1885e-02	0.2778e-02	0.4838e-02	0.6683e-02	0.7807e-02
0.2768e-02	0.8598e-01	0.7143e-01	0.7613e-04							
OH Coil	0.2018e-01	0.2018e-01	0.1408e-01	0.1408e-01	0.3189e-02	0.3189e-02	0.1498e-01	0.1498e-01	0.3286e-01	0.3286e-01
0.7143e-01	0.7143e-01	0.8725e+00	0.3629e-03							
plasma	0.7993e-04	0.7993e-04	0.1452e-03	0.1452e-03	0.3858e-04	0.3858e-04	0.2854e-03	0.2854e-03	0.4681e-03	0.4681e-03
0.7613e-04	0.7613e-04	0.3629e-03	0.4876e-05							

**********end of inductance output *********

******* PF Coil Power Conversion *****

PF Coil power and MVA requirements :

time (sec)	res. power (MW)	tot mva (MVA)
0.00	0.	0.
0.00	0.	0.
30.00	1.374e+00	2.960e+01
30.00	1.374e+00	-1.861e+02
36.00	1.731e+00	4.005e+02
36.00	1.731e+00	2.700e+01
42.00	1.926e+00	2.901e+01
42.00	1.926e+00	2.129e+00
842.00	2.130e+00	2.305e+00
842.00	2.130e+00	-2.552e+02
854.00	0.	0.
854.00	0.	0.

breakdown of power (MVA) requirement per pf coil group
power in MW, paranthesis values are MVA

time(sec) :	0.00000	30.00000	36.00000	42.00000	842.00000
pf coil : 1					
	0.0000 (0.0000)	0.2013 (4.7212)	0.1403 (-5.0037)	0.1456 (-0.3396)	0.1429 (0.1393)
	0.0000 (0.0000)	0.2013 (-6.7341)	0.1403 (-0.3414)	0.1456 (0.1419)	0.1429 (-6.9743)
pf coil : 2					
	0.0000 (0.0000)	0.2013 (4.7212)	0.1403 (-5.0037)	0.1456 (-0.3396)	0.1429 (0.1393)
	0.0000 (0.0000)	0.2013 (-6.7341)	0.1403 (-0.3414)	0.1456 (0.1419)	0.1429 (-6.9743)
pf coil : 3					
	0.0000 (0.0000)	0.0986 (4.7497)	0.1000 (0.4194)	0.1948 (0.3289)	0.2010 (0.2020)
	0.0000 (0.0000)	0.0986 (0.0035)	0.1000 (0.3203)	0.1948 (0.1966)	0.2010 (-21.6444)
pf coil : 4					
	0.0000 (0.0000)	0.0986 (4.7497)	0.1000 (0.4194)	0.1948 (0.3289)	0.2010 (0.2020)
	0.0000 (0.0000)	0.0986 (0.0035)	0.1000 (0.3203)	0.1948 (0.1966)	0.2010 (-21.6444)
pf coil : 5					
	0.0000 (0.0000)	0.1948 (0.1261)	0.0146 (-0.1145)	0.0238 (-0.0167)	0.0334 (0.0331)
	0.0000 (0.0000)	0.1948 (0.6678)	0.0146 (-0.0162)	0.0238 (0.0227)	0.0334 (0.1059)
pf coil : 6					
	0.0000 (0.0000)	0.1948 (0.1261)	0.0146 (-0.1145)	0.0238 (-0.0167)	0.0334 (0.0331)
	0.0000 (0.0000)	0.1948 (0.6678)	0.0146 (-0.0162)	0.0238 (0.0227)	0.0334 (0.1059)
pf coil : 7					
	0.0000 (0.0000)	0.0096 (0.3898)	0.1548 (40.4058)	0.1761 (3.0110)	0.1997 (0.2223)
	0.0000 (0.0000)	0.0096 (-10.0151)	0.1548 (2.0049)	0.1761 (0.1974)	0.1997 (-21.3910)
pf coil : 8					
	0.0000 (0.0000)	0.0096 (0.3898)	0.1548 (40.4058)	0.1761 (3.0110)	0.1997 (0.2223)
	0.0000 (0.0000)	0.0096 (-10.0151)	0.1548 (2.0049)	0.1761 (0.1974)	0.1997 (-21.3910)
pf coil : 9					
	0.0000 (0.0000)	0.0001 (-0.0470)	0.1631 (14.3078)	0.1812 (6.7036)	0.2003 (0.2617)
	0.0000 (0.0000)	0.0001 (2.4794)	0.1631 (6.3507)	0.1812 (0.2301)	0.2003 (-63.0650)
pf coil : 10					

```
   0.0000 (   0.0000)     0.0001 (  -0.0478)     0.1631 (  94.3078)     0.1812 (   6.7035)     0.2003 (   0.2817)
   0.0000 (   0.0000)     0.0001 (   2.4794)     0.1631 (   6.3507)     0.1812 (   0.2381)     0.2003 ( -53.9650)
pf coil :  11
   0.0000 (   0.0000)     0.1745 (   2.7976)     0.1389 (  10.9828)     0.1641 (   1.4960)     0.2011 (   0.2121)
   0.0000 (   0.0000)     0.1745 ( -21.5927)     0.1389 (   1.3284)     0.1641 (   0.1741)     0.2011 (  -5.9163)
pf coil :  12
   0.0000 (   0.0000)     0.1745 (   2.7976)     0.1389 (  10.9828)     0.1641 (   1.4960)     0.2011 (   0.2121)
   0.0000 (   0.0000)     0.1745 ( -21.5927)     0.1389 (   1.3284)     0.1641 (   0.1741)     0.2011 (  -5.9163)
OHC :
   0.0000 (   0.0000)     0.0328 (   2.2898)     0.1337 (  96.1468)     0.1860 (   6.6388)     0.1018 (   0.2341)
   0.0000 (   0.0000)     0.0328 ( -47.3116)     0.1337 (   6.1192)     0.1860 (   0.2054)     0.1018 ( -38.8796)


      pfckts, number of pf coil circuits                          13.00
      spsmva, sum of psmva of all pf coil circuits                894.7
      apsmva, average psmva of all pf coil circuits               68.82
      tcpfppsm, cost of all pulsed power supplies, $m             22.37
      tcpfclm, cost of all pf circuit l&c, $M                     5.123


      arcktpm,ave. r power of the pf circuits, kw                 198.3
      acptmax, av. max current/turn of the pf ckts, ka            24.62
      spfbusl, sum of the bus lengths of the pf ckts, m           2131.
      tcpfbsm, cost of all the pf bussing, $m                     2.624
      tcpfbpsm, cost of burn phase power supplies, $m             2.670


      vpfskv, maximum pf coil voltage, kv                         0.000
      ensxpfm, max. sum of x energy in pf ckts mj                 1544.
      tcpfbkm, cost of all dc ckt. breakers, $m                   0.1600e-01
      tcpfdrm, cost of all energy d-resistors, $m                 0.2194
      tcscpm, cost of pf ac ckt protection, $m                    0.9760


      tcpfsm, total cost of PF Conv. Sys. (M$)                    32.92
      engtpfm, maximum resistive energy of all the
           pf circuits over the entire cycle, mJ                  1899.


      bpsfm2, floor area of the burn power supplies
           of the pf coils, m2                                    441.9
      ppsfm2, floor area for the pulsed power supplies
           of the pf coils, m2                                    873.2
      bkrfm2, floor are for the dc ckt breakers, m2               322.2
      pfbldgm2, total building floor area for the pf
           coil power supplies, m2                                1637.
      pfbldgm3, building volume for the pfcoil power
           supplies, m3                                           9824.


******* End of PF Power Conversion **********



******** Start of Energy Storage ********
```

All pulsed power taken Utility line

Energy storage system parameters.

tburn---burn time, seconds	400.0
tfinal--total cycle time, seconds	854.0
pseff---power supply efficiency	0.9200
ereff---energy recovery efficiency	0.7500
dmeff---MGF drive motor efficiency	0.8000
pwrfac1-pulsed P.S. power factor	0.6000
pwrfac2-plasma heating P.S. power factor	0.8500
pwrfac3-MGF drive motor power factor	0.7500

Power supply energy and load data:

acpfmva-peak ac mva of the P.F. coil P.S.	740.1
acphmva-peak mva of the plasma heating P.S.	220.9
acptmva-total peak mva = acpfmva + acphmva	961.1
acptmw---total peak power demand, mw	631.9
phtgmj---plasma heating energy /cycle, mj	0.1302e+06
engtpfm-energy to P.F. coil P.S. /cycle, mj	1599.
acptmj---total pulsed energy /cycle, mj	0.1520e+06

MGF energy storage data:

fmgmw---maximum MGF power output, mw	0.
fmgmva---maximum MGF mva output, mva	0.
fmgmj---MGF energy /cycle, mj	0.
fmgrmj---energy recovery /cycle, mj	0.
fmgdmw---ave. power to MGF motor, mw	0.
fmgdmva-ave. mva to MGF motor, mva	0.
tcfmgm, total cost of the mgf energy storage system	0.

Power and energy from the utility line:

ulpmw---max. pulsed mw from utility line	631.9
ulpmva---max. pulsed mva from utility line	961.1
ulpmj---pulsed energy from the utility line, mj	0.1520e+06

flccfm2, floor area needed for the load control center (m2)	117.1
fmgfm2, floor area needed for mgf units (m2)	0.
esbldgm2, building floor area for the energy storage system (m2)	117.1
esbldgm2, building volume space for the energy storage system (m3)	702.8

********** End of Energy Storage **********

******* Start of Vacuum Output *********

PUMPDOWN TO BASE PRESSURE

fw outgassing rate (Pa-m/s)	(rat)	0.1300e-07

total outgassing load (Pa-m^3/s)	(ogas)	0.235e-04
base pressure required (Pa)	(pbase)	0.26#e-05
required N2 pump speed	(s(1))	9.0577
N2 pump speed provided (m^3/s)	(snet(1))	14.8729

PUMPDOWN BETWEEN BURNS

plasma chamber volume (m^3)	(volume)	90.5358
pressure in plasma chamber after burn (Pa)	(pend)	0.219e+00
pressure in plasma chamber before start of burn (Pa)	(pstart)	0.219e-02
dwell time between burns (s)	(tdwell)	100.0000
required DT pump speed (m^3/s)	(s(2))	4.5377
DT speed provided (m^3/s)	(snet(2))	29.6453

HELIUM ASH REMOVAL

gas pressure in divertor chamber (Pa)	(pdiv)	0.12#e+00
fraction of He gas in divertor chamber	(fhe)	0.1271
required He pump speed (m^3/s)	(s(3))	29.6453
He speed provided (m^3/s)	(snet(3))	32.1884

DT REMOVAL AT FUELING RATE

DT fueling rate (kg/s)	(frate)	0.714e-05
required DT pump speed (m^3/s)	(s(4))	29.6453
DT speed provided (m^3/s)	(snet(4))	29.6453

The vacuum pumping system size is governed by the requirements for
DT removal at fueling rate

number of large pump ducts	(nduct)	32
diameter of passage from div. to ducts (m)	(d(1max))	0.3147
length of passage (m)	(l1)	1.7400
diameter of ducts (m)	(dout)	0.3776
length of ducts from div. passage to elbow (m)	(l2)	5.2500
length of ducts from elbow to vac. pumps (m)	(l3)	2.0000
number of turbopumps	(npump)	64

Vacuum Pumping System Costs

cost of ducts = $ 2287435.
cost of duct shielding* = $ 0.
cost of l&c and leak detection = $ 1000000.
cost of roughing/backing pumps = $ 720000.
cost of hi-vacuum pumps = $ 5440000.
cost of large isolation valve = $ 4911548.
total cost of vacuum pumping system = $ 28038983.

********* End of Vacuum Output **************

********** Reactor Vault Output **********

INPUT

DT Neutron Wall load	1.233e+00	MW/m**2
Major radius	2.995e+00	m
Outer Shield Radius	5.240e+00	m
Inner Reactor Vault radius	1.705e+01	m
Total shield Thickness	1.270e+00	m

OUTPUT

Wall Thickness of The Reactor Vault	1.760e+00	m
Roof Thickness of The Reactor Vault	9.690e-01	m

********* End of Reactor Vault **********

****************** Plant Buildings System ******************

vrcl	internal volume of reactor building (to tritium module)	6.211e+04
wrbl	distance from center of tokamak to building wall (to reactor vault shield module)	1.705e+01
efloor	effective floor area to ac power	7.312e+04
rbv	volume of reactor building	7.920e+04
rmbv	volume of reactor maintenance building	6.174e+04
wsv	volume of warmshop	4.242e+04
triv	volume of tritium building	3.313e+04
elev	volume of electrical building	3.550e+04
conv	volume of control building	2.000e+04
cryv	volume of cryogenics building	1.667e+04
admv	volume of administration building	5.000e+04
shov	volume of shops	1.000e+05

******* End of Building Output ********

******** Tritium Output **********

*burn time	(s)	=	800.
*fusion power	(mw)	=	300.
*dwell time	(s)	=	100.
*ramp time	(s)	=	40.
*plant availibility		=	0.30
*ion density	(ions/m**3)	=	8.00e+20
*beam (trit) efficiency		=	0.2

```
  *beam  (deut) efficiency                =      0.2
  *(deut)neutral beam          (kamp)     =      0.044
  *(trit)neutral beam          (kamp)     =      0.044
tritium and fuel processing parameters

  tritium initial load/burn (g)           =      0.02
  number of burn          (cycles/d)      =      91.1
  tritium burnup           (g/cycle)      =      0.45
  tritium burnup                (g/d)     =      40.9
  tritium exhaust          (g/cycle)      =       8.4
  tritium exhaust               (g/d)     =    765.6
  tritium to plasma        (g/cycle)      =       8.0
  tritium fueling               (g/d)     =    886.5
  tritium fueling              (g/yr)     =   0.88e+05
  tritium proc. -plasma       (kg/s)      =   0.98e-05
  tritium separated-blkt        (g/d)     =      17.9
  tritium bred                  (g/d)     =      40.5
  tritium perm/div              (g/d)     =       0.1
  tritium perm/fw               (g/d)     =       0.1
  tritium proc.losses          (g/yr)     =       9.3
  tritium weight frac.-pellet             =       0.6
deuterium and neutral beam system

  d burned per day              (g/d)     =      27.4
  d total pellets               (g/d)     =    194.7
  d injected neut beam          (g/d)     =     60.603
  d load  beam pumps            (g/d)     =    274.412
  t pumped-neut beams           (g/d)     =   0.0001
  d total fueling               (g/d)     =    537.0
tritium inventories

  trit -diverter                  (g)     =     10.0
  trit -fw structure              (g)     =     30.0
  trit -plas vacuum pumps         (g)     =     16.5
  trit -surge tank                (g)     =     33.6
  trit -storage (reserve)         (g)     =    886.5
  trit -fuel cleanup unit         (g)     =      2.0
  trit -cryo distill              (g)     =     92.4
  trit -gaseous waste             (g)     =      1.9
  trit -lines                     (g)     =      0.9
  trit -fueler                    (g)     =     12.0
  trit -breeder blanket           (g)     =    207.1
  trit - blanket proc             (g)     =     43.2
  trit -primary coolant           (g)     =      0.0
  trit -prim coolant proc         (g)     =      0.0
  trit -trit neut beam pump       (g)     =     17.2
  trit -deut neut beam pump       (g)     =   0.004
  total tritium inventory         (g)     =  1264.0
3 salt: 2 li/oxide; 1 libe; 0 flibe

  blanket type                            =      3.00
  breeding ratio                          =      0.99
  tritium bred                  (g/d)     =     40.47
  tritium decay                (g/yr)     =     70.70
  *cost of t                ($/curie)     =      1.50
  annual tritium consumption(g)           =   0.12e+03
  annual cost of tritium          ($)     =   0.18e+07
  startup cost of tritium         ($)     =   0.18e+08
tritium system capital costs

  cap cost fuel cleanup           ($)     =   0.12e+07
  cap cost cryo still             ($)     =   0.18e+07
  cap cost transfer pumps         ($)     =   0.12e+06
  cap cost gas waste proc         ($)     =   0.48e+06
```

```
  cap cost control systems  ($)  =    0.23e+07
  cap cost solid waste      ($)  =    0.18e+06
  cap cost uninter. power   ($)  =    0.17e+06
  cap cost emerg. generator ($)  =    0.61e+06
  cap cost integration      ($)  =    0.55e+06
  cap cost trit receiving   ($)  =    0.28e+06
  cap cost trit shippers    ($)  =    0.12e+06
  cap cost trit storage     ($)  =    0.93e+06
  cap cost anal/inv systems ($)  =    0.20e+07
  cap cost glovebox/secdary ($)  =    0.12e+07
  cap cost emerg proc       ($)  =    0.84e+07
  cap cost tritium monitors ($)  =    0.14e+08
  cap cost water recovery   ($)  =    0.
  cap cost blkt processing  ($)  =    0.25e+08
  cap cost atmospheric proc ($)  =    0.15e+08
  cap cost plasma proc      ($)  =    0.69e+07
  cap cost storage/secondary($)  =    0.53e+07
  cap cost monitors/atmosp  ($)  =    0.29e+08
  cap cost water proc       ($)  =    0.
  cap cost blank/coolnt proc($)  =    0.25e+08
  cap cost total - trit proc($)  =    0.66e+08
   feedrate (kg/s)               =    0.28e+01
   in -t concentration (ci/kg)   =    0.18e+02
   front end -1=vpce,2=el        =    0.18e+01
   front end enrichment          =    0.90e+04
   type of water 1.=h,0=d        =    0.10e+01
   salt removal                  =    0.00e+00
   return feed(kg/s)             =    0.28e+01
   out-t concentration (ci/kg)   =    0.90e+01
   cryogenic refrigeration (mw)  =    0.13e-04
   electrical power load (mw)    =    0.
   steam energy requirement (mw) =    0.93e+01
   correction factor -scott      =    0.10e+01
  cleanup1=diffuser,2=molesieve  =    0.10e+01
 operating costs

  op cost - plasma proc      ($)  =     0.10e+07
  op cost - blanket proc     ($)  =     0.10e+07
  op cost - atmosphere proc  ($)  =     0.10e+07
  op cost - water proc       ($)  =     0.10e+07
  total op cost - trit proc  ($)  =     0.40e+07
 equipment sizes

  equip -plasma proc.      (m**3)  =    1500.
  equip -blanket proc.     (m**3)  =    4009.
  equip -atmosphere proc.  (m**3)  =    1472.
  equip -emergency  proc.  (m**3)  =    1174.
  equip -water  proc.      (m**3)  =       0.
  equip -other proc.       (m**3)  =     500.
  equip -total trit proc.  (m**3)  =    8281.
 power requirements

  power - plasma proc.       (mw)  =       0.5
  power  - blanket proc      (mw)  =       9.3
  power  - atmosphere proc   (mw)  =       2.0
  power  - emergency  proc   (mw)  =       0.6
  power  - water proc        (mw)  =       0.0
  power  - other proc        (mw)  =       0.5
  total power - trit proc    (mw)  =      12.3
atmospheric tritium recovery-reactor hall

  accident release           (g)  =    10.00
  initial t conc.     (uci/m**3)  =     0.16e+07
 *cleanup time              (hr)  =   120.00
```

```
        *volume of reactor hall (m**3)  =    0.62e+05
        *cleanup efficiency             =    0.90
        *t level stacked    (uci/m**3)  =   50.00
         atr  flow rate       (m**3/s)  =    1.65
         vent rate            (m**3/s)  =    0.14e+00
         tritium release         (ci)   =    3.11
         tritium vented to env.  (ci)   =    0.04
       atmospheric tritium recovery- hot cell

         accident release          (g)  =   10.00
         initial t conc.     (uci/m**3)  =    0.16e+07
        *cleanup time              (hr)  =  120.00
        *volume of  hot cell    (m**3)   =    0.62e+05
        *cleanup efficiency             =    0.90
        *t level stacked    (uci/m**3)  =   50.00
         atr  flow rate       (m**3/s)  =    0.00
         vent rate            (m**3/s)  =    0.14e+00
         tritium release         (ci)   =    3.09
         tritium vented to env.  (ci)   =    0.04
       atmospheric tritium recovery-trit bldg

         accident release          (g)  =   10.00
         initial t conc.     (uci/m**3)  =    0.29e+07
        *cleanup time              (hr)  =  120.00
        *volume of trit bldg    (m**3)   =    0.33e+05
        *cleanup efficiency             =    0.90
        *t level stacked    (uci/m**3)  =   50.00
         atr  flow rate       (m**3/s)  =    0.00
         vent rate            (m**3/s)  =    0.77e-01
         tritium release         (ci)   =    1.66
         tritium vented to env.  (ci)   =    0.79


********* End of Tritium Output *******

      ****************** Heat Transport System ******************

      fwht    heat removal from first wall (Mw)                  98.072
      divht   heat removal from divertor plates (Mw)             31.691
      blht    heat removal from blankets (Mw)                     0.000
      shdht   heat removal from shield (Mw)                     363.400
      pnbht   heat removal from neutral beams (Mw)               86.132
      echht   heat removal from ech (Mw)                          0.000
      plhht   heat removal from lh (Mw)                          21.489
      cryht   heat removal from cryogenic plant (Mw)             19.231
      vacht   heat removal from vacuum pumps (Mw)                 0.600
      tritht  heat removal from tritium plant (Mw)               12.279
      helpow  total cryogenic load at 4.2K (Mw)                   0.030
      facht   heat removal from facilities(Mw)                   27.200
      rnphx   number of primary heat exchangers                   3.261
      rnihx   number of intermediate heat exchangers             13.944
      ctht    total plant heat rejection (Mw/                   686.994

  ********** End of Heat Transport **********
```

******** AC POWER SYSTEM OUTPUT ************

@ Inputs from other system code modules
& User-selected inputs
* Outputs to other system code modules

@	basemw,	facility base power load, MW	5.00
@	efloor,	effective total floor space, SQ.M	73123.74
@	pkwpm2,	power needed per floor area, KW/SQ.M	0.15
	fcsht,	total power to facility loads, MW	27.76
@	fmgdmw,	power to mgf units, MW	0.00
@	acpfmva,	pf pulsed power at pwrfacl (1), MW	740.11
@	bpsmw,	power to burn power supplies, MW	2.50
@	bdvmw,	power to divertor coil supplies, MW	0.00
@	wtfmw,	power to tf coil power supplies, MW	2.90
@	pheatmw,	power to plasma heating supplies, MW	172.70
@	crymw,	power to cryogenic comp. motors, MW	19.23
@	vacmw,	power to vacuum pump motors, MW	0.50
&	htpmw,	power to hts pump motors, MW	10.00
@	t2pmw,	power to tritium processing, MW	12.20
*	pacpmw,	total pulsed power system load, MW	236.23

(1 - see energy storage)

&	hvlkv,	pulsed power utility line voltage, KV	230.00
	n3pht,	number of 3 phase transformers	2.00
	tmva,	max. mva of each transformer, MVA	125.00
	pnbkrs,	number of 13.8kv circuit breakers	16.00
	bkrmva,	short circuit mva of circuit bkrs, MVA	1250.00
&	fvlkv,	facility power line voltage, KV	115.00
	ftmva,	max. mva of facility transformer, MVA	30.00
	fnbkrs,	number of 13.8kv circuit breakers	5.00
	fbkmva,	short circuit mva of circuit bkrs, MVA	500.00

AC POWER SUMMARY

*	pacpmw,	total pulsed power system load, MW (power to the heat transfer system)	236.23
&	hvlkv,	pulsed power utility line voltage, KV	230.00
	fcsht,	total facility power load, MW	27.76
&	fvlkv,	facility power line voltage, KV	115.00

AC POWER COST SUMMARY

	cpacpm,	cost of the pulsed power system, $M	7.97
	cfacpm,	cost of facility ac power system, $M	1.20
	c2dgm,	cost of 2 DGs (480v, 2500kw ea.), $M	1.60
	c4nbpm,	cost of 4 no-break power supplies, $M	0.40
	clvdsm,	cost of LV power distribution, $M	2.70
*	ctacpm,	installed cost of ac power system, $M	13.95

********** End of AC Power ************

******* Maintanance Equipment Output ********

Equipment-Item	Unit cost ($K)	Test cell	Hot cell	Mockup	Total ($K)
Servo-manipulator (bridge-mounted)	2000.0	1.0	1.0	0.5	5000.0
Power manipulator (bridge-mounted)	500.0	1.0	1.0	0.5	1250.0
Robot arm (floor-mounted)	100.0	1.0	1.0	1.0	300.0
Mechanical manipulator (thru-the-wall)	100.0	0.0	5.0	1.0	600.0
Mobile manipulator	1000.0	1.0	0.0	1.0	2000.0
In-vessel manipulator system	1300.0	2.0	0.0	1.0	3900.0
Leak detection system	000.0	1.0	0.0	0.0	000.0
Small "hand" tools	500.0	1.0	1.0	1.0	1500.0
Lifting fixtures, slings, etc.	250.0	1.0	1.0	0.0	500.0
Shielded windows	250.0	4.0	5.0	1.0	2500.0
Transporter for large components	500.0	1.0	0.0	0.0	500.0
Transporter for small components	250.0	2.0	0.0	0.0	500.0
Welders - structural	100.0	1.0	1.0	0.0	200.0
Welders - piping	150.0	1.0	1.0	0.0	300.0
Cutters - structural	100.0	1.0	1.0	0.0	200.0
Cutters - piping	150.0	1.0	1.0	0.0	300.0
Sector module transporter	500.0	1.0	0.0	0.0	500.0
Manipulator end-effectors	500.0	1.0	1.0	1.0	1500.0
Decontamination (Decon cell)	1000.0	1.0	0.0	0.0	1000.0
Decontamination (Hot cell)	100.0	0.0	1.0	0.0	100.0
Rad-waste handling (Hot cell)	1000.0	0.0	1.0	0.0	1000.0
Waste handling casks	500.0	0.0	1.0	0.0	500.0
Transfer lock (into test cell)	1000.0	1.0	0.0	0.0	1000.0
Cell lighting and audio	100.0	1.0	1.0	0.5	250.0
Closed circuit TV	100.0	1.0	1.0	0.5	250.0
Blanket module handling	500.0	1.0	0.0	0.0	500.0
					28450.0
Warm Cell (@10% of above)					2845.0
					31295.0

********* End of Maintanance Output *********

********** I & C Output **********

PROCESS I&C COST ESTIMATE

* tcopsc-TOTAL COST OF PROCESS I&C $ 21.00M

PLASMA DIAGNOSTICS COST ESTIMATE TABLE

fprodpar-fusion product particle diagnostics group
nohp-no. of diagnostic types in group k for H2 phase
nodp-no. of diagnostic types in group k added for D2 phase
nctp-no. of diagnostic types in group k added for T phase
tmcpdm-average cost of a diagnostic type in group k, $M
hpdgcm-cost of diagnostics in group k for H2 phase, $M
dpdgcm-cost of diagnostics in group k added for D2 phase, $M
tpdgcm-cost of diagnostics in group k added for T phase, $M

k	diag.grp	nohp	nodp	notp	tmcpdm	hpdgcm	dpdgcm	tpdgcm	total
1	edensity	2	2	2	1.00	3.60	3.60	3.80	11.00
2	e.temp	2	2	2	1.60	3.20	3.20	3.40	9.80
3	ion temp	3	2	2	1.00	5.40	3.60	4.00	13.00
4	impurity	3	2	2	0.85	2.55	1.70	2.00	6.25
5	pwr loss	2	2	2	0.50	1.00	1.00	1.10	3.10
6	magnetic	3	2	2	0.35	1.05	0.70	0.80	2.55
7	p.instab	3	2	1	0.85	2.55	1.70	1.85	5.30
8	fprodpar	1	3	2	0.95	0.95	2.00	2.10	5.90
9	environ	3	3	2	0.85	2.55	2.55	1.00	6.90
10	miscel	6	0	10	0.50	3.00	4.00	5.10	12.10

TOTAL COST OF DIAGNOSTICS 25.05 24.90 28.15 $ 78.90M
(Using MEDIUM Diagnostics) * tcopdg

ARCHIVING COMPUTER HARDWARE

* tcarch-computer archiving $ 10.00M

TOTAL I&C & PLASMA DIAGNOSTICS COST SUMMARY
(Through The Tritium Phase)

* tcopsc-total cost of process I&C cost, $M 21.00
* tcopdg-total cost of plasma diagnostics, $M 78.9
* tcarch-total cost of archiving & processing, $M 10.00

* tcscdg-TOTAL COST OF DIAGNOSTICS & I&C $106.90M

COST RANGE USING I&C & DIAGNOSTIC DEFAULTS FOR TRITIUM PHASE
LOW Diagnostics tcscdg= $ 67M
MEDIUM Diagnostics tcscdg= $ 107M
HIGH Diagnostics tcscdg= $ 170M

********** End of I & C Output **********

****

the starting point used 37 iterations
the optimization used 0 iterations
there were 37 physics calls

***** computer usage output *****

cpu= 0.634e+01 s io= 0.421e+00 s sys= 0.190e-01 s
n total= 37 n calls= 37
09:02:58 10/00/87

ORNL FEDC-87-7
Dist. Category UC-423, 424

INTERNAL DISTRIBUTION

1. C. A. Flanagan
2. J. D. Galambos
3. J. R. Haines
4. P. N. Haubenreich
5. D. R. Hicks
6. S. S. Kalsi
7. M. S. Lubell
8. Y-K. M. Peng
9. R. K. Richards
10. R. L. Reid
11. M. J. Saltmarsh
12. R. O. Sayer
13. E. C. Selcow
14. T. E. Shannon
15. J. Sheffield
16. P. T. Spampinato
17. D. J. Strickler
18. S. L. Thomson
19. N. A. Uckan
20. T. Uckan
21–22. Laboratory Records Department
23. Laboratory Records, ORNL-RC
24. Document Reference Section
25. Central Research Library
26. Fusion Energy Division Library
27–28. Fusion Energy Division Publications Office
29. ORNL Patent Office

EXTERNAL DISTRIBUTION

30. G. E. Gorker, 1727 Marlyn Way, San Jose, CA 95125
31. W. L. Barr, Lawrence Livermore National Laboratory, P.O. Box 5511 (L-644), Livermore, CA 94550
32. C. G. Bathke, Controlled Thermonuclear Research Division, Los Alamos National Laboratory, P.O. Box 1663, MS F641, Los Alamos, NM 87545
33. J. N. Brooks, Argonne National Laboratory, 9700 South Cass Avenue, Bldg. 205, Argonne, IL 60439
34. R. H. Bulmer, Lawrence Livermore National Laboratory, P.O. Box 5511 (L-644), Livermore, CA 94550
35. A. Busigin, Ontario Hydro, 700 University Avenue, H11-F26, Toronto, Ontario, Canada, M5G1X6
36. P. F. DuBois, Lawrence Livermore National Laboratory, P.O. Box 5511 (L-630), Livermore, CA 94550
37. M. E. Fensternacher, Lawrence Livermore National Laboratory, P.O. Box 5511 (L-644), Livermore, CA 94550
38. J. Fink, Lawrence Livermore National Laboratory, P.O. Box 5511 (L-644), Livermore, CA 94550
39. P. A. Finn, Argonne National Laboratory, 9700 South Cass Avenue, Bldg. 205, Argonne, IL 60439

40. Y. Gohar, Argonne National Laboratory, 9700 South Cass Avenue, Bldg. 205, Argonne, IL 60439
41. A. M. Hassanein, Argonne National Laboratory, 9700 South Cass Avenue, Bldg. 205, Argonne, IL 60439
42. S. K. Ho, Lawrence Livermore National Laboratory, P.O. Box 5511 (L-644), Livermore, CA 94550
43. K. M. Kalyanam, Ontario Hydro, 700 University Avenue, H11-F26, Toronto, Ontario, Canada, M5G1X6
44. J. A. Kerns, Lawrence Livermore National Laboratory, P.O. Box 5511 (L-538), Livermore, CA 94550
45. J. D. Lee, Lawrence Livermore National Laboratory, P.O. Box 5511 (L-644), Livermore, CA 94550
46. J. R. Miller, Lawrence Livermore National Laboratory, P.O. Box 5511 (L-643), Livermore, CA 94550
47. R. L. Miller, Controlled Thermonuclear Research Division, Los Alamos National Laboratory, P.O. Box 1663, MS-F641, Los Alamos, NM 87545
48. J. O. Myall, Lawrence Livermore National Laboratory, P.O. Box 5511 (L-635), Livermore, CA 94550
49. L. J. Perkins, Lawrence Livermore National Laboratory, P.O. Box 5511 (L-644), Livermore, CA 94550
50. C. E. Wagner, JAYCOR, P.O. Box 85154, San Diego, CA 92138
51. R. S. Willms, Controlled Thermonuclear Research Division, Los Alamos National Laboratory, P.O. Box 1663, MS C348, Los Alamos, NM 87545
52. M. A. Abdou, Boelter Hall, University of California, Los Angeles, CA 90024
53. J. L. Anderson, CMB-3, Mail Stop 348, Los Alamos National Laboratory, P.O. Box 1633, Los Alamos, NM 87545
54. C. C. Baker, FPP/208, Argonne National Laboratory, 9700 South Cass Avenue, Argonne, IL 60439
55. D. Baldwin, University of Texasm RLM 11.22, Austin, TX 78712
56. D. S. Beard, Office of Fusion Energy, Office of Energy Research, ER-531 Germantown, U.S. Department of Energy, Washington, DC 20545
57. R. Botwin, C47-05, Grumman Aerospace Corporation, P.O. Box 31, Bethpage, NY 11714
58. J. D. Callen, Department of Nuclear Engineering, University of Wisconsin, Madison, WI 53706-1687
59. J. F. Clarke, Director for Fusion Energy, Office of Energy Research, ER-50 Germantown, U.S. Department of Energy, Washington, DC 20545
60. D. R. Cohn, MIT Plasma Fusion Center, 167 Albany Street, NW 16-140, Cambridge, MA 02139
61. R. W. Conn, Department of Chemical, Nuclear, and Thermal Engineering, Boelter Hall, University of California, Los Angeles, CA 90024
62. J. G. Crocker, EG&G Idaho, P.O. Box 1625, Idaho Falls, ID 83401

63. G. R. Dalton, Department of Nuclear Engineering Science, Nuclear Science Center, University of Florida, Gainesville, FL 32611
64. R. C. Davidson, Massachusetts Institute of Technology, 77 Massachusetts Avenue, Cambridge, MA 02139
65. N. A. Davies, Office of the Associate Director, Office of Fusion Energy, Office of Energy Research, ER-51 Germantown, U.S. Department of Energy, Washington, DC 20545
66. S. O. Dean, Director, Fusion Power Associates, Inc., 2 Professional Drive, Suite 249, Gaithersburg, MD 20760
67. D. DeFreece, E451, Building 81/1/B7, McDonnell Douglas Astronautics Company, P.O. Box 516, St. Louis, MO 63166
68. R. S. Devoto, Lawrence Livermore National Laboratory, P.O. Box 5511, L-644, Livermore, CA 94550
69. J. N. Doggett, Lawrence Livermore National Laboratory, P.O. Box 5511, L-441, Livermore, CA 94550
70. R. J. Dowling, Office of Fusion Energy, Office of Energy Research, ER-55, Germantown, U.S. Department of Energy, Washington, DC 20545
71. H. Dreicer, Division Leader, CRT, Los Alamos National Laboratory, P.O. Box 1663, Los Alamos, NM 87545
72. F. Engelmann, The NET Team, Max-Planck-Institut fur Plasmaphysik, D-8046 Garching, Federal Republic of Germany
73. H. K. Forsen, Bechtel Group, Inc., Research and Engineering, P.O. Box 3965, San Francisco, CA 94119
74. J. W. French, Princeton Plasma Physics Laboratory, P.O. Box 451, Princeton, NJ 08543
75. S. D. Frey, U.S. Department of Energy, Oak Ridge Operations, P.O. Box E, Room 2115, Oak Ridge, TN 37831
76. N. Fugisawa, Japan Atomic Energy Research Institute, Naka Fusion Reserach Establishment, Naka-machi, Naka-gun, Ibaraki-ken 311-02, Japan
77. H. P. Furth, Director, Princeton Plasma Physics Laboratory, P.O. Box 451, Princeton, NJ 08543
78. J. R. Gilleland, Lawrence Livermore National Laboratory, P.O. Box 5511, Livermore, CA 94550
79. R. W. Gould, Department of Applied Physics, California Institute of Technology, Pasadena, CA 91125
80. R. A. Gross, Plasma Research Laboratory, Columbia University, New York, NY 10027
81. C. D. Henning, Lawrence Livermore National Laboratory, P.O. Box 5511, Livermore, CA 94550
82. J. Holdren, University of California, Berkeley, CA 94720
83. T. R. James, Office of Fusion Energy, Office of Energy Research, ER-55, Germantown, U.S. Department of Energy, Washington, DC 20545

84. J. B. Joyce, Princeton Plasma Physics Laboratory, P.O. Box 451, Princeton, NJ 08543
85. T. Kammash, University of Michigan, Cooley Building, North Campus, Department of Nuclear Engineering, Ann Arbor, MI 48109
86. R. A. Krakowski, CTR-12, Mail Stop 641, Los Alamos National Laboratory, P.O. Box 1663, Los Alamos, NM 87545
87. G. L. Kulcinski, University of Wisconsin, Department of Nuclear Engineering, Engineering Research Building, Room 439, 1500 Johnson Drive, Madison, WI 53706
88. R. K. Linford, Los Alamos National Laboratory, P.O. Box 1663, Los Alamos, NM 87545
89. B. G. Logan, Lawrence Livermore National Laboratory, P.O. Box 5511, L-644, Livermore, CA 94550
90. W. Marton, Office of Fusion Energy, Office of Energy Research, ER-55 Germantown, U.S. Department of Energy, Washington, DC 20545
91. R. F. Mattas, Argonne National Laboratory, 9700 S. Cass Acenue, Argonne, IL 60439
92. D. M. Meade, Princeton Plasma Physics Laboratory, P.O. Box 451, Princeton, NJ 08543
93. G. H. Miley, University of Illinois, Nuclear Engineering Laboratory, 103 S. Goodwin Avenue, Urbana, IL 61801
94. D. B. Montgomery, MIT Plasma Fusion Center, 167 Albany Street, Cambridge, MA 02139
95. A. L. Opdenaker, Office of Fusion Energy, Office of Energy Research, ER-532 Germantown, U.S. Department of Energy, Washington, DC 20545
96. D. Overskei, GA Technologies, P.O. Box 85608, San Diego, CA 92138
97. R. R. Parker, Plasma Fusion Center, Massachusetts Institute of Technology, 167 Albany Street, Cambridge, MA 02139
98. B. Pease, Culham Laboratory, Abingdon, Oxfordshire OX14 3DB, United Kingdom
99. F. W. Perkins, Princeton Plasma Physics Laboratory, P.O. Box 451, Princeton, NJ 08543
100. M. Porkolab, Plasma Fusion Center Massachusetts Institute of Technology, 167 Albany Street, Cambridge, MA 02139
101. D. E. Post, Princeton Plasma Physics Laboratory, P.O. Box 451, Princeton, NJ 08543
102. F. A. Puhn, GA Technologies, Inc., P.O. Box 81608, San Diego, CA 92138
103. M. Roberts, International Program, Office of Fusion Energy, Office of Energy Research, ER-52 Germantown, U.S. Department of Energy, Washington, DC 20545
104. P. H. Rutherford, Princeton Plasma Physics Laboratory, P.O. Box 451, Princeton, NJ 08543

105. J. A. Schmidt, Princeton Plasma Physics Laboratory, P.O. Box 451, Princeton, NJ 08543
106. K. R. Schultz, GA Technologies P.O. Box 85608, San Diego, CA 92138
107. G. V. Sheffield, Princeton Plasma Physics Laboratory, P.O. Box 451, Princeton, NJ 08543
108. W. M. Stacey, Jr., Georgia Institute of Technology, Fusion Research Center, Cherrry-Emerson Building, Atlanta, GA 30332
109. R. D. Stambaugh, GA Technologies P.O. Box 85608, San Diego, CA 92138
110. R. R. Stasko, Canadian Fusion Fuels Technology Project, 2700 Lakeshore Road West, Mississauga, Ontario L5J 1K3
111. D. Steiner, Rensselaer Polytechnic Institute, Nuclear Engineering Department, NES Building, Tibbets Avenue, Troy, NY 12181
112. L. E. Strawbridge, Westinghouse Electric Corporation, P.O. Box 158, Madison, PA 15663
113. F. Thomas, B-20-5, Grumman Aerospace Corporation, Bethpage, NY 11714
114. K. I. Thomassen, Lawrence Livermore National Laboratory, P.O. Box 5511, Livermore, CA 94550
115. R. J. Thome, Francis Bitter National Magnet Laboratory, 170 Albany Street, Cambridge, MA 02139
116. H. Weitzner, New York University, 251 Mercer Street, New York, NY 10012
117. J. C. Wesley, GA Technologies, Inc., P.O. Box 81608, San Diego, CA 92138
118. J. W. Willis, Office of Fusion Energy, Office of Energy Research, ER-55, Germantown, U.S. Department of Energy, Washington, DC 20545
119. K. M. Young, Princeton Plasma Physics Laboratory, P.O. Box 451, Princeton, NJ 08543
120. Bibliothek, Max-Planck Institut fur Plasmaphysik, D-8046 Garching, Federal Republic of Germany
121. Bibliothek, Institut fur Plasmaphysik, KFA, Postfach 1913, D-5170 Julich, Federal Republic of Germany
122. Library, CEN/Cadarache, F-13108 Saint-Paul-lez-Durance, France
123. Documentation S.I.G.N., Departement de la Physique du Plasma et de la Fusion Controlee, Centre d'Etudes Nucleaires, B.P. 85, Centre du Tri, 38041 Grenoble Cedex, France
124. Library, Centre de Recherches en Physique des Plasmas, 21 Avenue des Bains, 1007 Lausanne, Switzerland
125. Library, Culham Laboratory, UKAEA, Abingdon, Oxfordshire, OX14 3DB, England
126. Library, FOM Instituut voor Plasmafysica, Rijnhuizen, Edisonbaan 14, 3439 MN Nieuwegein, The Netherlands
127. J. Shang-Xian, Graduate School, Academia Sinica, P.O. Box 3908, Beijing, China (PRC)

128. Library, Institute for Plasma Physics, Nagoya University, Nagoya 464, Japan
129. Library, International Centre for Theoretical Physics, Trieste, Italy
130. Library, JET Joint Undertaking, Abingdon, Oxfordshire, OX14 3EA, England
131. Library, Laboratorio Gas Ionizzati, CP 65, I-00044 Frascati, Rome, Italy
132. Plasma Research Laboratory, Australian National Laboratory, P.O. Box 4, Canberra, ACT 2000, Australia
133. Thermonuclear Library, Japan Atomic Energy Research Institute, Tokai Research Establishment, Tokai, Ibaraki-ken, Japan
134. Library, Plasma Physics Laboratory, Kyoto University, Gokasho, Uji, Kyoto 611, Japan
135. Office of the Assistant Manager for Energy Research and Development, U.S. Department of Energy, Oak Ridge Operations, P.O. Box E, Oak Ridge, TN 37831
136. Bibliothek, KfK Karlsruhe GmbH, Postfach 3640, D-7500 Karlsruhe 1, Federal Republic of Germany
137. Library, Japan Atomic Energy Research Institute, Naka-machi, Naka-gun, Ibaraki-ken 311-02, Japan

138–187. Given distribution as shown in OSTI-4500, Magnetic Fusion Energy (Distribution Category UC423 and 424: Reactor Materials and Fusion Systems)

•U S GOVERNMENT PRINTING OFFICE